Pergamon

Prog. Part. Nucl. Phys., Vol. 39, pp. 503–564, 1997

0146-6410/97 $32.00 + 0.00

S0146-6410(97)00049-5

Photon and Gluon Induced Processes in Relativistic Heavy-Ion Collisions

F. KRAUSS, M. GREINER and G. SOFF

Institut für Theoretische Physik, Technische Universität, D-01062 Dresden, Germany

Abstract : Relativistic heavy–ion collisions at RHIC and LHC represent an intense source for photon induced processes. The strong transverse electromagnetic fields of the colliding heavy ions can be described as an equivalent swarm of photons, which leads to the Equivalent Photon Approximation. Cross sections and production rates for various heavy particles are estimated for two–photon fusion processes. An equivalent photon can also interact with the other colliding nucleus. Processes like Coulomb dissociation and photon–gluon fusion are investigated. The latter allows for a deduction of the in–medium gluon distribution. We also discuss the production of Z^0 bosons, Higgs bosons and top quarks in central heavy-ion collisions.

Contents

Chapter 1

Introduction

The two accelerators "Relativistic Heavy-Ion Collider" (RHIC) scheduled for 1999 and "Large Hadron Collider" (LHC) scheduled for 2004/2008 offer the possibility to investigate heavy-ion collisions at extremely high energies. At RHIC Au-Au collisions are designed with a collision energy of $E = 108$ GeV/u in the center of momentum of the colliding heavy ions. The Pb-Pb mode at LHC will allow for collision energies of $E = 2.75$ TeV/u; in Ca-Ca collisions one can even reach $E = 3.75$ TeV/u. The main emphasis will be on central nuclear collisions to study properties of nuclear matter under extreme conditions. It is speculated to observe a possible phase transition of nuclear and hadronic matter into a quark-gluon plasma at sufficiently large nuclear densities. Besides this mainstream effort there are also other facts worth considering, which can be labelled loosely as "Non Quark Gluon Plasma Physics": Two-photon fusion processes into exotic particles, photon-gluon fusion processes and pomeron exchange in peripheral collisions, and also production processes of exotic particles in central collisions.
As a charged nucleus moves with nearly the speed of light, its electromagnetic field becomes transverse to its velocity. Due to the overlap of the strong transverse electromagnetic fields of the two colliding nuclei, very large coherent energy densities can be reached, which represent sources for the electromagnetic production of exotic particles. The equivalent photon approximation allows a rather simple and straightforward calculation of these processes: Since the electric and magnetic field associated with one nucleus take on the same absolute value, this transverse electromagnetic field can be simulated by an equivalent swarm of photons. Thus the collision of the two transverse electromagnetic fields can be described as the collision of two equivalent swarms of photons, where two photons, one of each swarm, may fuse to produce exotic particles.
To have a rough estimate of the energies contained in the strong transverse electromagnetic fields we consider the maximum available equivalent photon frequencies, which can be derived from the uncertainty principle:

$$\Delta t \cdot \Delta E \simeq 1 \quad \Longrightarrow \quad \frac{R}{\gamma v} \cdot \omega \simeq 1 \quad \overset{v \to c}{\Longrightarrow} \quad \omega_{\max} \simeq \frac{\gamma}{R} \,. \tag{1.1}$$

Δt is the collision time, γ is the Lorentz contraction factor, R denotes the nuclear radius and v the velocity of the nucleus ($c = 1$). At RHIC energies ($\gamma = 108$) a Au beam will contain photon energies up to about 3 GeV. For the Pb-mode at LHC energies ($\gamma = 2750$) photons appear with energies up to about 80 GeV contained in the electromagnetic fields. Even larger photon energies of about 180 GeV might be reached in a Ca beam at LHC energies ($\gamma = 3750$). Hence, the fusion of two high-energy equivalent photons can lead to the production of exotic elementary particle states which have masses up to about 5 GeV (RHIC), 150 GeV (LHC, Pb-mode) and 300 GeV (LHC, Ca-mode), respectively. Those particles are as heavy as the heavy nuclei themselves.
Due to the coherence effect of the strong Lorentz contracted electromagnetic fields of the charged heavy ions the particle production cross section is proportional to Z^4. Considering Pb-Pb collisions, this immediately leads to an enhancement factor of 10^7 in the particle cross sections in comparison to e^+e^- collisions.
The idea to produce such exotic particles via two-photon fusion processes has been suggested in Ref. [67]. Since then several authors have contributed, we list their references in connection with the specific

particles considered: $\mu^{\pm}$–leptons [131, 69, 34, 32, 26, 67, 13], $\tau^{\pm}$–leptons [131, 69, 32, 67, 13], light mesons (π^0, $\pi^{\pm}$, η, η', $K^{\pm}$, ...) [69, 24, 23, 67, 94], heavy mesons (η_c, χ_c, η_b) [131, 24, 20, 23, 67, 94], glueballs [69, 95], c and b quarks [131, 65], $W^{\pm}$–bosons [138, 99, 100, 67], Standard Model Higgs bosons [69, 138, 33, 34, 101, 49, 37, 96, 5, 6, 14, 92, 68, 99, 100, 67], Higgs bosons from the Minimal Supersymmetric Extension of the Standard Model [69, 99], supersymmetric particles [69, 100, 108], and even magnetic monopoles [80].

Two–photon fusion processes are of course not the only photon induced processes to occur in peripheral heavy–ion collisions. A photon from one of the equivalent photon swarms can also directly interact with the other nucleus. This leads to the Coulomb dissociation of the latter as it emits one or several nucleons or even disintegrates. This process represents a major contribution to the beam loss, which limits the collider luminosity. The Coulomb dissociation cross section has been calculated in Refs. [23, 19, 132] for the Pb–mode at LHC, in [35] for the Ca–mode at LHC and in [109, 130] for the Au–Au collisions at RHIC.

As a very hard photon from one equivalent swarm of photons penetrates into the other nucleus it is able to resolve the partonic structure of the nucleus and to interact with the quarks and gluons. Photon–gluon fusion leads to the production of a quark pair. In the case of b–quarks this process represents the main background for the two–photon production of an intermediate–mass Higgs boson [79]. Since the open flavors fragment into mesons this process also contributes to the production of exotic mesons, maybe even unexpected heavy mesons.

The production of heavy-quark pairs by photon-gluon fusion can also be used to extract informations about the gluon distribution function of a bound nucleon inside a nucleus, i.e. in a nuclear medium [79, 72, 19]. This contributes to a better understanding of the EMC effect.

Another possibility to hunt for exotic particles can be performed in central ultrarelativistic heavy–ion collisions. In case of Pb-Pb collisions we have to deal with 208 nucleons impinging on about 208 nucleons. If the quarks as individual constituents are considered, we are confrontated with a collision scenario of 624 quarks on 624 quarks, still without counting the other partons, e.g. gluons and sea quarks. A simple geometric estimate leads to the number of single nucleon-nucleon collisions as $A^{4/3}$, i.e. about 1230 for a Pb-Pb collision. This means that Pb-Pb collisions are favoured by about three orders of magnitude compared to pp collisions. But on the other hand the expected c.m. energy and the expected luminosity in pp collisions are by a factor 2.5 and by about seven orders of magnitude, respectively, larger than in Pb-Pb collisions. As a result, particle production rates in central collisions seem to be smaller by about four orders of magnitude compared to pp collisions. For the collision of Ca on Ca only two orders of magnitude difference appear. But one might ask whether coherent and collective effects may contribute to particle production. The cooperative interactions of many constituents could provide sufficient energy to produce heavy particles even if there is not enough energy to produce this particle in a single parton-parton collision [120]. For example, the production of Higgs bosons in central ultrarelativistic heavy-ion collisions has discussed in a nuclear density build-up [56]; however, the production rates even seem to be rather small.

This review intends to summarize a wide range of "Non Quark Gluon Plasma" aspects in relativistic heavy–ion collisions. In section 2 we provide an introduction into the foundation of the Equivalent Photon Approximation. First a derivation from classical electrodynamics is given. But also an exhaustive justification from QED is presented. We also give a detailled derivation of the Equivalent Photon cross section for two–photon fusion into a charged boson pair, which shows the relevant approximations to be taken in a very illustrative way. Section 3 is devoted to applications of the equivalent photon approximation to two photon–photon fusion processes in relativistic heavy–ion collisions. The electromagnetic production of mesons, leptons, quarks, supersymmetric particles and Higgs–bosons is considered. The Coulomb dissociation represents the opener of Section 4 on "Single Photon Processes". Some emphasis is put on photon–gluon processes, which help to deduce the gluon distribution in a nuclear medium. Section 5 reviews some aspects of the production of exotic particles in central collisions. Some future investigations are outlined in Section 6, which constitutes the Conclusions.

Chapter 2

Equivalent Photon Approximation

A nucleus moving at nearly the speed of light has almost transverse electromagnetic fields; the electric and magnetic fields have the same absolute value and are perpendicular to each other. Therefore an observer can not distinguish between these transverse electromagnetic fields and an equivalent swarm of photons, see Fig.2.1 Equating the energy flux of the electromagnetic fields through a transverse plane with the energy content of the equivalent photon swarm yields the equivalent photon distribution $n(\omega)$, which tells how many photons with frequency ω do occur. This derivation is presented in the first Subsection.

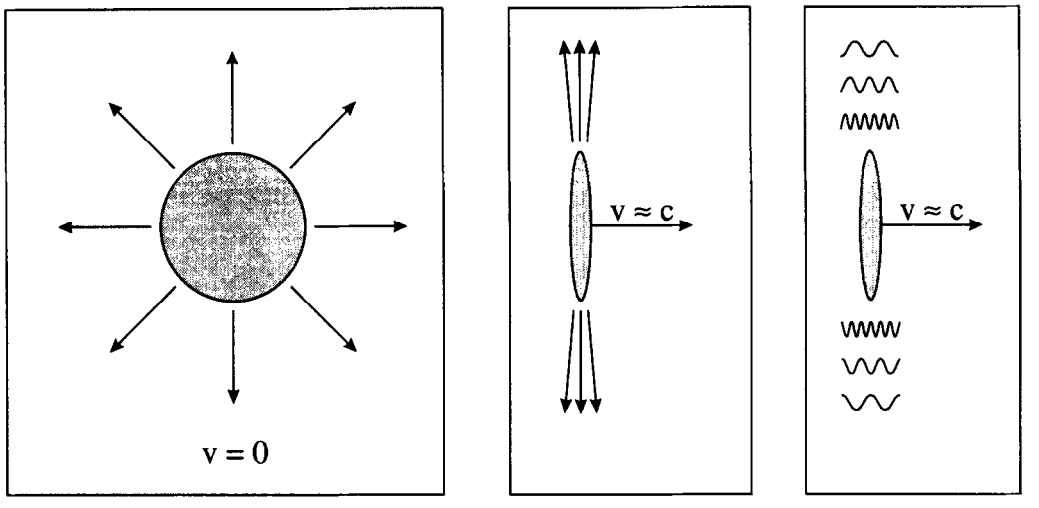

Figure 2.1: Fermis idea leading to the Equivalent Photon Approximation: As the velocity of the charge approaches the speed of light, its electromagnetic field becomes Lorentz–contracted (b) and similar to a parallel–moving photon–cloud (c).

This is already the idea of the *Equivalent Photon Approximation.* It has been first developed by E. Fermi [57]. Often this method is also called *Weizsäcker–Williams–Method* as E. J. Williams [135] and C. F. v. Weizsäcker [134] independently extended Fermis idea. A good review of results and various

applications of the *Equivalent Photon Approximation* can be found in the articles of C. A. Bertulani and G. Baur [28] and of J. Eichler [52]; we will solely concentrate on applications in (ultra-) relativistic heavy-ion collisions.
Given now the classical equivalent photon distribution, it is straightforward to estimate, for example, the electromagnetic production cross section of particles in a heavy-ion collision in the following way:

$$\sigma^{\mathrm{EPA}}_{A_1A_2\to A_1A_2X} = \int \mathrm{d}\omega_1 \int \mathrm{d}\omega_2 \; n_1(\omega_1)\, n_2(\omega_2)\, \sigma_{\gamma\gamma\to X}(\omega_1,\omega_2) \quad ; \tag{2.1}$$

two photons steming from the two colliding swarms of equivalent photons fuse to produce the particle X. $\sigma_{\gamma\gamma\to X}$ represents the elementary two-photon fusion cross section. The cross section (2.1) is called the equivalent photon cross section. However, some caution has to be taken; the following points have to be clarified in detail:
The exotic particles we are interested in have masses, which come close to the maximum frequencies contained in the electromagnetic fields; therefore they will be produced, where the electromagnetic interaction energy is largest. That occurs at small impact parameters in the vicinity of the nuclear surfaces. On the other hand, central collisions have to be excluded in order to have a rather clean experimental trigger on peripheral collisions. Naturally the question arises, how much do small impact parameters contribute to the total equivalent photon cross section (2.1)? – The equivalent photon cross section (2.1) consists of a quantum mechanical part ($\sigma_{\gamma\gamma\to X}$) and a classical part ($n_1n_2$). It is not clear, how good this ansatz approximates the full quantum mechanical cross section $\sigma_{A_1A_2\to A_1A_2X}$? – Therefore there is a need to derive the equivalent photon cross section directly from QED and to generalize this method to include an impact parameter dependence and quantum effects! This will be done in Subsections 2.2 and 2.3.

2.1 Classical equivalent photon distribution

In order to determine the classical equivalent photon distribution $n(\omega)$ we first calculate the electromagnetic field of a charge distribution moving with $v \approx c$ on a straight trajectory; see Fig. 2.1. In the observers system K the inhomogeneous wave equation for the electromagnetic vector–potential in Lorentz gauge reads

$$\partial_\mu\partial^\mu A^\nu(x) = j^\nu(x) \quad ; \tag{2.2}$$

note that here Heaviside-Lorentz units have been chosen. In the reference system K' of the moving charge the current–density is

$$j'^\nu(x') = \rho(\vec{x}')\, u'^\nu = \rho(|\vec{x}'|)\, u'^\nu \quad , \tag{2.3}$$

where $u'^\nu = (1,0,0,0)$ is the four–velocity of the spherical symmetric charge distribution. The Fourier transformed current–density results as

$$j'^\nu(k') = \int\limits_{-\infty}^{\infty} d^4x'\, e^{ik'x'}\, j'^\nu(x') = 2\pi\, \delta(\omega')\, \rho(|\vec{k}'|)\cdot u'^\nu = 2\pi\, \delta(k'\cdot u')\, \rho(\sqrt{-k'^2})\cdot u'^\nu \tag{2.4}$$

with $k'^\nu = (\omega', \vec{k}')$. This result is written in a covariant way; consequently, we can drop the primes and switch back to the observer system. Here $u^\nu = \gamma(1,0,0,v)$ and $k^\nu = (\omega, \vec{k})$, where we have chosen the z–axis as the direction of the Lorentz–boost γ between the two systems.
We use (2.4) to solve the equation for the vector–potential. Fourier transformation of (2.2) yields

$$A^\nu(k) = -\frac{1}{k^2} j^\nu(k) = -2\pi\, \delta(k\cdot u)\, \frac{\rho(\sqrt{-k^2})}{k^2}\, u^\nu = Z\, r(k)\, u^\nu \,, \tag{2.5}$$

where we have introduced the abbreviation

$$r(k) = \frac{1}{Z}(-2\pi)\, \delta(k\cdot u)\, \frac{\rho(\sqrt{-k^2})}{k^2} = -2\pi\, e\, \delta(k\cdot u)\, \frac{F(-k^2)}{k^2} \,, \tag{2.6}$$

with the normalized elastic nuclear charge formfactor $F(-k^2) = \rho(-k^2)/Ze$ and the nuclear charge number Z. The delta function enforces the validity of the Lorentz-gauge $k_\nu A^\nu = 0$ and the transversality of the photons. Furthermore, we deduce, that

$$\gamma(\omega - vk_z) = 0 \quad , \tag{2.7}$$

which leads to

$$k^2 = \omega^2 - k_z^2 - \vec{k}_\perp^2 = -\left(\frac{\omega}{v\gamma}\right)^2 - \vec{k}_\perp^2 \approx -\left(\frac{\omega}{\gamma}\right)^2 - \vec{k}_\perp^2 \quad ; \tag{2.8}$$

the last step holds in the limit $v \approx c = 1$. The subscript $\perp$ labels the transverse components of a vector, in this case the x- and y-components.
Now we can calculate the components of the electromagnetic field-strength tensor $F^{\mu\nu}$. Its Fourier transform is given by

$$F^{\mu\nu}(k) = -i(k^\mu A^\nu(k) - k^\nu A^\mu(k)) \quad . \tag{2.9}$$

As $\vec{u}_\perp = \vec{A}_\perp(k) = 0$, the transverse components of the electric and magnetic field read

$$\begin{aligned} \vec{E}_\perp(k) &= -i\,A^0(k)\,\vec{k}_\perp \\ \vec{B}_\perp(k) &= \vec{v} \times \vec{E}_\perp(k) = -ivA^0(k)(-k_y, k_x, 0)^T \quad . \end{aligned} \tag{2.10}$$

The longitudinal components of the field strengths vanish in the limit $v \to c = 1$ [82]. In this limit the following relations hold as well:

$$|\vec{E}| = |\vec{B}|, \quad \vec{E} \perp \vec{B}, \quad \vec{E} \perp \vec{v} \quad \text{and} \quad \vec{B} \perp \vec{v} \quad . \tag{2.11}$$

This justifies the idea of the *Equivalent Photon Approximation* to interpret this electromagnetic field as an equivalent swarm of photons.
To extract the equivalent photon spectrum $n(\omega)$, which depends on the photon frequency ω, we have to consider the energy flux of the electromagnetic field through a plane perpendicular to the direction of the moving charge distribution. The flux of the fields is provided by the Poynting vector

$$\vec{S}(\vec{r},t) = \vec{E}(\vec{r},t) \times \vec{B}(\vec{r},t) \xrightarrow{v \to c} |\vec{E}(\vec{r},t)|^2\,\vec{v}. \tag{2.12}$$

The last step holds due to the relations (2.10) and (2.11). Of course the Poynting vector points in the direction of the charges' velocity. Now we require that the energy flux of the fields through a transverse plane is identical to the energy flux of the equivalent photons:

$$\int_{-\infty}^{\infty} dt \int d\vec{x}_\perp \cdot \vec{S}(\vec{r},t) \stackrel{!}{=} \int_0^\infty d\omega\, \omega \cdot n(\omega) \tag{2.13}$$

A partial Fourier transformation of $\vec{E}(\vec{k},\omega)$ in z-direction,

$$\begin{aligned} \vec{E}(z,\vec{k}_\perp,\omega) &= \int_{-\infty}^{\infty} \frac{dk_z}{2\pi} e^{ik_z z}\, \vec{E}_\perp(k_\perp,\omega) \\ &= 2\pi i\gamma(Ze)\,\vec{k}_\perp \cdot \int_{-\infty}^{\infty} \frac{dk_z}{2\pi}\, e^{ik_z z}\, \frac{F(-k^2)}{k^2}\, \delta(k \cdot u) \\ &= (Ze)\frac{-i\vec{k}_\perp}{v}\, e^{i\omega z/v} \cdot \frac{F\left(\left(\frac{\omega}{v\gamma}\right)^2 + \vec{k}_\perp^2\right)}{\left(\frac{\omega}{v\gamma}\right)^2 + \vec{k}_\perp^2} \quad , \end{aligned} \tag{2.14}$$

leads to

$$|\vec{E}_\perp(z,\vec{k}_\perp,\omega)|^2 = (Ze)^2\frac{\vec{k}_\perp^2}{v^2}\left[\frac{F\left(\left(\frac{\omega}{v\gamma}\right)^2+\vec{k}_\perp^2\right)}{\left(\frac{\omega}{v\gamma}\right)^2+\vec{k}_\perp^2}\right]^2 \approx (Ze)^2\left[\frac{F\left(\left(\frac{\omega}{\gamma}\right)^2+\vec{k}_\perp^2\right)}{\left(\frac{\omega}{\gamma}\right)^2+\vec{k}_\perp^2}\right]^2\vec{k}_\perp^2 \quad . \tag{2.15}$$

Performing again a Fourier transformation with respect to the time coordinate in (2.13) and using the obvious identity $|\vec{E}_\perp(z,\vec{k}_\perp,\omega)|^2 = |\vec{E}_\perp(z,\vec{k}_\perp,-\omega)|^2$ the photon spectrum is follows as

$$\begin{aligned} n(\omega) &= \frac{1}{\pi\omega}\int d\vec{x}_\perp|\vec{E}_\perp(\vec{r},\omega)|^2 = \frac{1}{\pi\omega}\int_0^\infty\frac{d^2k_\perp}{(2\pi)^2}\cdot|\vec{E}_\perp(z,\vec{k}_\perp,\omega)|^2 \\ &= \frac{(Ze)^2}{\pi\omega}\int_0^\infty\frac{d^2k_\perp}{(2\pi)^2}\left[\frac{F\left(\left(\frac{\omega}{\gamma}\right)^2+\vec{k}_\perp^2\right)}{\left(\frac{\omega}{\gamma}\right)^2+\vec{k}_\perp^2}\right]^2\vec{k}_\perp^2 \quad , \end{aligned} \tag{2.16}$$

where Parsevals identity has been used. Finally, we change to a new integration variable,

$$\kappa^2 = -k^2 = \left(\frac{\omega}{\gamma}\right)^2+\vec{k}_\perp^2 \quad , \tag{2.17}$$

and obtain

$$n(\omega) = \frac{2\alpha_{\rm QED}Z^2}{\pi\omega}\int_{\omega/\gamma}^\infty d\kappa\,\frac{\kappa^2-\left(\frac{\omega}{\gamma}\right)^2}{\kappa^3}\cdot F^2(\kappa^2) \quad . \tag{2.18}$$

Notice again, that this expression only holds in the limit $v \to c$, where the longitudinal components of the electromagnetic field can be neglected. Notice also, that the photon spectrum depends quadratically on the nuclear charge number Z. Due to this fact the cross section (2.1) for elastic two-photon production scales with Z^4.

We will use three different form factors: one for a homogeneously charged sphere labelled by the subscript *hcs* [125, 67, 119], one gaussian-shaped with subscript *gauss* [125, 49] and a point-like one with subscript *pt* [125, 37, 24]. They are given by

$$\begin{aligned} F_{\rm hcs}(k^2) &= 3\cdot\frac{j_1(kR)}{kR} \quad , \\ F_{\rm gauss}(k^2) &= \exp\left(\frac{k^2}{2Q_0^2}\right) \quad , \\ F_{\rm pt}(k^2) &= 1 \quad , \end{aligned} \tag{2.19}$$

respectively. R represents the radius of the nucleus, Q_0 is a fit parameter to the nuclear shape and j_1 denotes a spherical Bessel function. The formfactors are depicted in Fig. 2.2.

The maximum photon energy ω_0 contained in the swarm of equivalent photons can be estimated by the uncertainty principle as the inverse of the Lorentz-contracted nuclear radius:

$$\omega_0 = \frac{\gamma}{R} \quad . \tag{2.20}$$

With the substitution $z = \kappa R$ Eq. (2.18) can be cast into ($v \approx 1$)

$$\begin{aligned} n(\omega) &= \frac{2\alpha_{QED}Z^2}{\pi\omega}\cdot f\left(\frac{\omega}{\omega_0}\right) \quad , \\ f(x) &= \int_x^\infty dz\,\frac{z^2-x^2}{z^3}\left[F\left(\frac{z^2}{R^2}\right)\right]^2 \quad . \end{aligned} \tag{2.21}$$

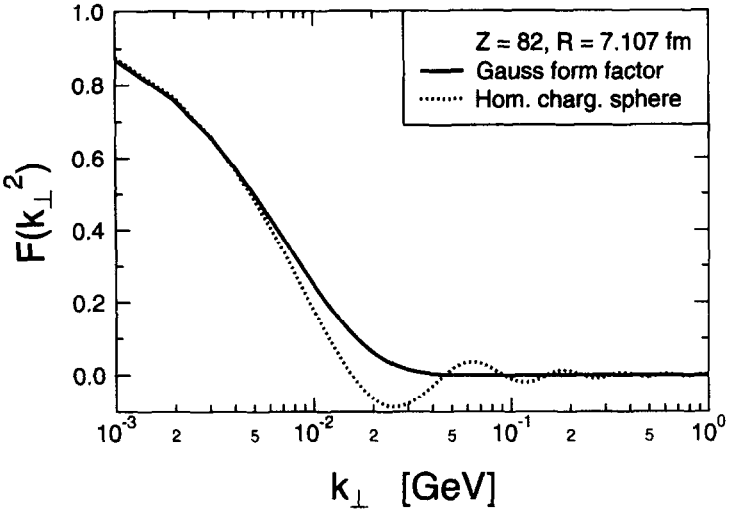

Figure 2.2: Different nuclear charge form factors for a Pb-nucleus. Already for $k_\perp = 1/R \approx 30$ MeV they converge to zero.

For the point-like form factor the integral in (2.21) diverges for large z, i.e. for large transverse momenta $k_\perp$. Hence, a cut-off $(k_\perp)_{\max} = 1/R$ is introduced, which we relate to the inverse of the nuclear radius. We arrive at

$$f_{\rm pt}(x) = \frac{1}{2}\left[\ln(1+x^{-2}) + \frac{1}{1+x^{-2}} - 1\right] \quad . \tag{2.22}$$

For a homogeneously charged sphere we obtain

$$\begin{aligned} f_{\rm hcs}(x) \;=\; & \frac{3}{16x^6} + \frac{3}{8x^4} - \cos(2x)\left[\frac{3}{16x^6} + \frac{7}{40x^2} + \frac{1}{20}\right] \\ & - \sin(2x)\left[\frac{3}{8x^5} + \frac{1}{10x^3} - \frac{9}{20x} - \frac{x}{10}\right] - \mathrm{Ci}(2x)\left(1 + \frac{x^5}{5}\right) \end{aligned} \tag{2.23}$$

with the integral-cosine

$$\mathrm{Ci}(x) = -\int_x^\infty dt\, \frac{\cos t}{t} \quad . \tag{2.24}$$

For a Gaussian shaped nucleus we find

$$f_{\rm gauss}(x) = \frac{1}{2}\left(1 + \frac{x^2}{Q_0^2 R^2}\right) \mathrm{E}_1\left(\frac{x^2}{Q_0^2 R^2}\right) - \frac{1}{2}\exp\left(-\frac{x^2}{Q_0^2 R^2}\right) \tag{2.25}$$

with

$$\mathrm{E}_1(x) = \int_x^\infty dt\, \frac{e^{-t}}{t} \quad . \tag{2.26}$$

The photon spectra for the different form factors are displayed in Fig. 2.3. We realize that except for the point-like form factor the different form factors do not modify the photon spectra for $\omega < \omega_0$. Only for $\omega > \omega_0$ some minor differences occur between the equivalent photon distribution with the Gaussian form factor and the form factor of a homogeneously charged sphere.

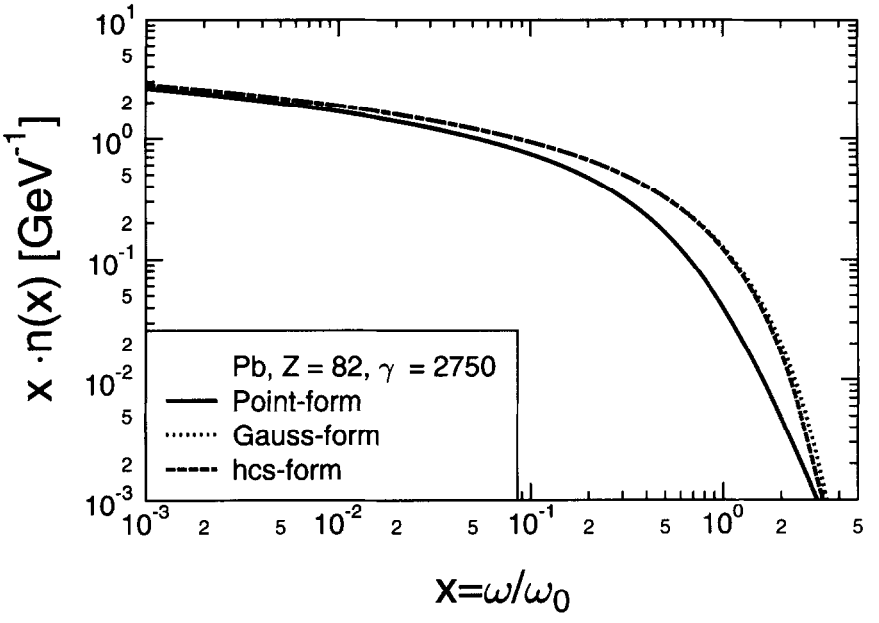

Figure 2.3: Equivalent photon distributions for different charge form factors of a Pb nucleus.

2.2 Impact–parameter dependence

The classical equivalent photon distribution $n(\omega)$ tells us how many photons with frequency ω are contained in the equivalent swarm of photons simulating the strong transverse electromagnetic fields of a charged nucleus moving with nearly the speed of light. However, we have no information on how many photons with a given frequency do occur at a certain transverse distance from the straight trajectory of the nucleus. We have lost this information because in the identification (2.13) an integration over the whole transverse plane has been performed on the left hand side. We can recover this information once we generalize (2.13) to

$$\int_{-\infty}^{\infty} \mathrm{d}t \int \mathrm{d}\vec{x_\perp} \cdot \vec{S}(\vec{r},t) \stackrel{!}{=} \int_0^{\infty} \mathrm{d}\omega \int \mathrm{d}\vec{x_\perp}\, \omega\, n(\omega, \vec{x_\perp}) \tag{2.27}$$

and consider the energy flux through an infinitesimal element $\mathrm{d}\vec{x_\perp}$ of the transverse plane instead of the full transverse plane. We get:

$$\begin{aligned} n(\omega,\vec{x}_\perp) &= \frac{1}{\pi\omega}\left|\vec{E}_\perp(\omega,\vec{x}_\perp)\right|^2 \\ &= \frac{4Z^2\alpha_{QED}}{\omega}\left|\int \frac{d^2\vec{k}_\perp}{(2\pi)^2}\vec{k}_\perp \frac{F\left(\vec{k}_\perp^2+\left(\frac{\omega}{\gamma}\right)^2\right)}{\vec{k}_\perp^2+\left(\frac{\omega}{\gamma}\right)^2} e^{i\vec{x}_\perp\cdot\vec{k}_\perp}\right|^2 \\ &= \frac{Z^2\alpha_{QED}}{\pi^2\omega}\left|\int_0^{\infty} dk_\perp\, k_\perp^2 \frac{F\left({k_\perp}^2+\left(\frac{\omega}{\gamma}\right)^2\right)}{{k_\perp}^2+\left(\frac{\omega}{\gamma}\right)^2} J_1(x_\perp k_\perp)\right|^2 , \end{aligned} \tag{2.28}$$

where J_1 is a Bessel function. The form factors (2.19) approach fast enough zero for the $k_\perp \to \infty$ asymptotics, so that the integral (2.28) converges. For extended nuclei the integral has to be calculated numerically, but for a point-like nucleus the photon distribution can be expressed in closed form:

$$\begin{aligned} n_{\rm pt}(\omega, x_\perp) &= \frac{Z^2\alpha_{QED}\omega}{\pi^2\gamma^2}\left[K_1\left(\frac{\omega x_\perp}{\gamma}\right)^2\right]^2 \\ &\to \frac{Z^2\alpha_{QED}}{2\pi\gamma x_\perp}\exp\left(\frac{2\omega x_\perp}{\gamma}\right) \qquad \text{for } \frac{\omega x_\perp}{\gamma} \to \infty \\ &\to \frac{Z^2\alpha_{QED}}{\pi^2\omega x_\perp^2} \qquad \text{for } \frac{\omega x_\perp}{\gamma} \to 0 \ . \end{aligned} \tag{2.29}$$

In Fig. 2.4 we depict the impact-parameter dependent photon distribution for different form factors and different values of ω in dependence on the transverse distance $x_\perp$.

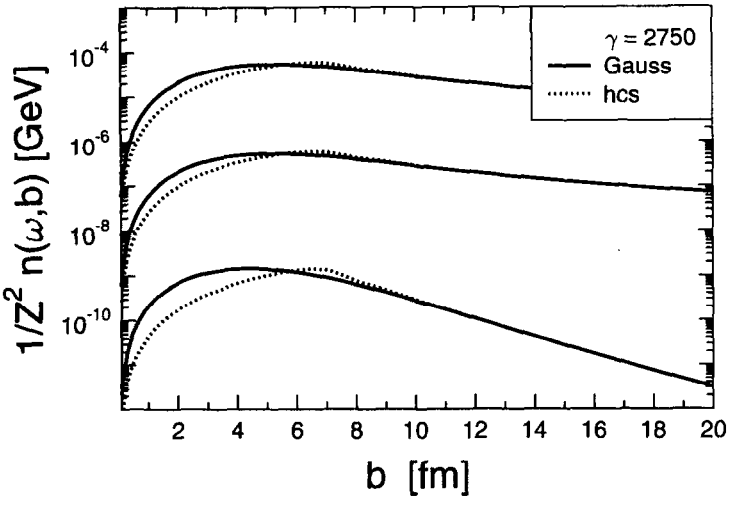

Figure 2.4: Impact-parameter dependent equivalent photon distribution $n(\omega, b)$ for different charge formfactors of a Pb nucleus. From top to bottom the photon energies are $\omega = 10$ MeV, $\omega = 1$ GeV and $\omega = 100$ GeV.

With the expression for the impact-parameter dependent equivalent photon distribution given in Eq. (2.28) we are tempted to generalize the electromagnetic production cross section (2.1) in a heavy-ion collision to

$$\sigma^{\rm EPA}_{A_1A_2\to A_1A_2X} = \int {\rm d}\omega_1 \int {\rm d}\omega_2 \int {\rm d}^2b \int {\rm d}^2\vec{x_\perp}\ n(\omega_1, \vec{x_\perp} - \vec{b})\, n(\omega_2, \vec{x_\perp})\, \sigma_{\gamma\gamma\to X}(\omega_1, \omega_2)\,, \tag{2.30}$$

which would allow us to introduce further cuts on the impact parameter $\vec{b}$ in order to discard central or semi-central collisions and to concentrate on the peripheral collisions with no hadronic background. It turns out that the expression (2.30) is not correct because it neglects polarization effects for the interaction of the two photons. Hence, a solid derivation is in order and this means to start the description of two-photon fusion processes in relativistic heavy-ion collisions directly from *QED*. We

will extend our previous considerations to deduce the correct impact-parameter dependence for the equivalent photon cross sections.

We will use the external field approximation, where the electromagnetic potentials are treated classically. The two nuclei are supposed to move with constant velocities on straight parallel trajectories, which have a distance $\vec{b}$. The electromagnetic potentials then follow again from $\Box A^\mu = j^\mu$:

$$\begin{aligned} A_1^\mu(k_1) &= Z\, e^{\mathrm{i}k_1\cdot b}\, r_1(k_1)\, u_1^\mu \quad , \\ A_2^\mu(k_2) &= Z\, r_2(k_2)\, u_2^\mu \quad ; \end{aligned} \tag{2.31}$$

consult Eq. (2.5). The velocities are $u_1 = \gamma(1, v, 0, 0)$ and $u_2 = \gamma(1, -v, 0, 0)$ in the collider system. The total cross section for the electromagnetic production of particles in a heavy-ion collision is given as the integral of the transition probability, which is the square of the S-matrix element, over the phase space of the outgoing produced particles and the impact parameter $\vec{b}$:

$$\begin{aligned} \sigma_{A_1A_2\to A_1A_2X} = \int \mathrm{d}^2b \left(\prod_i \int \mathrm{d}^3\tilde{p}_i\right) \Bigg| \int \frac{\mathrm{d}^4k_1}{(2\pi)^4} \int \frac{\mathrm{d}^4k_2}{(2\pi)^4} \left[A_1^\mu(k_1,\vec{b})\, \Gamma_{\mu\nu}(k_1,k_2,p_i)\, A_2^\nu(k_2)\right] \cdot \\ \cdot (2\pi)^4\, \delta^4\left(k_1 + k_2 - \sum_i p_i\right)\Bigg|^2 \end{aligned} \tag{2.32}$$

with $\mathrm{d}^3\tilde{p} = (1/2E)\mathrm{d}^3p/(2\pi)^3$ for bosons and $\mathrm{d}^3\tilde{p} = (m/E)\mathrm{d}^3p/(2\pi)^3$ for fermions; the electromagnetic potentials do enter in the S-matrix element as does the transition current $\Gamma_{\mu\nu}(2\pi)^4\delta^4(k_1 + k_2 - \sum_i p_i)$, where the δ-function guarantees energy-momentum conservation and the vertex function $\Gamma_{\mu\nu}$ describes the interaction of the two virtual photons with the produced outgoing particles. Expressions for $\Gamma_{\mu\nu}$ are given for example in Ref. [126]; for the process $\gamma\gamma \to b^+b^-$, where two photons fuse into a pair of charged bosons, see also Eq. (2.35) and Fig. 2.5.

Within the external field approximation the expression (2.32) is still exact. It is now to introduce reasonable approximations, which will lead to the equivalent photon cross section (2.1) and a correct generalisation of Eq. (2.30). It is our goal to separate the fusion process of two virtual photons into an emission process of equivalent photons and a successive fusion process of two real photons. Real photons are massless since the square of their four-momentum $k = (\omega, 0, 0, \omega)$ is zero; the first component of k represents the photon energy, whereas the last three components represent the photon momentum, which we have chosen along the z-axis. Actually the relation $k^2 = 0$ is the result of an exact cancellation of two big quantities. The four-momentum of the virtual photons $k = (\omega, \vec{k_\perp}, \omega/v)$, where v is the velocity of the moving heavy ion, is determined by the classical electromagnetic potentials. The virtual photons are not massless, since $k^2 = -\omega^2/\gamma^2 - \vec{k_\perp}^2$ as $v \to c = 1$; see Eq. (2.17). Again this relation traces back to a cancellation of two big quantities, but in this case not to exactly zero. This motivates the following assumption:

$$\mathcal{O}\left(|\vec{k_\perp}|\right) = \mathcal{O}\left(\frac{\omega}{\gamma}\right) = \frac{1}{\gamma}\mathcal{O}(\omega) = \frac{1}{\gamma}\mathcal{O}(k_\parallel) \quad ; \tag{2.33}$$

the Lorentz contraction factor $\gamma = (1 - v^2)^{-1/2}$ assumes values of several hundreds to thousands in our cases of interest (RHIC, LHC). Further support for relation (2.33) can be given from the equivalent photon distribution $n(\omega)$ itself, where the main contributions to the integral in (2.16) originate from the regime $|\vec{k_\perp}| \leq \omega/\gamma$. Applying relation (2.33), does not mean that $|\vec{k_\perp}|$ and ω/γ can simply be set equal to zero in the invariant matrix element $A_1^\mu\Gamma_{\mu\nu}A_2^\nu$; in fact, if we would do so, the invariant matrix element would vanish. This becomes clear, if we again have a closer look on the expression (2.16) for the equivalent photon distribution; the factor $|\vec{k_\perp}|^2$ has still to be extracted from the invariant matrix element appearing in (2.32)! As a consequence special care has to be taken, when applying relation (2.33) to the invariant matrix element. We indicate two derivations: The direct calculation is very intuitive, but rather tedious; details are only given for the two-photon fusion into a pair of charged bosons. The more general approach [126] makes use of gauge invariance in order to separate the emission and fusion of the two virtual photons.

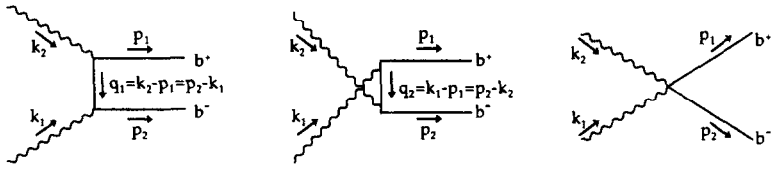

Figure 2.5: Feynman diagrams for boson-pair production by two real photons.

2.2.1 Derivation of the equivalent photon cross section for the production of charged boson pairs

As an explicit example we discuss the two-photon fusion process into a pair of charged spin-0 bosons. At first we concentrate on the elementary fusion cross section:

$$\sigma_{\gamma\gamma\to b^+b^-} = \frac{1}{2\omega_1\omega_2} \int \frac{\mathrm{d}^3p_1}{2E_1} \int \frac{\mathrm{d}^3p_2}{2E_2} \frac{1}{4} \sum_{\epsilon_1,\epsilon_2} |\Gamma^{\mu\nu}\epsilon_{1\mu}\epsilon_{2\nu}|^2 \, \delta^4(p_1+p_2-k_1-k_2)\,, \tag{2.34}$$

where ϵ_1 and ϵ_2 are the corresponding polarisation vectors of the two photons. The notation of the four vectors are: $p_1 = (E_1, \vec{p}_1)$, $p_2 = (E_2, \vec{p}_2)$, $k_1 = (\omega_1, \omega_1, 0, 0)$ and $k_2 = (\omega_2, -\omega_2, 0, 0)$. The transition current $\Gamma^{\mu\nu}$ reflects the lowest order Feynman diagrams depicted in Figure 2.5 and is given by the expression:

$$\Gamma^{\mu\nu} = -\frac{i\,e^2}{q_1^2-m^2}(p_2^\mu+q_1^\mu)\,(q_1^\nu-p_1^\nu) - \frac{i\,e^2}{q_2^2-m^2}(q_2^\mu-p_1^\mu)(p_2^\nu+q_2^\nu) + 2\,i\,e^2\,g^{\mu\nu} \quad . \tag{2.35}$$

The polarisation vectors of the photons are fixed by $\epsilon_1 = (0, \vec{\epsilon}_1, 0)$ and $\epsilon_2 = (0, \vec{\epsilon}_2, 0)$. With

$$\sigma_{\gamma\gamma\to b^+b^-} = \frac{1}{2}\left(\sigma_{\parallel}^{\gamma\gamma\to b^+b^-} + \sigma_{\perp}^{\gamma\gamma\to b^+b^-}\right) \tag{2.36}$$

we then get for the polarisation dependent cross sections:

$$\begin{aligned}\sigma_{\parallel}^{\gamma\gamma\to b^+b^-} &= \frac{1}{2\omega_1\omega_2} \int \frac{\mathrm{d}^3p_1}{2E_1} \int \frac{\mathrm{d}^3p_2}{2E_2}\, \delta^4(p_1+p_2-k_1-k_2)\, \frac{2\,e^4}{(k_1\cdot p_1)^2(k_2\cdot p_1)^2} \\ &\times \Big\{2\,(k_1\cdot p_1)^2(k_2\cdot p_1)^2 - 2\,(k_1\cdot p_1)(k_2\cdot p_1)\,[(k_1\cdot p_1)+(k_2\cdot p_1)]\,\vec{p}_{1\perp}^{\,2} \\ &+\Big[(k_1\cdot p_1)+(k_2\cdot p_1)\Big]^2 (p_{1x}^4+p_{1y}^4)\Big\}\end{aligned} \tag{2.37}$$

and

$$\begin{aligned}\sigma_{\perp}^{\gamma\gamma\to b^+b^-} &= \frac{1}{2\omega_1\omega_2} \int \frac{\mathrm{d}^3p_1}{2E_1} \int \frac{\mathrm{d}^3p_2}{2E_2}\, \delta^4(p_1+p_2-k_1-k_2) \\ &\times \frac{4\,e^4}{(k_1\cdot p_1)^2(k_2\cdot p_1)^2}\,\Big[(k_1\cdot p_1)+(k_2\cdot p_1)\Big]^2 p_{1x}^2\, p_{1y}^2\,,\end{aligned} \tag{2.38}$$

where $\parallel$ symbolizes that the polarisation vectors of the two incoming photons are parallel to each other whereas $\perp$ stands for the orthogonality of the polarisation vectors. Carrying out the integrations finally leads to the two-photon fusion cross sections stated in Section 3.1. The expressions (2.37) and (2.38) are of tremendous use to derive the correct impact-parameter dependent generalization of the equivalent photon approach.

Within the external field approximation the total production cross section (2.32) for a boson pair becomes

$$\begin{aligned}\sigma_{A_1A_2\to b^+b^-} &= (2\pi)^2 Z^4 \int \mathrm{d}^2b \int \frac{\mathrm{d}^3p_1}{2E_1} \int \frac{\mathrm{d}^3p_2}{2E_2} \\ &\times \left| \int \frac{\mathrm{d}^4k_1}{(2\pi)^4}\, r_1(k_1)\, e^{i k_1\cdot b} \int \frac{\mathrm{d}^4k_2}{(2\pi)^4}\, r_2(k_2)\, \delta^4(p_1+p_2-k_1-k_2)\, \Gamma^{\mu\nu}(k_i,p_i)\, u_{1\mu}\, u_{2\nu} \right|^2\end{aligned} \tag{2.39}$$

Note the similiarity of the invariant matrix element $\Gamma^{\mu\nu}\, u_{1\mu}\, u_{2\nu}$ with the one in (2.34), where the only difference is the replacement $\epsilon \leftrightarrow u$. From the 12 δ-functions in the expression (2.39) it follows that $\omega_i = \omega_i'$ and $k_{iz} = k_{iz}'$, where the primed quantities result from the square in (2.39). If we were to carry out the integration over the impact parameter, an additional two-dimensional δ-functions $\delta(\vec{k}_{1\perp} - \vec{k}_{1\perp}')$ would show up, which would lead to $k_1 = k_1'$ and $k_2 = k_2'$. But we will not integrate over d^2b; instead we go on integrating over d^4k_2', $\mathrm{d}\omega_1'$, $\mathrm{d}k_{1z}'$, $\mathrm{d}k_{1z}$ and $\mathrm{d}k_{2z}$. Introducing the new integration variable $q = (0, 0, \vec{q}_\perp) = k_1 - k_1' = k_2' - k_2$ the cross section (2.39) then reads:

$$\begin{aligned}
\sigma_{A_1A_2\to b+b-} &= \frac{8\, Z^4\, e^4}{v^3\, \gamma^4} \int \mathrm{d}^2b \int \mathrm{d}\omega_1 \int \mathrm{d}\omega_2 \int \frac{\mathrm{d}^2k_{1\perp}}{(2\pi)^2} \int \frac{\mathrm{d}^2k_{2\perp}}{(2\pi)^2} \int \frac{\mathrm{d}^2q}{(2\pi)^2}\, e^{-i\vec{q}\cdot\vec{b}} \\
&\times \frac{F(-k_1^2)}{k_1^2} \frac{F(-(k_1-q)^2)}{(k_1-q)^2} \frac{F(-k_2^2)}{k_2^2} \frac{F(-(k_2-q)^2)}{(k_2-q)^2} \\
&\times \int \frac{\mathrm{d}^3p_1}{2\,E_1} \int \frac{\mathrm{d}^3p_2}{2\,E_2} \left[(\Gamma^{\mu\nu}(k_i,p_i)\, u_{1\mu}\, u_{2\nu})\, (\Gamma^{\mu\nu *}(k_i',p_i)\, u_{1\mu}\, u_{2\nu}) \right] \delta^4(p_1 + p_2 - k_1 - k_2)
\end{aligned} \tag{2.40}$$

with $k_1 = (\omega_1, \omega_1/v, \vec{k}_{1\perp})$, $k_2 = (\omega_2, -\omega_2/v, \vec{k}_{2\perp})$, $k_1' = (\omega_1, \omega_1/v, \vec{k}_{1\perp} - \vec{q}_\perp)$ and $k_2' = (\omega_2, \omega_2/v, \vec{k}_{2\perp} + \vec{q}_\perp)$. Since we do not deal with real photons, the square of the photon momenta are not equal to zero but for example $-k_1^2 = \omega_1/(v^2\gamma^2) + \vec{k}_{1\perp}^2$. This form of the cross section is especially suited for the derivation of the impact-parameter dependent equivalent photon cross section.

Let us now again turn our attention to the reduced invariant matrix element of eq. (2.39), which can be rewritten as

$$\Gamma^{\mu\nu}(k_i,p_i)\, u_{1\mu}\, u_{2\nu} = 2\, i\, e^2 \left\{ 2\, \frac{(p_2\cdot u_1)\,(p_1\cdot u_2)}{k_2^2 - 2(k_2\cdot p_1)} + 2\, \frac{(p_2\cdot u_2)\,(p_1\cdot u_1)}{k_1^2 - 2(k_1\cdot p_1)} + (u_1\cdot u_2) \right\}. \tag{2.41}$$

It is then most convenient to rewrite the scalar products including the four-velocities as

$$\begin{aligned}
(p_2\cdot u_1) &= \gamma\,(E_2 - v p_{2z}) = \gamma\,[E_2 - p_{2z} + (1-v)p_{2z}] \\
&= \frac{\gamma}{\omega_1} \left[(k_1\cdot p_2) + \frac{\omega_1 p_{2z}}{v\gamma^2} + \vec{k}_{1\perp}\cdot\vec{p}_{2\perp} \right].
\end{aligned} \tag{2.42}$$

Analogously it follows that

$$\begin{aligned}
(p_1\cdot u_2) &= \frac{\gamma}{\omega_2} \left[(k_2\cdot p_1) - \frac{\omega_2 p_{1z}}{v\gamma^2} + \vec{k}_{2\perp}\cdot\vec{p}_{1\perp} \right], \\
(p_2\cdot u_2) &= \frac{\gamma}{\omega_2} \left[(k_2\cdot p_2) - \frac{\omega_2 p_{2z}}{v\gamma^2} + \vec{k}_{2\perp}\cdot\vec{p}_{2\perp} \right], \\
(p_1\cdot u_1) &= \frac{\gamma}{\omega_1} \left[(k_1\cdot p_1) + \frac{\omega_1 p_{1z}}{v\gamma^2} + \vec{k}_{1\perp}\cdot\vec{p}_{1\perp} \right], \\
(u_1\cdot u_2) &= \frac{\gamma^2}{\omega_1\omega_2} \left[(k_1\cdot k_2) - \frac{1+v^2}{v^2\gamma^2}\omega_1\omega_2 + \vec{k}_{1\perp}\cdot\vec{k}_{2\perp} \right].
\end{aligned} \tag{2.43}$$

Furthermore, noting that $k_i^2 \ll (k_i\cdot p_1)$, the denominators appearing in eq. (2.41) can be transformed into

$$\frac{1}{k_i^2 - 2(k_i\cdot p_1)} = \frac{(-1)}{2(k_i\cdot p_1)} \left[1 + \frac{k_i^2}{2(k_i\cdot p_1)} + \mathcal{O}\left(\frac{1}{\gamma^4}\right) \right]. \tag{2.44}$$

We go on inserting all Eqs. (2.42)–(2.44) into Eq. (2.41). Keeping all terms up to the order $[\omega^6/\gamma^2] = [\omega^4\vec{k}_\perp^2]$ yields for the reduced invariant matrix element:

$$\begin{aligned}
\Gamma^{\mu\nu}(k_i,p_i)\, u_{1\mu}\, u_{2\nu} \approx\ & \frac{\gamma^2}{\omega_1\omega_2} \frac{-2ie^2}{(k_1\cdot p_1)\,(k_2\cdot p_1)} \Big\{ (k_1\cdot p_1)\,(k_2\cdot p_1) \left[\vec{k}_{1\perp}\cdot\vec{k}_{2\perp} \right] \\
& - \left[(k_1\cdot p_1) + (k_2\cdot p_1) \right] (\vec{k}_{1\perp}\cdot\vec{p}_{1\perp})\,(\vec{k}_{2\perp}\cdot\vec{p}_{1\perp}) \Big\}.
\end{aligned} \tag{2.45}$$

Taking the square as in (2.40) yields

$$
\begin{aligned}
&(\Gamma^{\mu\nu}(k_i,p_i)\,u_{1\mu}\,u_{2\nu})(\Gamma^{\mu\nu *}(k_i',p_i)\,u_{1\mu}\,u_{2\nu}) \;=\\
&\frac{\gamma^4}{\omega_1^2\omega_2^2}\,\frac{4\,e^4}{(k_1\cdot p_1)^2\,(k_2\cdot p_1)^2}\\
&\times\Big\{(k_1\cdot p_1)\,(k_2\cdot p_1)\,\Big[\vec{k}_{1\perp}\cdot\vec{k}_{2\perp}\Big]-\Big[(k_1\cdot p_1)+(k_2\cdot p_1)\Big]\,\Big[(\vec{k}_{1\perp}\cdot\vec{p}_{1\perp})\,(\vec{k}_{2\perp}\cdot\vec{p}_{1\perp})\Big]\Big\}\\
&\times\Big\{(k_1\cdot p_1)\,(k_2\cdot p_1)\,\Big[(\vec{k}_{1\perp}-\vec{q})\cdot(\vec{k}_{2\perp}+\vec{q})\Big]\\
&\quad-\Big[(k_1\cdot p_1)+(k_2\cdot p_1)\Big]\,\Big[((\vec{k}_{1\perp}-\vec{q})\cdot\vec{p}_{1\perp})\,((\vec{k}_{2\perp}+\vec{q})\cdot\vec{p}_{1\perp})\Big]\Big\}\;,
\end{aligned}
\tag{2.46}
$$

where we have employed $(k_1\cdot p_1)\approx(k_1'\cdot p_1)\approx\omega_1E_1-\omega_1p_{1z}$ and $(k_2\cdot p_1)\approx(k_2'\cdot p_1)\approx\omega_1E_1+\omega_1p_{1z}$. We employ the substitutions

$$
\begin{aligned}
&\Big[\vec{k}_{1\perp}\cdot\vec{k}_{2\perp}\Big]\Big[((\vec{k}_{1\perp}-\vec{q})\cdot\vec{p}_{1\perp})\,((\vec{k}_{2\perp}+\vec{q})\cdot\vec{p}_{1\perp})\Big]+\Big[(\vec{k}_{1\perp}-\vec{q})\cdot(\vec{k}_{2\perp}+\vec{q})\Big]\Big[(\vec{k}_{1\perp}\cdot\vec{p}_{1\perp})\,(\vec{k}_{2\perp}\cdot\vec{p}_{1\perp})\Big]\\
&\qquad\longrightarrow\;2\,\Big[\vec{k}_{1\perp}\cdot\vec{k}_{2\perp}\Big]\Big[(\vec{k}_{1\perp}-\vec{q})\cdot(\vec{k}_{2\perp}+\vec{q})\Big]\,p_{1x}^2
\end{aligned}
\tag{2.47}
$$

and

$$
\begin{aligned}
&\Big[(\vec{k}_{1\perp}\cdot\vec{p}_{1\perp})\,(\vec{k}_{2\perp}\cdot\vec{p}_{1\perp})\Big]\Big[((\vec{k}_{1\perp}-\vec{q})\cdot\vec{p}_{1\perp})\,((\vec{k}_{2\perp}+\vec{q})\cdot\vec{p}_{1\perp})\Big]\\
&\longrightarrow\;\Big[\vec{k}_{1\perp}\cdot\vec{k}_{2\perp}\Big]\Big[(\vec{k}_{1\perp}-\vec{q})\cdot(\vec{k}_{2\perp}+\vec{q})\Big]\,p_{1x}^4+\Big[\vec{k}_{1\perp}\times\vec{k}_{2\perp}\Big]\Big[(\vec{k}_{1\perp}-\vec{q})\times(\vec{k}_{2\perp}+\vec{q})\Big]\,p_{1x}^2\,p_{1y}^2
\end{aligned}
\tag{2.48}
$$

because of the integrations $\int\mathrm{d}p_{1x}\;p_{1x}^2=\int\mathrm{d}p_{1y}\;p_{1y}^2$ and $\int\mathrm{d}p_{1x}\;p_{1x}=\int\mathrm{d}p_{1y}\;p_{1y}=0$ appearing in Eq. (2.40). With this we can identify the real polarization dependent $\gamma\gamma$-fusion cross sections of Eqs. (2.37) and (2.38). The differential cross section then finally leads to

$$
\begin{aligned}
\sigma_{A_1A_2\to A_1A_2b^+b^-} &= \int\mathrm{d}^2b\int\mathrm{d}\omega_1\int\mathrm{d}\omega_2\,\Big[n_{\parallel}(\omega_1,\omega_2;\vec{b})\,\sigma^{\parallel}_{\gamma\gamma\to b^+b^-}(\omega_1,\omega_2)\\
&\qquad+n_{\perp}(\omega_1,\omega_2;\vec{b})\,\sigma^{\perp}_{\gamma\gamma\to b^+b^-}(\omega_1,\omega_2)\Big]\\
&= \int\mathrm{d}\omega_1\int\mathrm{d}\omega_2\,n_1(\omega_1)\,n_2(\omega_2)\,\sigma_{\gamma\gamma\to b^+b^-}(\omega_1,\omega_2)\quad .
\end{aligned}
\tag{2.49}
$$

The two-photon distribution

$$
\begin{aligned}
n_{\parallel}(\omega_1,\omega_2;\vec{b}) &= \frac{1}{\pi^2\omega_1\omega_2}\int\mathrm{d}^2x_\perp\,\Big|\vec{E}_{1\perp}(\omega_1,\vec{x}_\perp-\vec{b})\cdot\vec{E}_{2\perp}(\omega_2,\vec{x}_\perp)\Big|^2\\
&= \int\mathrm{d}^2x_\perp\;n(\omega_1;\vec{x}_\perp-\vec{b})\,n(\omega_2;\vec{x}_\perp)\,\left(\frac{(\vec{x}_\perp-\vec{b})\cdot\vec{x}_\perp}{|\vec{x}_\perp-\vec{b}|\,|\vec{x}_\perp|}\right)^2
\end{aligned}
\tag{2.50}
$$

depends on the transverse electromagnetic fields $\vec{E}_{1\perp}$ and $\vec{E}_{2\perp}$ of the two heavy ions; for $n_\perp(\omega_1,\omega_2;\vec{b})$ the dot product in the expression (2.50) simply has to be replaced by a cross product. The two-photon distribution function essentially contains a product of one-photon distribution functions. The integration over $x_\perp$ means that the photon-photon interaction can take place over the whole transversal plane resulting in a product of local one-photon distribution functions. The geometric expression in large brackets appears due to the polarization dependence of the two photons. This point deviates from the treatment of Papageorgiu [100, 101].

An integration over the impact parameter in (2.49) leads to the total equivalent photon cross section (2.1). Omitting the integration over $\vec{b}$, yields the correct impact-parameter dependent equivalent cross section for the production of a pair of charged bosons.

2.2.2 General derivation of the equivalent photon cross section

The rather cumbersome direct derivation of the equivalent photon cross section (2.49) from lowest order QED (within the semiclassical approximation) has been given for the two photon fusion process into

a pair of charged spin-0 bosons. For the production of other particle species like neutral (scalar or pseudoscalar) bosons or fermions this approach has to be repeated from scratch in order to validate an equivalent expression. Especially for the production of fermions this task is very time-consuming as traces of γ-matrices have to be manipulated and an expansion of the invariant matrix element $|u_{1\mu}\Gamma^{\mu\nu}u_{2\nu}|^2$ has to be performed up to fourth order in $\vec{k}_\perp$. Hence, there is a need for a quite general derivation, which is independent of the particle species to be produced.
We make use of gauge invariance of the S-matrix element entering into (2.32), which leads to the conservation of the transition current, i.e.

$$k_1^\mu \Gamma_{\mu\nu} = k_2^\nu \Gamma_{\mu\nu} = 0 \quad . \tag{2.51}$$

Its time-like coordinate may be expressed by its space-like components (latin indices run only over the transverse plane):

$$\begin{aligned} \Gamma^{0\nu}(k_1 k_2; p_i) &= -\frac{k_{1i}\Gamma^{i\nu} + k_{1z}\Gamma^{3\nu}}{k_{10}} \quad , \\ \Gamma^{\mu 0}(k_1 k_2; p_i) &= -\frac{k_{2i}\Gamma^{\mu i} + k_{2z}\Gamma^{\mu 3}}{k_{20}} . \end{aligned} \tag{2.52}$$

The nuclei move on straight trajectories and thus $k_z/k^0 = \pm 1/v$; consult Eq. (2.7). We obtain

$$u_{1\mu}u_{2\nu}\Gamma^{\mu\nu} = \gamma^2 \frac{k_{1i}}{k_{10}}\frac{k_{2j}}{k_{20}}\Gamma^{ij} + \frac{1}{v}\left(\frac{k_{2j}}{k_{20}}\Gamma^{3j} - \frac{k_{1i}}{k_{10}}\Gamma^{i3}\right) - \frac{1}{\gamma^2 v^2}\Gamma^{33} \quad . \tag{2.53}$$

Precisely at this point we introduce the decisive approximation (2.33): the ratios k_{1i}/k_{10} or k_{2i}/k_{20} are of the order $1/\gamma$, which leaves the first term in (2.53) to be dominant over the remaining two terms by the order γ. Hence, we approximate

$$u_{1\mu}u_{2\nu}\Gamma^{\mu\nu} \approx \gamma^2 \frac{k_{1i}}{\omega_1}\frac{k_{2j}}{\omega_2}\Gamma^{ij} \quad . \tag{2.54}$$

On the right hand side now appears the vertex function $\Gamma^{ij} = \Gamma^{ij}(\omega_1, \omega_2; p_i)$ for real photons, which have transverse polarisations. This identification is the heart of the equivalent photon approach! Except for a flux factor the integration of the square of the vertex function $|\Gamma^{ij}|^2\delta^4(k_1 + k_2 - \sum_i p_i)$ over the phase space of the produced outgoing particles leads to the polarized two-photon fusion cross sections $\sigma^{\parallel}_{\gamma\gamma\to X}(\omega_1, \omega_2)$ and $\sigma^{\perp}_{\gamma\gamma\to X}(\omega_1, \omega_2)$, for which the polarisation vectors of the two photons are parallel and perpendicular to each other, respectively. Observe, that the transverse components k_{1i} and k_{2j} of the virtual photons coming from the two heavy-ion lines are extracted in the transformation (2.54); this is a very important point because the square of them will lead to quantities like $\vec{k}^2_{1\perp}$ and $\vec{k}^2_{2\perp}$, which are so desperately needed to make an identification with the equivalent photon distributions.
Using the transformation (2.54) and performing most of the integrations in the expression (2.32) we arrive at

$$\begin{aligned} \sigma_{A_1A_2\to A_1A_2X} &= \int \mathrm{d}^2b \int \mathrm{d}\omega_1 \int \mathrm{d}\omega_2 \left[n_\parallel(\omega_1, \omega_2; \vec{b})\,\sigma^{\parallel}_{\gamma\gamma\to X}(\omega_1, \omega_2) + n_\perp(\omega_1, \omega_2; \vec{b})\,\sigma^{\perp}_{\gamma\gamma\to X}(\omega_1, \omega_2)\right] \\ &= \int \mathrm{d}\omega_1 \int \mathrm{d}\omega_2\, n_1(\omega_1)\, n_2(\omega_2)\, \sigma_{\gamma\gamma\to X}(\omega_1, \omega_2) \quad ; \end{aligned} \tag{2.55}$$

all further technical details of this derivation have been given in Ref. [126]. $\sigma^{\parallel}_{\gamma\gamma\to X}$ and $\sigma^{\perp}_{\gamma\gamma\to X}$ represent the polarized two-photon fusion cross sections and add up to yield the total two-photon fusion cross section $\sigma_{\gamma\gamma\to X} = (\sigma^{\parallel}_{\gamma\gamma\to X} + \sigma^{\perp}_{\gamma\gamma\to X})/2$.
The second step in Eq. (2.55) illustrates, that we have indeed derived the equivalent photon cross section (2.1) from QED directly. If we skip the integration over the impact parameter in Eq. (2.49), we come up with a correct impact parameter dependent differential equivalent photon cross section!

We have succeeded to derive an impact-parameter dependent generalization of the Equivalent Photon Approximation for two-photon fusion processes in relativistic heavy-ion collisions. A semiclassical approach has been chosen as the electromagnetic potentials of the charged heavy ions moving on classical

trajectories have been considered; all the rest, i.e. the interaction of the two virtual photons and the production of the new particles, has been described by QED (in lowest order). Two approaches have been followed: the first resembles a strategy by brute force whereas the other using the conservation of the transition current is much more elegant and general. There is one more approach around [68]: again we can make use of the gauge freedom of the S-matrix element to transform the four-velocity u^μ into a polarization-like four-vector, i.e. $u^\mu \to u^\mu + \alpha k^\mu = h(k)\epsilon^\mu$. With a suitable choice of α (or $h(k)$, respectively) a straightforward identification with the real two-photon subprocess becomes feasible.

Similiar impact parameter dependent cross sections were obtained in Refs. [24, 37]:

$$\sigma^{WW} = \int \mathrm{d}\omega_1 \int \mathrm{d}\omega_2 \left[J_{\|}(\omega_1,\omega_2)\ \sigma_{\|}(\omega_1,\omega_2) + J_{\perp}(\omega_1,\omega_2)\ \sigma_{\perp}(\omega_1,\omega_2) \right] \tag{2.56}$$

with

$$\begin{aligned} J_{\|} &= 2\pi \int_R \mathrm{d}b_1\ b_1 \int_R \mathrm{d}b_2\ b_2 \int_0^{2\pi} \mathrm{d}\phi\ n(\omega_1,b_1)\ n(\omega_2,b_2)\ \cos^2\phi\ \Theta(b-2R)\,, \\ J_{\perp} &= 2\pi \int_R \mathrm{d}b_1\ b_1 \int_R \mathrm{d}b_2\ b_2 \int_0^{2\pi} \mathrm{d}\phi\ n(\omega_1,b_1)\ n(\omega_2,b_2)\ \sin^2\phi\ \Theta(b-2R) \end{aligned} \tag{2.57}$$

where $b^2 = b_1^2 + b_2^2 - 2b_1 b_2 \cos\phi$. After some transformations this leads to the same result but the integration over the transverse plane $x_\perp$ is here performed with the black-disk approximation ($|\vec{x}_\perp| \geq R, |\vec{x}_\perp - \vec{b}| \geq R$), which is a little different from our description.

One word of caution has to be mentioned: the equivalent photon approximation can only be applied to particle production with particle masses larger than $|\vec{k}_\perp|_{\max} \approx 1/R$. Therefore the equivalent photon method can not be used for e^+e^- pair production in heavy-ion collisions. Phenomenologically this is easy to understand because the Compton wavelength of the electron is larger than the nuclear radius. In fact, if one takes a closer look on the propagator, it has the denominator like $1/(q^2 - m^2)$, where q is the momentum transfer $q = k - p$ with the photon momentum k and the momentum p of the produced particle of mass m. The denominator of the propagator

$$\frac{1}{q^2 - m^2} = \frac{1}{k^2 - 2(p \cdot k)} \tag{2.58}$$

has to be transformed into the propagator where only real photons are coupling, i.e. $k^2 = 0$. The approximation one has to perform reads $|k^2| \ll |2(p \cdot k)|$. With $k = (\omega, \vec{k}_\perp, \omega/v)$, $p = (E, \vec{p}_\perp, \sqrt{E^2 - m^2 - \vec{p}_\perp^{\,2}})$ and $m \ll \omega$ we deduce in the CM system of the two photons, that the transverse momentum of the photon has to be much smaller than the mass of the produced particle, i.e. $m \gg |\vec{k}_\perp|$. In Pb-Pb collisions for example the photon have transverse momenta up to the inverse nuclear radius, thus $|\vec{k}_\perp|_{\max} \approx 1/R \approx 30$ MeV. The electron is unique in the sense, that all other particles produced by two photons are heavier. Therefore electron-positron production has to be calculated without using the equivalent photon approach; the exact cross section has to be evaluated [17, 73, 76, 77]. Of special interest is the e^+e^--production with capture; this process sets limits to the collider luminosity and due to its non-perturbative character it is also of fundamental interest [9, 18]. A comprehensive review is presented in the book of Eichler and Meyerhof [53].

2.3 Equivalent photon approximation for virtual photons

So far we have employed the external field approximation for all derivations of the equivalent photon cross section, i.e. we identified the classical electromagnetic fields of heavy ions moving with constant velocity on straight lines with the equivalent photon swarm. Although we are convinced that this quasi-classical approximation is justified for high energetic heavy-ion collisions, we feel that it is nevertheless

worth discussing the impact of small derivations from the straight line motion. The small deflections of the two projectiles introduce a non-negligible virtuality of the equivalent photons, so that the question arises how large of a deflection angle is admissible to guarantee the validity of the equivalent photon approach. For an exemplary demonstration we choose pp-collisions instead of heavy-ion collisions leading to the production of a pair of fermions. In the following we will use some results given in the article of Budnev et al. [36]. We keep this very technical subsection rather short and compressed as it is not of relevance for the various applications to be presented in sections 3 and 4.
We start our derivation with the full cross section for photoproduction of fermions with fermionic photon sources:

$$d\sigma = \frac{1}{4\sqrt{(p_1p_2)^2 - m_1^2m_2^2}} \cdot (4\pi\alpha_{\rm QED})^2\, \mathrm{T}_1^{\mu\mu'}\mathrm{T}_2^{\nu\nu'}\mathrm{M}^*_{\mu'\nu'}\mathrm{M}_{\mu\nu}\, \frac{(2\pi)^4\delta^4(q_1+q_2-P)\, d\tilde{P}\, d^3p_1'\, d^3p_2'}{2E_1'\, 2E_2'\, (2\pi)^6} \tag{2.59}$$

In this equation the first term on the right hand side is the flow factor for the incoming particles. The second one contains the elementary matrix elements M for the transition $\gamma^*\gamma^* \to X$ and the density matrices T_i for the emission of a photon with momentum q_i by the i-th particle. The last term reflects the conservation of four-momentum and the phase-space integrations over the outgoing photon sources denoted by d^3p_i' and the phace space $d\tilde{P}$ of the produced system.
First we focus on the photon density matrices. They are given by the usual tensor for the emission of a virtual photon by a fermion multiplied with $(q^{-2})^2$ stemming from the photon propagator. Notice, that this photon density is not diagonal reflecting the polarisation of the photons. It is given by

$$\begin{aligned}\mathrm{T}^{\mu\nu} &= \frac{1}{2q^4}\mathrm{Tr}\left[(\not{p}+m_P)\Gamma^\mu(\not{p}'+m_P)\Gamma^\nu\right] \\ &= \frac{1}{q^2}\left[\left[g^{\mu\nu}-\frac{q^\mu q^\nu}{q^2}\right]H_2(q^2)+\left[\frac{(2p-q)^\mu(2p-q)^\nu}{q^2}\right]H_1(q^2)\right].\end{aligned} \tag{2.60}$$

For structureless point-like particles like leptons the Γ^μ are given by the usual Dirac matrices γ^μ and the form factors are $H_{1/2}(q^2) = 1$. For particles with structure this changes of course; for protons the form factors are given by

$$\Gamma^\mu = \gamma^\mu F_1(q^2) - i\frac{\sigma^{\mu\mu'}q_{\mu'}}{2m}F_2(q^2)\,, \tag{2.61}$$

$$H_1(q^2) = F_1^2(q^2) - \frac{q^2}{4m^2}F_2^2(q^2) = \frac{4m^2G_E^2(q^2) - q^2G_M^2(q^2)}{4m^2-q^2}\,, \tag{2.62}$$

$$H_2(q^2) = G_M^2(q^2). \tag{2.63}$$

F_1 and F_2 are given in the usual Sachs combinations for the elastic electric and magnetic form factors G_E and G_M. In our calculations we use the common dipole form factors :

$$\begin{aligned}G_E(q^2) &= \frac{1}{(1-q^2/q_0^2)^2}\,, \\ G_M(q^2) &= (1+\mu_P)\cdot G_E(q^2)\end{aligned} \tag{2.64}$$

with $q_0^2 = 0.71\,\mathrm{GeV}^2$. Of course these elastic form factors are only valid as long as the proton remains intact. In other words, our expressions for the cross sections are valid as long as we consider elastic photoproduction. Obviously this sets limits on the energy fraction carried away by the photon and its virtuality.
Integrated over the phase space of the produced particle state the corresponding matrix elements read

$$\mathrm{M}_{\mu'\nu'\mu\nu} = \frac{1}{2}\int d\tilde{P}\,(2\pi)^4\,\delta^4(q_1+q_2-P)\,\mathrm{M}^*_{\mu'\nu'}\mathrm{M}_{\mu\nu}. \tag{2.65}$$

Gauge invariance ensures that

$$q_{1,2}^{\mu,\nu} \mathrm{M}_{\mu'\nu'\mu\nu} = 0. \tag{2.66}$$

so that the term $q_i^\mu q_i^\nu / q_i^2$ of the completeness relation

$$\sum_a (-1)^a \epsilon^{*\mu}(a) \epsilon^\nu(a) \;=\; g^{\mu\nu} - \frac{q^\mu q^\nu}{q^2}. \tag{2.67}$$

vanishes. Consequently we insert the completeness relation in between the matrices T and M of equation (2.59). This results in a 3×3-matrix for the photon-density

$$\mathrm{T}^{ab} = \mathrm{T}^{\mu\nu} \epsilon_\mu^*(a) \epsilon_\nu(b), \tag{2.68}$$

where the helicity labels a, b stand for $+, -, 0$ which reflect transverse and longitudinal polarisations, respectively. A similar expression in the helicity basis can be obtained for the production-matrix elements. They are connected to elementary cross sections for $\gamma^*\gamma^* \to f\bar{f}$ via

$$\begin{aligned}
\sigma_{TT} &= \frac{1}{2} \frac{(\mathrm{M}^{++,++} + \mathrm{M}^{+-,+-})}{2\sqrt{X}} \\
&= \frac{\pi \alpha_{\mathrm{QED}}^2}{X} \left((q_1 q_2) L \left[2 + \frac{2m_f^2}{x} - \left(\frac{2m_f^2}{q_1 q_2} \right)^2 + \frac{q_1^2 + q_2^2}{x} + \frac{q_1^2 q_2^2 s_{\gamma\gamma}}{2x(q_1 q_2)^2} + \frac{3}{4} \left(\frac{q_1^2 q_2^2}{x(q_1 q_2)} \right)^2 \right] \right. \\
&\qquad \left. - \Delta t \left[1 + \frac{m_f^2}{x} + \frac{q_1^2 + q_2^2}{x} + \frac{q_1^2 q_2^2}{T} + \frac{3}{4} \frac{q_1^2 q_2^2}{x^2} \right] \right), \\
\sigma_{TT}^{\text{Spin-flip}} &= \frac{\mathrm{M}^{++,--}}{2\sqrt{X}} \\
&= -\frac{\pi \alpha_{\mathrm{QED}}^2}{4X} \left(\frac{2\Delta t}{x} \left[2m_f^2 + \frac{(q_1^2 - q_2^2)^2}{s_{\gamma\gamma}} + \frac{3}{2} \frac{q_1^2 q_2^2}{x} \right] \right. \\
&\qquad \left. + \frac{L}{(q_1 q_2)} \left[16 m_f^4 - 16 m_f^2 (q_1^2 + q_2^2) - 4 q_1^2 q_2^2 \left(2 + \frac{2m_f^2}{x} + \frac{q_1^2 + q_2^2}{x} - \frac{3}{4} \frac{q_1^2 q_2^2}{x(q_1 q_2)} \right) \right] \right), \\
\sigma_{TS} &= \frac{\mathrm{M}^{0+,0+}}{2\sqrt{X}} \\
&= -\frac{\pi \alpha_{\mathrm{QED}}^2 q_2^2}{Xx} \left(\Delta t \left[1 + \frac{q_1^2}{T} \left(6m_f^2 + q_1^2 + \frac{3}{2} \frac{q_1^2 q_2^2}{x^2} \right) \right] \right. \\
&\qquad \left. - \frac{L}{(q_1 q_2)} \left[4m_f^2 x + q_1^2 (s_{\gamma\gamma} + 2m_f^2) + q_1^2 \left(q_1^2 + q_2^2 + \frac{3}{2} \frac{q_1^2 q_2^2}{x} \right) \right] \right),
\end{aligned} \tag{2.69}$$

where we used the following short-hand notations:

$$\begin{aligned}
s_{\gamma\gamma} &= (q_1 + q_2)^2, \\
X &= (q_1 q_2)^2 - q_1^2 q_2^2, \\
x &= \frac{X}{s_{\gamma\gamma}}, \\
\Delta t &= \sqrt{4x(s_{\gamma\gamma} - 4m_f^2)}, \\
T &= 4xm_f^2 + q_1^2 q_2^2, \\
L &= \ln \frac{\left(q_1 q_2 + \frac{1}{2} \Delta t \right)^2}{T}.
\end{aligned}$$

As one can easily see longitudinal polarisations result in a factor of roughly $q^2/s_{\gamma\gamma}$, which leads to a suppression in the region of $q^2 < s_{\gamma\gamma}$.
Obviously only the two contributions σ_{TT} are left to survive for $q_i^2 \to 0$. In this limit they reduce to the well-known elementary cross sections for $\gamma\gamma \to f\bar{f}$ in the corresponding helicity decomposition. Additional cross sections are due to more scalar photons and due to antisymmetric helicity combinations occuring for polarised photon sources.
The transformation of Eq. (2.59) to the helicity basis yields

$$d\sigma = \frac{8\alpha_{\rm QED}^2\pi^2}{q_1^2 q_2^2}\sqrt{\frac{(q_1q_2)^2 - q_1^2q_2^2}{(p_1p_2)^2 - m_1^2m_2^2}}\cdot\frac{d^3p_1'\,d^3p_2'}{2E_1'\,2E_2'\,(2\pi)^6} \times\left[4\mathrm{T}_1^{++}\mathrm{T}_2^{++}\,\sigma_{TT} + 2|\mathrm{T}_1^{+-}\mathrm{T}_2^{+-}|\cos 2\tilde{\phi}\;\sigma_{TT}^{\rm spin-flip} + \text{terms involving scalar photons}\right] \quad (2.70)$$

The numerator in the square root is due to the factor X in Eq. (2.69). The integration is over the phase space of the outgoing sources. The angle $\tilde{\phi}$ is the correlation angle of the scattering planes of the outgoing particles in the photons c. m. s..

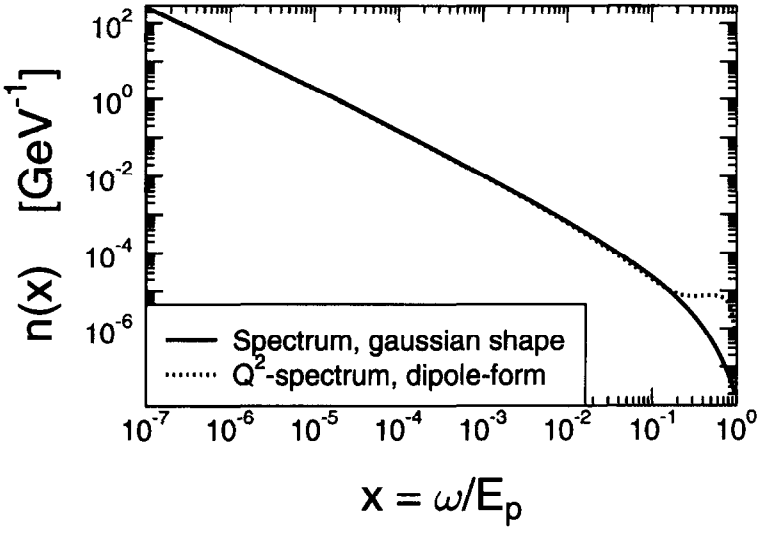

Figure 2.6: The photon spectra for protons. For the spectrum obtained by considering small deflection angles we integrated over $0 \le \theta \le 0.003$. For the equivalent photon spectrum we employed a Gaussian shape for the proton with parameter $Q_0^2 = Q_{0,\rm dipole}^2 = 0.71\,\mathrm{GeV}^2$.

We now perform a transformation to polar coordinates for the phase–space integral; it then reads

$$\frac{d^3p_1'\,d^3p_2'}{2E_1'\,2E_2'\,(2\pi)^6} = \frac{\pi\,s}{2[(p_1p_2)^2 - m_1^2m_2^2]}\cdot\frac{dq_1^2\,dq_2^2\,d\omega_1\,d\omega_2\,d\phi}{128\pi^6}, \quad (2.71)$$

where ϕ is the already mentioned correlation angle in the c. m. s. of the colliding particles.

In the limit of small scattering angles the following relations hold :

$$\begin{aligned}
\tilde{\phi} &\approx \phi\,, \\
\mathrm{T}_i^{++} = \mathrm{T}_i^{--} &\approx \frac{2E^2}{\omega_i^2}\cdot\left[\left(1-\frac{\omega_i}{E}\right)\left(1-\left|\frac{q_{i,\min}^2}{q_i^2}\right|\right)H_1(q_i^2)+\frac{\omega_1^2}{2E^2}H_2(q_1^2)\right] \\
&= \frac{2}{x_i^2}\cdot\left[(1-x_i)\left(1-\left|\frac{q_{i,\min}^2}{q_i^2}\right|\right)H_1(q_i^2)+\frac{x_i^2}{2}H_2(q_i^2)\right]\,, \qquad (2.72) \\
\left|\mathrm{T}_i^{+-}\right| &= \mathrm{T}_i^{++}-H_2(q_i^2). \qquad (2.73)
\end{aligned}$$

Defining "relative polarisations"

$$\xi_i = \frac{\left|T_i^{+-}\right|}{T^{++}} \qquad (2.74)$$

we can write Eq. (2.70) as

$$d\sigma = \left(\sigma_{TT}+\frac{1}{2}\xi_1\xi_2\cos(2\phi)\,\sigma_{TT}^{\text{Spin-flip}}\right)dn_1dn_2\frac{d\phi}{2\pi} \qquad (2.75)$$

with

$$dn_i(\omega_i,q_i^2) = \frac{\alpha_{\text{QED}}}{2\pi}\,\mathrm{T}_i^{++}\frac{\omega_i d\omega_i dq_i^2}{E^2q_i^2}. \qquad (2.76)$$

Here the dn_i are the differential photon–distribution functions for virtual transverse polarised photons. We compare this photon distribution integrated over the region of small angles θ_i with the equivalent photon spectrum (2.21). We consider pp–collisions with $\gamma = 3000$, where we have taken the usual dipole form factor for the protons emitting the virtual photons. For the equivalent photon spectrum we assumed a Gaussian shape for the proton with the parameter Q_0 from the dipole form factor. The striking fact of Fig. 2.6 is that the two spectra are nearly identical for low photon energies ω, whereas for the high energy region they differ.

Once again it should be noted that we only were able to neglect the scalar contributions to the cross section due to the relative smallness of the scalar components of the elementary cross sections compared to the transverse ones. Those scalar components are suppressed by a factor of q^2/M_{inv}^2. The photon spectra in dependence on Q^2 with two different fixed values of x are displayed in Fig. 2.7. In the full kinematics of two–photon production processes the matrices T_i depend on both photon momenta q_i. It is in the region of small scattering angles only, where they depend solely on one momentum.

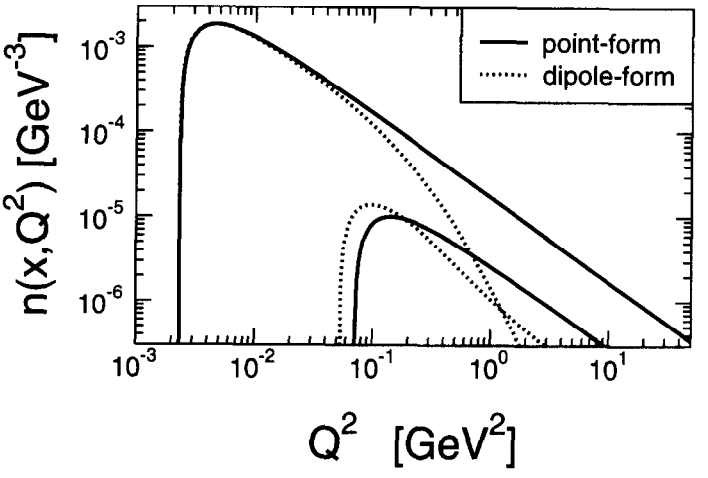

Figure 2.7: The photon spectra for protons in dependence on the virtuality Q^2. We took two different fixed values for x: $x = 0.05$ – the two upper lines – and $x = 0.25$ – the lower ones. Two different proton forms were taken into account, a point–like one and the dipole form with $Q^2_{0,\text{dipole}} = 0.71\,\text{GeV}^2$.

Chapter 3

Two–photon fusion processes

The idea to produce exotic particles not only in e^+e^-- and pp-collisions, but also in peripheral relativistic heavy-ion collisions via the strong transverse electromagnetic fields is very appealing. These processes could be investigated at the heavy-ion colliders RHIC and LHC almost for free: The main emphasis at these facilities is of course to search for signals from a Quark-Gluon-Plasma which is believed to be formed in central collisions. But there is also an overwhelming number of peripheral collisions with no hadronic interaction between the two colliding nuclei. This would represent a very clean environment for the electromagnetic particle production processes to be detected. The maximum photon frequency contained in the transverse electromagnetic fields is directly proportional to the inverse of the Lorentz-contracted nuclear radius, $\omega_{\max} \approx \gamma/R$. This amounts to $\omega_{\max} \approx 80$ GeV for the LHC Pb-mode with $\gamma = 2750$, $\omega_{\max} \approx 180$ GeV for the LHC Ca-mode with $\gamma = 3750$ and $\omega_{\max} \approx 3$ GeV for the RHIC Au-mode with $\gamma = 108$. Thus, particles such as exotic heavy mesons in the 1 GeV – 10 GeV mass range as well as even Higgs bosons and supersymmetric particles in the 100 GeV mass range could be produced. With the equivalent photon approach, presented in general in the previous Section, we will now evaluate cross sections and production rates.
In the first Subsection we list the relevant elementary two-photon cross sections to be used within the equivalent photon method. Some general features of the equivalent photon cross sections for particle production are discussed in the second Subsection. In the subsequent Subsections we then focus with increasing mass on the production of mesons, leptons, quarks, supersymmetric particles and Higgs bosons.

3.1 Elementary two-photon fusion cross sections

In general we have to distinguish between the two elementary two–photon cross sections $\sigma_{\parallel}^{\gamma\gamma\to X}(\omega_1,\omega_2)$ and $\sigma_{\perp}^{\gamma\gamma\to X}(\omega_1,\omega_2)$. For the first one the polarisation vectors of the two photons are parallel to each other whereas for the second one they are perpendicular to each other. The two cross sections with polarized photons add up to the total elementary two-photon cross section

$$\sigma^{\gamma\gamma\to X}(\omega_1,\omega_2) = \frac{1}{2}\left(\sigma_{\parallel}^{\gamma\gamma\to X}(\omega_1,\omega_2) + \sigma_{\perp}^{\gamma\gamma\to X}(\omega_1,\omega_2)\right) \quad , \tag{3.1}$$

which simply represents the average over all polarisations.
For the production of one (pseudo–) scalar boson we notice that it can only be produced when the polarisation vectors of the two photons are parallel (or perpendicular) to each other. The two-photon production cross section of those bosons is given by the following relation:

$$\sigma^{\gamma\gamma\to B_{s(ps)}}(s) = \frac{1}{2}\sigma_{\parallel(\perp)}^{\gamma\gamma\to B_{s(ps)}}(s) = (2J+1)\cdot\frac{8\pi^2}{m_B}\,\Gamma_{B_{s(ps)}\to\gamma\gamma}\cdot\delta(s-m_B^2) \quad . \tag{3.2}$$

Here, $s = 4\omega_1\omega_2$, Γ is the (usually measured) two-photon decay width and J denotes the spin of the boson. The delta function ensures total four-momentum conservation as physical particles can be produced only on-shell.

Charged bosons are produced in pairs. The elementary two-photon cross sections for the photonic subprocess are given in lowest order (see Figure 2.5) by

$$\sigma_{\parallel}^{\gamma\gamma\to b^+b^-} = \frac{2\pi\alpha^2}{s}\left[\sqrt{1-\frac{4m_b^2}{s}}\left(1+\frac{6m_b^2}{s}\right) - \frac{4m_b^2}{s}\left(2-\frac{6m_b^2}{s}\right)\ln\left(\frac{\sqrt{s}}{2m_b}+\sqrt{\frac{s}{4m_b^2}-1}\right)\right]\Theta(s-4m_b^2) \tag{3.3}$$

and

$$\sigma_{\perp}^{\gamma\gamma\to b^+b^-} = \frac{2\pi\alpha^2}{s}\left[\sqrt{1-\frac{4m_b^2}{s}}\left(1+\frac{2m_b^2}{s}\right) - \frac{4m_b^2}{s}\left(2-\frac{2m_b^2}{s}\right)\ln\left(\frac{\sqrt{s}}{2m_b}+\sqrt{\frac{s}{4m_b^2}-1}\right)\right]\Theta(s-4m_b^2) \quad . \tag{3.4}$$

Again the Mandelstam variable s is equal to $s = 4\omega_1\omega_2$ and m_b represents the mass of one charged boson; the step-function $\Theta(s-4m_b^2)$ guarantees, that the charged boson pair can only be produced, if the cm-energy of the two photons is larger or equal to twice the boson mass.

For the electromagnetic production of a fermion pair both the polarized scalar and pseudoscalar two-photon fusion cross section again contribute. In lowest order in α [36] they read

$$\sigma_{\parallel}^{\gamma\gamma\to f^+f^-} = \frac{4\pi\alpha^2}{s}\left[\left(1+\frac{4m_f^2}{s}-\frac{12m_f^4}{s^2}\right)2\ln\left(\frac{\sqrt{s}}{2m_f}+\sqrt{\frac{s}{4m_f^2}-1}\right) - \left(1+\frac{6m_f^2}{s}\right)\sqrt{1-\frac{4m_f^2}{s}}\right]\Theta(s-4m_f^2) \tag{3.5}$$

and

$$\sigma_{\perp}^{\gamma\gamma\to f^+f^-} = \frac{4\pi\alpha^2}{s}\left[\left(1+\frac{4m_f^2}{s}-\frac{4m_f^4}{s^2}\right)2\ln\left(\frac{\sqrt{s}}{2m_f}+\sqrt{\frac{s}{4m_f^2}-1}\right) - \left(1+\frac{2m_f^2}{s}\right)\sqrt{1-\frac{4m_f^2}{s}}\right]\Theta(s-4m_f^2) \quad ; \tag{3.6}$$

m_f represents the mass of the fermion.

3.2 General discussion

Before we present explicitly results for the production cross sections of specific particles, we discuss some general features of the equivalent photon cross sections: impact-parameter dependence, exclusion of central collisions and rapidity dependence.

Two elementary cross sections depending on the mutual polarization of the two photons enter into the expression (2.55) for the impact-parameter dependent cross section $d\sigma/db$. For the production of fermions or charged bosons both elementary cross sections contribute. However, due to the Yang-Theorem [140] a scalar boson can only be produced by two photons with polarizations parallel to each other, whereas a pseudoscalar boson only by two photons with polarizations perpendicular to each other. For the case of scalar spin-0-meson production only the first part of $d\sigma/db$ in (2.55) contributes since $\sigma_\perp = 0$.

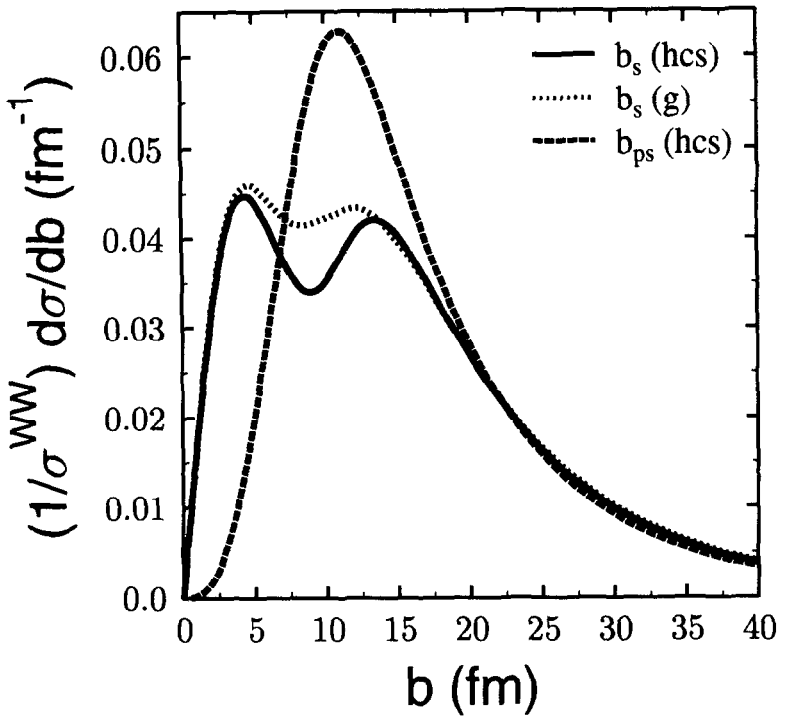

Figure 3.1: Impact parameter dependent cross section $d\sigma/db$ for scalar (s) and pseudoscalar (ps) boson production in a Pb-Pb collision for LHC energies ($\gamma = 3500$) taking a homogeneously charged sphere (hcs) and a Gaussian (g) formfactor into account. A particle mass of 100 GeV is assumed.

Figure 3.1 depicts the impact-parameter dependent cross section for the production of a scalar and a pseudoscalar boson with a mass of 100 GeV in a Pb-Pb collision for maximum LHC energies. For the production of a scalar boson a dip exists around $b \approx R$; it is a result of the two overlapping electromagnetic fields, which for this constellation are mostly perpendicular, but only the parallel part contributes (consult Eq. (2.50)). On the other hand, for the production of pseudoscalar mesons the maximum between R and $2R$ occurs due to the field constellation, where a large proportion of the electric fields are perpendicular to each other.

Furthermore, two different formfactors are considered in Figure 3.1. Taking the formfactor of a homogeneously charged sphere the dip is more pronounced than for the Gaussian formfactor which effectively smears out the nuclear surface. The lighter the produced particle the more the dip is smeared out because the particle has to be produced in a small volume, which should roughly be proportional to the cube of the particle Compton wavelength, so that for small particle masses this volume becomes relatively large and diminishes any structure. For the production of a pair of charged bosons or of a pair of fermions the scalar ($\parallel$) and pseudoscalar ($\perp$) part contribute together. Only if the pair is produced at threshold one of the two contributing parts vanishes: for the boson pair at threshold ($s = 4m_b^2$) it is the pseudoscalar part which diminishes because the pair is created with no kinetic energy in the cm-system of the two photons and therefore can be understood as a composite scalar boson. Hence, a double-hump structure appears in the differential cross section $d\sigma/db$. For the fermion pair at threshold ($s = 4m_f^2$) it is the other way around: it represents a pseudoscalar boson, so that only $\sigma_\perp^{\gamma\gamma\to f^+f^-}$ contributes to $d\sigma/db$.

Small impact parameters have to be excluded in order to discard central collisions and the accompanying

large hadronic background for the particle detection; this motivates the introduction of a sharp cut–off impact parameter $b_C = 2R$, which leads to a reduced total cross section

$$\sigma^{\rm red}_{A_1A_2\to A_1A_2X} = \int\limits_{b_c}^{\infty} {\rm d}b \; \frac{{\rm d}\sigma_{A_1A_2\to A_1A_2X}}{{\rm d}b} \quad ; \tag{3.7}$$

R denotes the nuclear radius.

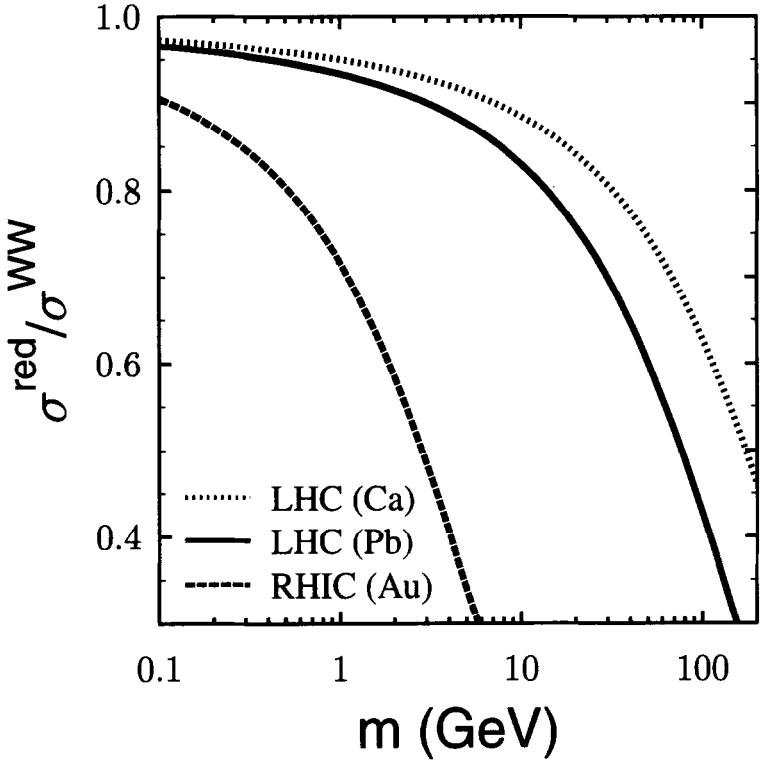

Figure 3.2: Reduction factor $\sigma^{\rm red}/\sigma^{\rm EPA}$ in dependence on the scalar boson mass for RHIC ($\gamma = 108$, Au) and LHC ($\gamma = 3000$, Pb; $\gamma = 3750$, Ca) energies.

In figure 3.2 the reduced cross section $\sigma^{\rm red}/\sigma^{\rm EPA}$ is shown in dependence on the produced boson mass m for RHIC and LHC energies. It is evident that the reduction gets larger as the considered boson mass increases. Whereas the reduction for the production of a 1 GeV boson for LHC energies leads to a somewhat less than 10% effect, it amounts already to 30% for RHIC energies. Since the maximum available photon energies at RHIC is about 3 GeV, the production of heavy mesons takes place in the vicinity of the strongest electromagnetic field densities, i.e. at small impact parameters. This indicates already that at RHIC it becomes almost impossible to search for electromagnetically produced unexpected heavy mesons in the mass range around 10 GeV. Ca-Ca collisions lead to a somewhat smaller reduction because of the smaller radius $R \approx 4.1$ fm in contrast to Pb with $R \approx 7.1$ fm. The reduction factors for the production of a pseudoscalar meson, charged mesons and fermions are quite similar to

the ones presented in Fig. 3.2. Another, maybe more sophisticated reduction employs the Glauber approximation with an absorption factor [92]:

$$\sigma^{\rm red} = \int {\rm d}b \, \frac{{\rm d}\sigma^{\rm EPA}}{{\rm d}b} \exp\{-A\, b\, \sigma_0 T(b)\} \, . \tag{3.8}$$

σ_0 is the total nucleon-nucleon cross section and $T(b)$ represents the profile function

$$T(b) = \int \frac{{\rm d}^2 q}{(2\pi)^2} F_1(q^2)\, F_2(q^2)\, {\rm e}^{{\rm i}qb} \, , \tag{3.9}$$

where F denotes the nuclear form factor. It turns out that this approach differs only to a minor extent from our simple cut–off introduced in (3.7).

The impact–parameter dependent cut–off introduced into the equivalent photon cross sections is not the only one relevant for a rigorous comparison with future experimental data. Usually a detector has no full 4π-coverage. At least this is the case for the proposed ALICE detector designed for the LHC heavy-ion experiments; it will have a polar angle coverage of $\pi/4 \leq \Theta \leq 3\pi/4$. Hence, produced particles moving closely to the heavy-ion beam axis will not be detected. – According to this perspective it is necessary to know the kinematical distributions of the produced particle system; in particular: transverse momentum and rapidity distributions.

First, we will discuss kinematical distributions for the produced particle state as a whole. In the equivalent photon approach the kinematics of the two photons can be easily described since they are on-mass shell and transverse [131]. The momentum of the produced particle state is therefore given by the total momentum

$$\begin{aligned} P &= (\omega_1 + \omega_2 \, , \, \vec{k}_{1\perp} + \vec{k}_{2\perp} \, , \, \frac{1}{v}(\omega_1 - \omega_2)) \\ &\approx (\omega_1 + \omega_2 \, , \, \vec{0} \, , \, \omega_1 - \omega_2) \quad . \end{aligned} \tag{3.10}$$

Actually, the particle state can have a small transverse momentum of twice the transverse momentum of the two photons, which is approximately $|\vec{k}_\perp|_{\rm max} \equiv 1/R$, i.e. approximately 30 MeV for Pb-Pb collisions. Compared to the longitudinal momentum $p_\parallel = \omega_1 - \omega_2$, which is of the order of several GeV, the transverse momentum of the produced particle state is negligible. As a consequence its cm-system will always move along the beam axis.

Instead of the two photon frequencies ω_1 and ω_2 we now introduce the center–of–momentum rapidity $y = \frac{1}{2} \ln \frac{E+P_\parallel}{E-P_\parallel} = \frac{1}{2} \ln \frac{\omega_1}{\omega_2}$, where according to (3.10) $E = \omega_1 + \omega_2$ and $P_\parallel = \omega_1 - \omega_2$, and the Mandelstam variable $s = 4\omega_1\omega_2 = 4\omega^2$. After a transformation of the integration variables in Eqs. (2.55) and (3.7), i.e. $\omega_1 = \omega\, {\rm e}^{+y}$ and $\omega_2 = \omega\, e^{-y}$, we then obtain

$$\begin{aligned} \frac{{\rm d}\sigma^{\rm red}}{{\rm d}y} &= \int_{2R}^{\infty} {\rm d}b \; 2\pi b \int {\rm d}\omega \; 2\omega \, \Big[n_\parallel(\omega\, {\rm e}^{+y}, \omega\, {\rm e}^{-y}; \vec{b}\,)\, \sigma_\parallel^{\gamma\gamma\to X}(s) \\ &\qquad + n_\perp(\omega\, {\rm e}^{+y}, \omega\, {\rm e}^{-y}; \vec{b}\,)\, \sigma_\perp^{\gamma\gamma\to X}(s) \Big] \, . \end{aligned} \tag{3.11}$$

ω is the photon energy in the center–of–momentum system of the two photons.

As an example the rapidity dependence of the differential cross section ${\rm d}\sigma^{\rm red}/{\rm d}y$ normalized to $\sigma^{\rm red}$ for the production of a fermion pair with four different masses m_f in a Pb-Pb collision at LHC energies ($\gamma = 3000$) is presented in Figure 3.3. As one expects from a symmetric collision, the rapidity distribution is symmetrically peaked around $y = 0$; therefore, we only present the rapidity dependence for positive values. The rapidity distributions for heavier fermion masses are more narrow around $y = 0$ than the corresponding ones for lighter fermion masses.

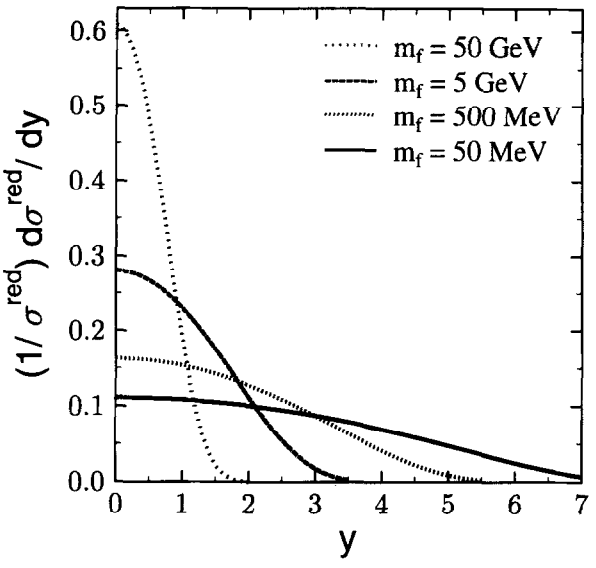

Figure 3.3: Normalized rapidity-dependent reduced cross section for fermion production for various masses m_f in Pb-Pb collisions at LHC energies ($\gamma = 3000$).

Only if the detector outline of the RHIC and LHC heavy-ion experiments would have a full rapidity coverage the expression (3.11) is relevant. The suggested detector of the ALICE collaboration at LHC will only cover charged particles in the polar angle range $45° \leq \Theta \leq 135°$, which corresponds to pseudorapidities of $\eta \leq 0.9$. In order to fully characterize the produced particle state not only its center-of-momentum rapidity, but also the rapidities of each single produced particle has to fall into this rapidity range. For example, both fermions of an electromagnetically produced ferimon pair have to be detected in order to reconstruct the invariant mass, the total rapidity and the total transverse momentum. This requirement to detect all particles in a rather narrow rapidity range of course reduces the observed productions rates.

The detection of the produced boson or fermion pairs requires to consider their individual rapidities $\bar{y}$ relative to the rapidity of the two-photon system. They are introduced by

$$\sigma_{\parallel/\perp}^{\gamma\gamma\to X} = \int\limits_{-\bar{y}_{\max}}^{\bar{y}_{\max}} \mathrm{d}\bar{y}\, \frac{\mathrm{d}\sigma_{\parallel/\perp}^{\gamma\gamma\to X}}{\mathrm{d}\bar{y}} \quad , \tag{3.12}$$

where $\bar{y}_{\max}$ is the maximum available single rapidity

$$\bar{y}_{\max} = \frac{1}{2} \ln \left(\frac{\varpi + \sqrt{\varpi^2 - m^2}}{\varpi - \sqrt{\varpi^2 - m^2}} \right) = \frac{1}{2} \ln \left(\frac{1+\beta}{1-\beta} \right) \tag{3.13}$$

with $\beta = (1 - 4m^2/s)^{1/2}$. m represents the particle mass and $s = 4\omega_1\omega_2 = 4\varpi^2$. The maximum available single rapidity is reached by a particle if it has no transverse momentum. It is considered in the center-of-momentum system of the two photons, which is identical with the rest system of the produced pair, so that one particle has the single rapidity $\bar{y}$ and the other $-\bar{y}$.

The ALICE detector cut $|\tan\theta| \geq 1 = a_{\mathrm{cut}}$ can be expressed in terms of rapidities:

$$\frac{\sinh|y \pm \bar{y}|}{\sqrt{1 - (1-\beta^2)\cosh^2\bar{y}}} \leq \frac{1}{a_{\mathrm{cut}}} \quad . \tag{3.14}$$

Then a modified cross section results, which takes the rapidity cuts into account:

$$\sigma^{\mathrm{cut}} = \int\limits_{\varpi_{\min}}^{\infty} \mathrm{d}\varpi\, 2\varpi \int\limits_{-y_{\mathrm{cut}}}^{y_{\mathrm{cut}}} \mathrm{d}y \int\limits_{2R}^{\infty} \mathrm{d}b\, 2\pi\, b \left[n_{\parallel}(\varpi \mathrm{e}^{+y}, \varpi \mathrm{e}^{-y}; \vec{b}\,)\, \tilde{\sigma}_{\parallel}^{\gamma\gamma\to X}(s) \right.$$

$$+ n_\perp(\varpi e^{+y}, \varpi e^{-y}; \vec{b})\, \tilde{\sigma}_\perp^{\gamma\gamma\to X}(s)\Big] \quad , \tag{3.15}$$

where $\varpi_{\min} = m$. The limits of the rapidity integration results from (3.14) with $\bar{y} = 0$:

$$y_{\rm cut} = \operatorname{arcsinh}\left(\frac{\beta}{a_{\rm cut}}\right) \quad . \tag{3.16}$$

The modified elementary polarization dependent cross section are

$$\begin{aligned}
\tilde{\sigma}_\parallel^{\gamma\gamma\to b^+b^-} &= \frac{\pi\alpha^2}{s}\Big\{(-1-2\beta^2+3\beta^4)\bar{y}_{\rm cut} + 3(1-\beta^2)^2 \sinh\bar{y}_{\rm cut}\, \cosh\bar{y}_{\rm cut} + 2\tanh\bar{y}_{\rm cut}\Big\} \\
\tilde{\sigma}_\perp^{\gamma\gamma\to b^+b^-} &= \frac{\pi\alpha^2}{s}\Big\{(-3+2\beta^2+\beta^4)\bar{y}_{\rm cut} + (1-\beta^2)^2 \sinh\bar{y}_{\rm cut}\, \cosh\bar{y}_{\rm cut} + 2\tanh\bar{y}_{\rm cut}\Big\}
\end{aligned} \tag{3.17}$$

for the production of a boson pair and

$$\begin{aligned}
\tilde{\sigma}_\parallel^{\gamma\gamma\to f^+f^-} &= \frac{2\pi\alpha^2}{s}\Big\{(5+2\beta^2-3\beta^4)\bar{y}_{\rm cut} - 3(1-\beta^2)^2 \sinh\bar{y}_{\rm cut}\, \cosh\bar{y}_{\rm cut} - 2\tanh\bar{y}_{\rm cut}\Big\} \\
\tilde{\sigma}_\perp^{\gamma\gamma\to f^+f^-} &= \frac{2\pi\alpha^2}{s}\Big\{(7-2\beta^2-\beta^4)\bar{y}_{\rm cut} - (1-\beta^2)^2 \sinh\bar{y}_{\rm cut}\, \cosh\bar{y}_{\rm cut} - 2\tanh\bar{y}_{\rm cut}\Big\}
\end{aligned} \tag{3.18}$$

for the production of a fermion pair.
Besides the kinematical quantities s and β they also depend on the parameter $\bar{y}_{\rm cut}$, which follows from the cut condition by determining the maximum available single rapidity $\bar{y}$:

$$\bar{y}_{\rm cut} = \frac{1}{2}\ln\left(\frac{(1+\beta^2+a_{\rm cut}^2) + 2\sqrt{\beta^2(1+a_{\rm cut}^2) - a_{\rm cut}^2(1-\beta^2)\sinh^2 y}}{(1-\beta^2+a_{\rm cut}^2\, e^{2|y|})}\right) \quad . \tag{3.19}$$

Furthermore, for $\bar{y}_{\rm cut} \le \bar{y}_{\max}$ one has to apply

$$\tilde{\sigma}_{\parallel/\perp}^{\gamma\gamma\to b^+b^-/f^+f^-} = \sigma_{\parallel/\perp}^{\gamma\gamma\to b^+b^-/f^+f^-} \quad , \tag{3.20}$$

because no rapidities larger than the maximum single rapidity (3.13) are allowed.

In Figure 3.4 we show the rapidity distribution for the production of a fermion pair production the rapidity cuts for the ALICE detector. In contrast to Figure 3.3 the rapidity cut reduces the maximum measurable rapidities to about 0.8. The cut–off ensures that both fermions are measured. – For particle states with rather small masses the reduction in the cross section will be pronounced by more than one order of magnitude, but for those particle states with high masses, in which we are mainly interested in, the reduction is not too severe.

3.3 Production of neutral mesons

The two-photon processes in relativistic heavy-ion collisions are of particular interest for meson spectroscopy. Neutral mesons do not couple directly to the two photons, so that the latter probe the quark content of the mesonic final state. This information enters into the two-photon decay width $\Gamma_{B\to\gamma\gamma}$, which forms an essential part of the elementary two-photon production cross section (3.2). Hence, peripheral relativistic heavy-ion collisions offer the possibility to produce resonant heavy meson states, open $q\bar{q}$ (jets) as well as vector meson states and exotic QCD bound states like glueballs, hybrids or even many-quark systems, and to study their electromagnetic properties such as for example decay widths and form factors. – Furthermore, the heavy-ion option perfectly supplements the meson production observed in e^+e^--collisions. There, mesons with an even C quantum number can not be produced directly by e^+e^--annihilation; only by two-photon fusion processes. But then due to the enhancement factor

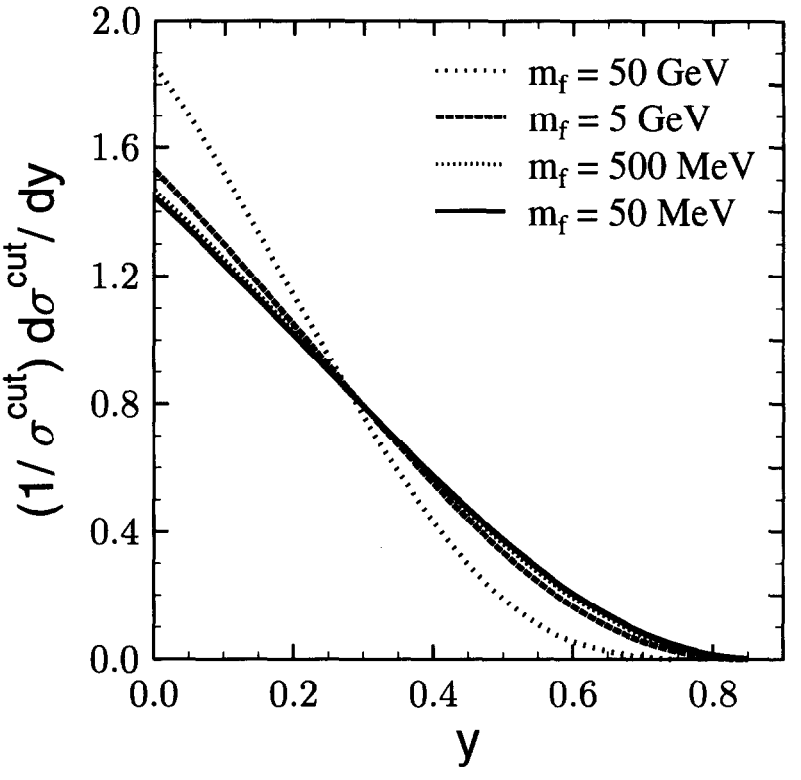

Figure 3.4: Normalized rapidity-dependent reduced cut cross section for fermion production with variable mass m_f in Pb-Pb collisions at LHC energies ($\gamma = 3000$).

Z^4 the $\gamma\gamma$-luminosities occuring in relativistic heavy-ion collisions exceed those achieved at existing or future e^+e^--colliders by many orders of magnitude [27, 110].

As can be deduced from the elementary cross section (3.2) for the production of a neutral boson we have assumed a narrow resonance. Usually a Breit-Wigner form is taken, which results in a resonant delta function for $\Gamma_{\gamma\gamma} \ll \Gamma_{\rm tot}$, where $\Gamma_{\rm tot}$ is the total decay width of the meson. Consequently, one integration in Eq. (2.55) is trivial due to the occuring delta function $\delta(s - m^2)$ in (3.2), where m is the meson mass and $s = 4\omega_1\omega_2$. To estimate the cross sections for the electromagnetic production of neutral mesons in peripheral ultrarelativistic heavy-ion collisions we take the corresponding two-photon decay widths from experimental data [103, 21, 84]; they are listed in Table 3.3 for various mesons.

The lightest meson known in nature is the pion π^0 with a mass of about $m_{\pi^0} = 135$ MeV and a two-photon decay width of $\Gamma_{\gamma\gamma} = 7.7 \pm 0.6$ eV. Because of the relative small mass most of the pions are produced outside the central collision region. Hence, the reduction of the total cross section with respect to the impact parameter cut $b_c = 2R$ has no dramatic consequences and is of the same order of magnitude as the uncertainty in the two-photon decay width. In a Au-Au collision at RHIC energies ($\gamma = 108$) we compute a total cross section of $\sigma^{\rm EPA} = 6.20$ mb and a reduced cross section of $\sigma^{\rm red} = 5.72$ mb, in a Pb-Pb collision at LHC energies ($\gamma = 2750$) we get $\sigma^{\rm EPA} = 44.05$ mb and $\sigma^{\rm red} = 42.94$ mb and in Ca-Ca collision at LHC energies ($\gamma = 3750$) we calculate $\sigma^{\rm EPA} = 0.177$ mb and $\sigma^{\rm red} = 0.167$ mb. In Table 3.2 we summarize the reduced cross sections of various mesons. These results are in fair agreement with similar calculations in Refs. [24, 94]. For the production of a mesonic state with high spin, e.g. $f_4(2050)$ with a decay width of $\Gamma_{\gamma\gamma} = 1.4$ keV, an additional factor of $(2J + 1) = 9$ increases the cross section.

Also heavier mesons which contain c and b quarks, as for example η_c, χ_c and η_b, can be produced in

meson	J^{PC}	m [GeV]	$\Gamma_{\gamma\gamma}$ [keV]
π^0	0^{-+}	0.135	0.0077
η	0^{-+}	0.547	0.51
$\eta'(958)$	0^{-+}	0.958	4.5
$f_0(975)$	0^{++}	0.974	0.25
$f_0(1250)$	0^{++}	1.250	3.4
$f_2(1270)$	2^{++}	1.275	3.19
$a_2(1320)$	2^{++}	1.318	1.14
$\pi_2(1670)$	2^{-+}	1.670	1.41
$f_4(2050)$	4^{++}	2.05	1.4
η_c	0^{-+}	2.98	6.3
χ_c	0^{++}	3.42	5.6
η_b	0^{-+}	9.37	0.4

Table 3.1: Properties of the mesons considered.

meson	$\gamma = 108$, Z = 79		$\gamma = 2750$, Z = 82		$\gamma = 3750$, Z = 20	
	σ^{tot} [μb]	σ^{red} [μb]	σ^{tot} [μb]	σ^{red} [μb]	σ^{tot} [μb]	σ^{red} [μb]
π^0	6198	5721	44056	42937	177	167
η	1528	1285	20689	19897	85.8	78.4
η'	1280	989	25984	24780	110	98.1
$f_0(975)$	126	90.9	2674	2496	11.3	9.88
$f_0(1250)$	488	332	12643	11728	53.8	46.5
f_2	1008	679	26616	24674	113	97.9
a_2	377	252	10304	9542	43.9	37.9
π_2	155	104	5500	5188	23.6	20.6
f_4	38.3	22.1	1758	1605	7.62	6.39
η_c	7.19	3.66	598	555	2.64	2.21
χ_c	3.00	1.36	343	290	1.44	1.15
η_b	$1.4 \cdot 10^{-4}$	$2.0 \cdot 10^{-5}$	0.466	0.406	$1.9 \cdot 10^{-3}$	$1.4 \cdot 10^{-3}$

Table 3.2: Cross sections for the production of different scalar and pseudoscalar mesons in two-photon processes mediated by various heavy-ion collisions at different energies. The second and third column refer to RHIC in the Au+Au-mode, whereas the last four columns refer to LHC in the Pb+Pb- and Ca+Ca-mode, respectively.

peripheral relativistic heavy-ion collisions [23, 67, 69, 94]. For the electromagnetic production of η_b we obtain reduced cross sections of $\sigma^{\text{red}} = 1.951 \cdot 10^{-5}\,\mu b$ for Au-Au collisions at RHIC ($\gamma = 108$), $\sigma^{\text{red}} = 0.406\,\mu b$ for Pb-Pb collisions at LHC ($\gamma = 2750$) and $\sigma^{\text{red}} = 1.356 \cdot 10^{-3}\,\mu b$ for Ca-Ca collisions at LHC ($\gamma = 3750$). With an expected RHIC (Au+Au) luminosity of $L = 2 \cdot 10^{26}$ cm^{-2} sec^{-1} and a beam time of 10^7 sec ($\approx 1/3$ year) we arrive at an integrated luminosity of $\mathcal{L} = 2.0$ /nb, which translates into 0.04 produced η_b per year. For LHC (Pb+Pb) we have $L = 1.6 \cdot 10^{27}$ cm^{-2} sec^{-1} and a beam time of 10^6 sec ($\approx 1/30$ year), which results in $\mathcal{L} = 1.6$ /nb; hence about 650 η_b-mesons can be produced per year. Recently it was discussed to accelerate Ca rather than Pb at LHC because of its much better Z/A ratio, which leads to a higher collision energy with $\gamma = 3750$ and, what is more important, to a more than three orders of magnitude larger luminosity, i.e. $\mathcal{L} = 4000$ / nb [35]. With the calculated reduced cross section for η_c production the expected particle production rate is about 5424 per beam year. This demonstrates that the various heavy-ion modes at LHC offer excellent opportunities to search for unexpected heavy mesons in the mass range of 10 GeV and above.

Other interesting mesons, which could be studied in peripheral ultrarelativistic heavy-ion collisions are glueballs or hybrids, which contain several gluons and quarks. These exotic particles are believed to

exist due to the self coupling of gluons and are predicted by QCD. Of course, pure glueballs consisting only of gluons can not be produced directly by two photons. However, the glueball states can mix with other hadronic states in order to form a new physical state, which in fact may decay into two photons. A definite experimental evidence for their existence has not been provided, but the general point of view is, that glueballs should be produced in reactions involving J/Ψ decays [61]. Several theoretical models describe the physical properties of various glueball states: MIT bag model, potential models, QCD sum rules, lattice gauge theory, flux-tube models, method of vacuum correlators [39, 48]. There are several exotic quantum number combinations J^{PC}, which are kinematically forbidden for $q\bar{q}$ states, e.g. 0^{--}, 0^{+-} and 1^{-+}, and would provide a direct evidence for the existence of glueballs.
Here we consider two glueball candidates, i.e. $\eta(1440)$ with mass m = 1440 MeV, $J^{PC} = 0^{-+}$ and $f_2(1720)$ with mass m = 1713 MeV, $J^{PC} = 2^{++}$ [103]. The two-photon decay width is the relevant quantity entering into the calculation of the reduced cross section. Several groups evaluated the two-photon decay width of $\eta(1440)$ with the above mentioned QCD models; the results are 4.3 keV [38], 2.5 keV [58, 7], 15.9 keV [75] and 3.7 keV [61]. From the experiment one can deduce an upper limit for the two-photon decay width of 3.2 keV [39]. The two-photon decay width of $f_2(1720)$ seems to be in the keV region [39], whereas the experimentel limits are below approximately 0.3 keV [87].
In Fig. 3.5 we present the reduced cross section of the two glueball candidates in dependence on their unknown two-photon decay width for RHIC and LHC energies. As we can see the calculated cross sections vary between 0.001 mb and 100 mb depending on the two-photon decay width. Assuming $\Gamma_{\gamma\gamma}$ = 1 keV about 10^5 glueballs are produced at RHIC with an assumed integrated luminosity of $\mathcal{L}$ = 2.0 / nb, whereas at LHC about 10^7 glueballs per year are produced in Pb-Pb collisions assuming $\mathcal{L}$ = 1.6 / nb and about 10^8 glueballs in Ca-Ca collisions with the higher integrated luminosity of $\mathcal{L}$ = 4000 / nb. These results agree with the ones from Ref. [95].

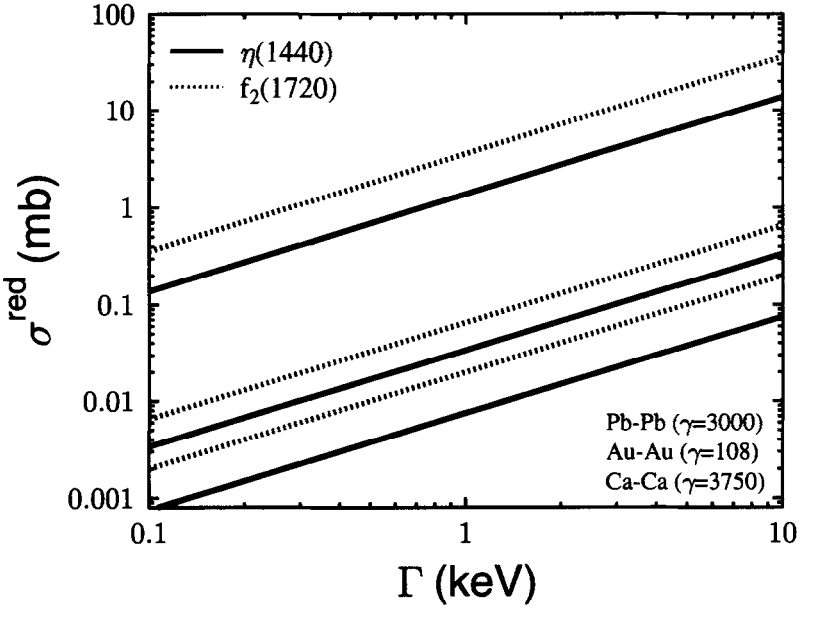

Figure 3.5: Reduced cross sections for the electromagnetic production of the two glueball candidates $\eta(1440)$ and $f_2(1720)$ for different collider systems. From top to bottom the lines refer to LHC in the Pb–mode, RHIC and LHC in the Ca–mode, respectively.

An additional possibility to produce mesons in peripheral ultrarelativistic heavy–ion collisions is given by Pomeron–Pomeron exchange [111]. For the case of light mesonic resonances cross sections are about

one order of magnitude larger compared to the two-photon fusion cross sections [94]. For the formation of charmed mesons they are comparable and for the production of bottom mesons the two-photon fusion process dominates the Pomeron-Pomeron process. The same comparison was performed for the production of glueballs [95].

3.4 Production of charged meson pairs

As for the neutral scalar and pseudoscalar mesons considered before the electromagnetic production of a pair of charged mesons in a relativistic heavy-ion collision would allow to study their properties as electromagnetic formfactors, decay modes and decay widths. – For our estimates we will assume the charged mesons to be pointlike charged bosons; hence, we will also neglect final state interactions. Table 3.3 lists the total and reduced equivalent photon cross sections (2.1) and (3.7), respectively.

meson	mass [GeV]	$\gamma = 108$, Z = 79		$\gamma = 2750$, Z = 82		$\gamma = 3750$, Z = 20	
		σ^{tot} [μb]	σ^{red} [μb]	σ^{tot} [μb]	σ^{red} [μb]	σ^{tot} [μb]	σ^{red} [μb]
$\pi^{\pm}$	0.140	14762	12159	181034	172005	749	676
$K^{\pm}$	0.494	218	145	6985	6452	30.0	25.6
$D^{\pm}$	1.87	0.599	0.219	178	155	0.821	0.609
$D_s^{\pm}$	1.97	0.449	0.158	153	133	0.789	0.522
$B^{\pm}$	5.28	$2.5 \cdot 10^{-4}$	$1.4 \cdot 10^{-5}$	7.64	6.00	0.039	0.021

Table 3.3: Cross sections for the production of different charged meson pairs in two–photon processes occuring in various heavy–ion collisions.

Again, these results demonstrate that only at the LHC facility heavy charged mesons can be produced in reasonable numbers. The rapidity cuts due to the ALICE detector layout mentioned in Section 3.2 further reduce the production rates of the heaviest charged mesons by only a factor of 2–3. With the RHIC collider there is hardly a chance to search for unexpected heavy charged mesons.

3.5 Production of leptons and quarks

The electromagnetic production of leptons in relativistic heavy-ion collisions is interesting for several reasons. On the one hand it can provide informations about the current collider luminosity [35] and on the other hand electromagnetic properties such as a hypothetical magnetic quadrupole moment of $\mu^{\pm}$ and $\tau^{\pm}$ can be studied [10] in order to test the point-like behavior of the leptons [10]. – The violation of unitary in case of e^+e^- pair production has been discussed by many authors; see for example [25, 29, 76]. Unfortunatly, the electromagnetic production of e^+e^- can not be described by the Weizsäcker-Williams approach because of the very low electron mass; we have already discussed this point at the end of Section 2.2. For the electromagnetic production of $\mu^{\pm}$ pairs of course no unitarity violation remains.

fermion	mass [GeV]	$\gamma = 108$, Z = 79		$\gamma = 2750$, Z = 82		$\gamma = 3750$, Z = 20	
		σ^{tot} [μb]	σ^{red} [μb]	σ^{tot} [mb]	σ^{red} [mb]	σ^{tot} [μb]	σ^{red} [μb]
$\mu^{\pm}$	0.1057	208329	177789	2360	2257	12303	11907
$\tau^{\pm}$	1.777	3.77	1.35	1.273	1.116	8.79	8.07
$c^{\pm}$	1.5	5.56	2.25	1.230	1.089	8.27	7.63
$b^{\pm}$	4.5			0.0028	0.0023	0.024	0.021

Table 3.4: Cross sections for the production of various fermion pairs in two–photon processes occuring in relativistic heavy–ion collisions.

In Table 3.4 we list the results for the equivalent photon cross sections (2.1) and (3.7) without and with impact-parameter cuts for the production of $\mu^{\pm}$ and $\tau^{\pm}$ pairs. In terms of production rates per year the reduced cross sections translate into $3.5 \cdot 10^8$ $\mu^{\pm}$ and $2.7 \cdot 10^3$ $\tau^{\pm}$ pairs for Au+Au collisions at RHIC with an integrated luminosity of $\mathcal{L} = 2.0$ / nb, $3.6 \cdot 10^9$ $\mu^{\pm}$ and $1.8 \cdot 10^6$ $\tau^{\pm}$ pairs for Pb+Pb collisions at LHC with an integrated luminosity of $\mathcal{L} = 1.6$ / nb, and $4.8 \cdot 10^{10}$ $\mu^{\pm}$ and $3.2 \cdot 10^7$ $\tau^{\pm}$ pairs for Ca+Ca collisions at LHC with an integrated luminosity of $\mathcal{L} = 4 \cdot 10^3$ / nb. These large numbers demonstrate that the heavy leptons indeed represent a very good measure to extract current beam luminosities.
Table 3.4 also lists the calculated cross sections for open heavy quark-pair production. The lowest order elementary two-photon fusion cross sections (3.5) and (3.6) have been corrected for the adequate electric charges of the quarks and for a factor due to the colour degrees of freedom. These cross sections represent approximate upper bounds for the production of heavy charged mesons; compare with the previous Section on $D^{\pm}$, $D_s^{\pm}$ and $B^{\pm}$ production. – Since the incoming two equivalent photons practically have no transverse momenta, the two quarks are produced with opposite $\vec{p}_{\perp}$. Replacing the elementary two-photon cross section $\sigma_{\gamma\gamma\to q\bar{q}}$ by $\mathrm{d}\sigma_{\gamma\gamma\to q\bar{q}}/\mathrm{d}p_{\perp}$ in the equivalent photon cross section (2.1) we are able to estimate the differential cross section $\mathrm{d}\sigma^{\mathrm{EPA}}_{\gamma\gamma\to q\bar{q}}/\mathrm{d}p_{\perp}$ with respect to the transverse momentum of a single quark. An expression for $\mathrm{d}\sigma_{\gamma\gamma\to q\bar{q}}/\mathrm{d}p_{\perp}$ is straightforwardly derived from the lowest order Feynman diagrams for the two-photon production of a fermion pair. The results for $b\bar{b}$- and $c\bar{c}$-production are depicted in Fig. (3.6). They indicate that for the $b\bar{b}$-case larger transverse momenta are pronounced over small transverse momenta; this is not the case for $c\bar{c}$-production. This effect is explained by the higher mass of the b-quark in connection with the elementary two-photon fusion cross section: for larger masses the fermions are more and more produced away from the beam axis.

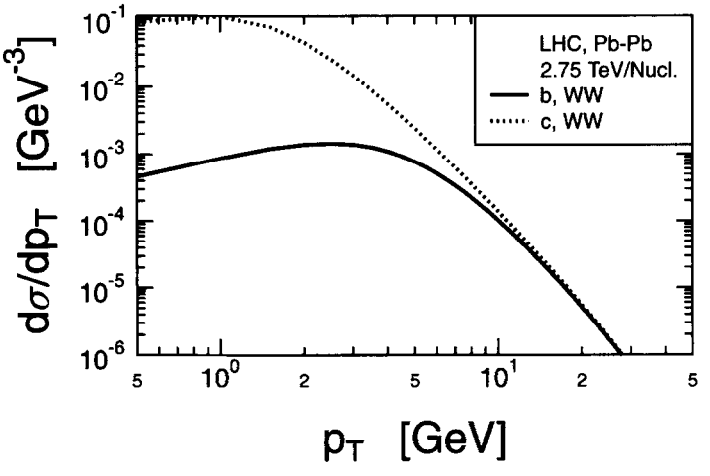

Figure 3.6: Differential equivalent photon cross section $\mathrm{d}\sigma/\mathrm{d}p_T$ for the production of b– and c–quark pairs in heavy-ion collisions at LHC.

QCD corrections for the production of quarks can not be neglected. This is due to the fact, that even in the region of heavy quarks like c– and b– quarks the strong coupling constant α_S can not be considered to be small. In first order perturbation theory the QCD corrections correspond to the emission of a

virtual or a soft real gluon. The modification of the elementary two-photon cross section for the process $\gamma\gamma \to q\bar{q}$ reads [50]:

$$\sigma^{(1)}_{\gamma\gamma\to q\bar{q}}(s_{\gamma\gamma}) = \sigma^{(0)}_{\gamma\gamma\to q\bar{q}}(s_{\gamma\gamma}) + \frac{4\pi\alpha^2 e_q^4 N_c}{s_{\gamma\gamma}}\sqrt{1-\frac{4m^2}{s_{\gamma\gamma}}}\left[1+\frac{4\alpha_s}{3\pi}\left(\frac{\pi^2}{2\sqrt{1-4m^2/s_{\gamma\gamma}}}-5+\frac{\pi^2}{4}\right)\right]. \quad (3.21)$$

Here, $\sigma^{(0)}_{\gamma\gamma\to q\bar{q}}(s_{\gamma\gamma})$ is equal to the lowest order expression given in expressions (3.5) and (3.6). Insertion of (3.21) into the equivalent photon cross section (2.1) leads to an 80% enhancement; this is illustrated in Fig. 3.7.

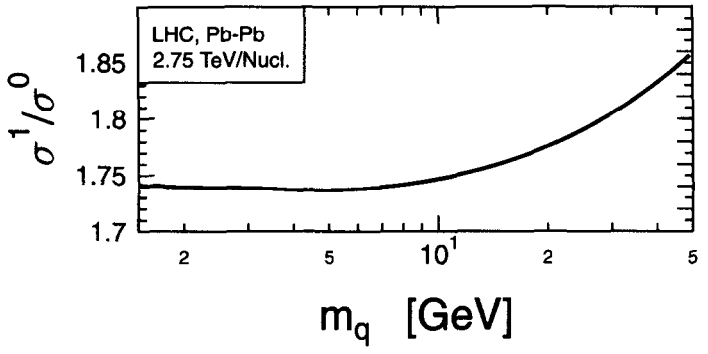

Figure 3.7: The ratio $\sigma^{(1)}(\text{EPA})/\sigma^{(0)}(\text{EPA})$ for quark pair production with variable quark mass m_q in Pb–Pb collisions at 2.75 TeV/Nucleon.

3.6 Production of supersymmetric particles

The concept of supersymmetry (SUSY) [91, 122] provides a promising candidate for the unifying description of all fundamental interactions in nature. SUSY requires a symmetry transformation between bosonic and fermionic degrees of freedom. Consequently bosons like gauge and Higgs bosons have supersymmetric fermionic partners, and fermions such as quarks and leptons have superpartners which are bosons. Except for the particle spin supersymmetric partners carry the same quantum numbers. It is a fundamental prediction of SUSY that every particle is related to a superpartner that differs by half a unit of spin. Furthermore, supersymmetric particles have to be created in pairs. Relatively model independent bounds on the masses of various supersymmetric particles are: $m_{\tilde{\chi}_1^\pm} > 45$ GeV, $m_{\tilde{\chi}_2^\pm} > 99$ GeV, $m_{\tilde{l}} > 45$ GeV ($\tilde{l} = \tilde{e}, \tilde{\mu}, \tilde{\tau}$) [103]. Considerable improvements of these mass bounds are expected from the energy upgrade of LEP II.

The electromagnetic production of supersymmetric particles in relativistic heavy-ion collisions has been studied in Refs. [69, 100, 108, 119]. In lowest order it is the charge of supersymmetric particles which determines the coupling to the two incoming equivalent photons, and it is their mass and the collider energy which determine the production cross sections. Consequently, the expressions for the elementary two-photon cross sections stated in Section 3.1 for the production of bosons and fermions can be applied. Due to the large masses ($m > 50$ GeV) of the supersymmetric particles, the Au+Au collisions at RHIC are not suited to produce such heavy particles. Also at LHC the Pb+Pb mode does not seem to be too

attractive because of its rather low integrated luminosity. Hence, the Ca+Ca mode at LHC appears to be most promising for the production of such heavy particles as supersymmetric particles. Fig. 3.8 depicts the reduced equivalent photon cross section (3.7) for the production of sbosons, which are supersymmetric partners of fermions, and sfermions, which are supersymmetric partners of bosons, in dependence on their assumed mass for Ca+Ca collisions with $\gamma = 3750$. With an integrated luminosity of $\mathcal{L} = 4 \cdot 10^3/\text{nb}$ this would lead to a production of 66 sfermion pairs and 354 sboson pairs with single mass $m = 50$ GeV per year.

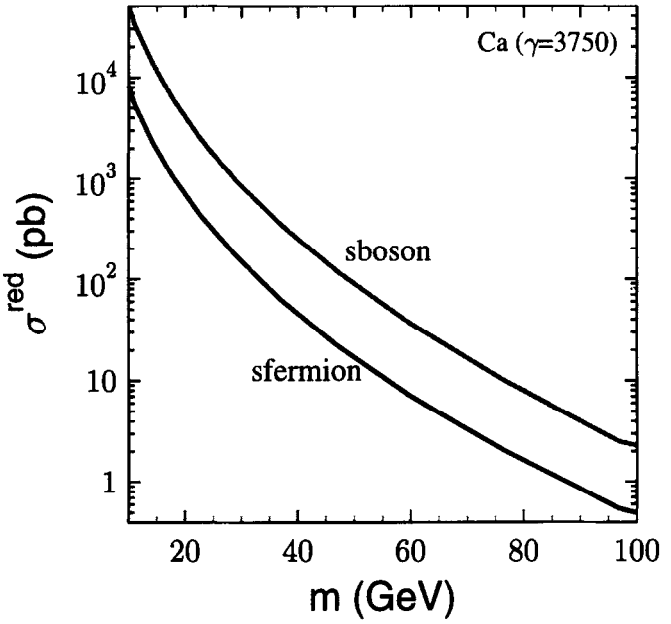

Figure 3.8: Reduced equivalent photon cross section σ_{red} for the production of sbosons and sfermions in dependence on their mass for Ca+Ca collisions at LHC ($\gamma = 3750$).

3.7 Production of Higgs bosons

After the recent detection of the top quark [1, 2], the existence of the Higgs boson remains the last important open question for a validation of the Standard Model. It is searched for at e^+e^- colliders (LEP) and at pp colliders (TEVATRON, LHC). But also relativistic heavy-ion collisions represent an opportunity to produce Higgs bosons via two-photon fusion in a rather clean environment. This option has been discussed intensively [5, 24, 37, 49, 66, 67, 68, 71, 92, 96, 99, 138] It turned out that due to the large background processes $\gamma\gamma \to b\bar{b}$ and $\gamma g \to b\bar{b}$ intermediate mass Higgs signals via the dominating decay into $b\bar{b}$ seem unlikely to be detectable; the production rates are too low. For the Ca+Ca mode at LHC the situation is different as it comes with a much higher luminosity and a slightly higher collision energy per nucleon. This possibility has been discussed in Refs. [101, 132].

The Higgs boson is a scalar boson. In order to calculate the equivalent photon cross sections we need to determine its two-photon decay width, which enters into the elementary two-photon cross section (3.2). It is given by

$$\Gamma_{H\to\gamma\gamma} = \frac{\alpha_{\text{QED}}^2}{8\sqrt{2}\pi^3} G_F m_H^3 |I|^2 , \tag{3.22}$$

where the dimensionless quantity

$$|I| = A_W + A_F + A_S. \tag{3.23}$$

reflects the contributions of W-bosons, fermions and ghosts in the triangle coupling between the Higgs boson and the two photons [22, 119]:

$$\begin{aligned} A_W &= \frac{3m_W^2}{m_H^2} + \frac{2m_W^2}{m_H^2}\left[2 - \frac{3m_W^2}{m_H^2}\right] g\left(\frac{m_W^2}{m_H^2}\right), \\ A_F &= -\sum_f \frac{e_f^2 m_f^2}{m_H^2}\left[2 - \left(\frac{4m_f^2}{m_H^2} - 1\right) g\left(\frac{m_f^2}{m_H^2}\right)\right], \\ A_S &= \frac{1}{2} - \frac{m_W^2}{m_H^2} g\left(\frac{m_W^2}{m_H^2}\right). \end{aligned} \tag{3.24}$$

The function g reads

$$g(x) = \begin{cases} 2\arcsin^2\left(\dfrac{1}{2\sqrt{x}}\right) & x \geq \frac{1}{4} \\ \dfrac{\pi^2}{2} - 2\ln^2\left[\dfrac{1+\sqrt{1-4x}}{2\sqrt{x}}\right] + 2i\pi \ln\left[\dfrac{1+\sqrt{1-4x}}{2\sqrt{x}}\right] & x < \frac{1}{4} \end{cases}. \tag{3.25}$$

The mass of the top quark has been set equal to $m_{\text{top}} = 175$ GeV.
Fig. 3.9 displays the calculated reduced cross section (3.7) for the production of the SM Higgs boson in Ca+Ca collisions at LHC ($\gamma = 3750$) in dependence on its mass. In the intermediate mass regime $m_Z < m_H < 2m_W$ the reduced cross section σ^{red} is approximately around 1 pb. The small enhancement around $m_H \approx 2m_W = 160$ GeV is due to the resonant behaviour of the W-boson running around in the triangle coupling between the Higgs boson and the two photons. Assuming a Higgs mass of $m_H = 100$ GeV and a luminosity of $L = 4 \cdot 10^{30}\text{cm}^{-2}\,\text{s}^{-1}$ with a running time of 10^6 (10^7) s for the Ca+Ca mode at LHC about 4 (40) SM Higgs bosons could be produced per year.

The main decay channel of the intermediate SM Higgs boson is into $b\bar{b}$ [74]. Therefore the irreducible background resulting from $\gamma\gamma \to b\bar{b}$ fusion processes has to be considered. The differential reduced cross section $\mathrm{d}\sigma/\mathrm{d}M_{b\bar{b}}$ with respect to the invariant mass $M_{b\bar{b}} = \sqrt{4\,\omega_1\omega_2}$ can be calculated from Eq. (3.7). With an optimistic mass resolution $\Delta M_{b\bar{b}} = 1$ GeV the Higgs signal surpasses the background signal for masses above 100 GeV. The statistical significance $N_s/\sqrt{N_s + N_b}$ with N_s and N_b denoting the number of signal and background events would be 4.5 for a SM Higgs boson with a 100 GeV mass and a LHC running time of about 1/3 year $= 10^7$ sec. Of course, larger mass resolutions and less beam time reduce the statistical significance.
Besides the direct background $\gamma\gamma \to b\bar{b}$ an additional background results from photon-gluon fusion into $b\bar{b}$ [72, 19]. A photon stemming from the one colliding nucleus penetrates into the other nucleus and fuses with one of its gluons. This process will be described in more detail in Sect. 4.2. The results for the differential cross section $\mathrm{d}\sigma/\mathrm{d}M_{b\bar{b}}$ for $\gamma g \to b\bar{b}$ in a Ca-Ca collision at LHC energies ($\gamma = 3750$) is also plotted in Fig. 3.9 assuming the optimistic mass resolution $\Delta M = 1$ GeV. Apparently this process overwhelms the production signal from the Higgs boson by about three orders of magnitude.
Kinematical cuts like rapidity cuts increase the ratio of signal to background events [132], but in view of the rather small absolute Higgs production rates no severe cuts can be introduced. As a consequence it appears that the intermediate mass SM Higgs boson will only be detectable in Ca+Ca collisions at LHC if a veto trigger on γg fusion events could be found. The difference between photon-photon fusion and photon-gluon fusion processes has to be studied in more detail. Since the $b\bar{b}$ quark pair produced by photon-gluon fusion is a color octet state, the quark pair has to radiate a gluon to become a singlet state. This automatically would lead to the disintegration of the Ca nucleus. Hence, a fragmentation

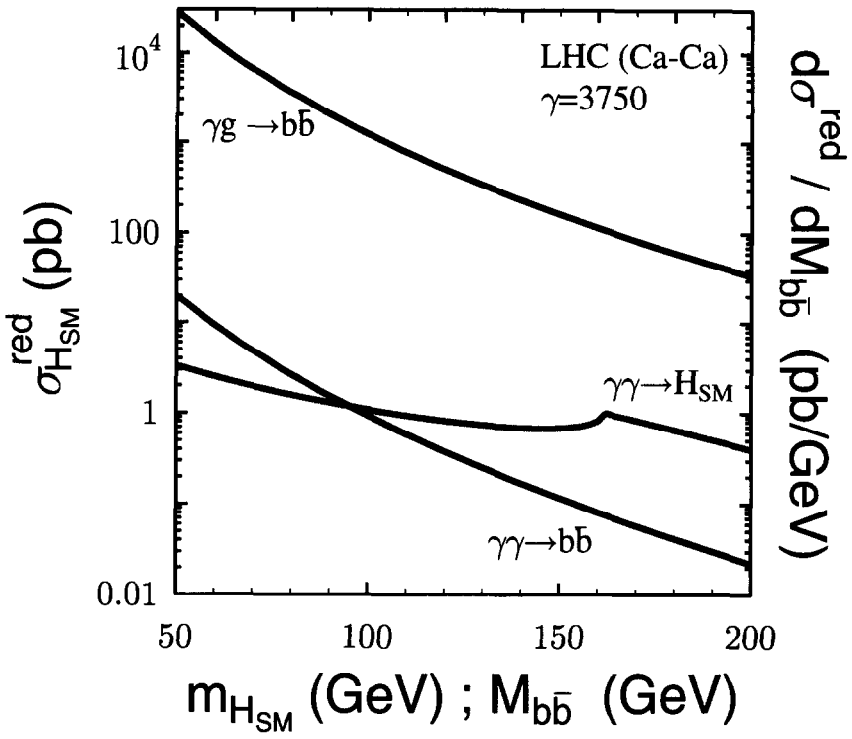

Figure 3.9: Reduced cross section $\sigma_{\rm red}$ for the electromagnetic production of a SM Higgs boson in dependence on its mass for the Ca+Ca collider mode at LHC. Also displayed are the differential cross sections $\mathrm{d}\sigma^{\rm red}/\mathrm{d}M_{b\bar{b}}$ for the two background contributions $\gamma\gamma \to b\bar{b}$ and $\gamma g \to b\bar{b}$.

trigger could be suitable to distinguish between $\gamma\gamma$ and γg processes. Furthermore, the quark pair resulting from two-photon processes in Ca-Ca collisions obtain a maximum total transverse momentum $\Delta p_\perp \approx 2/R \approx 100$ MeV in contrast to $\Delta p_\perp \approx 1/R + 1/r \approx 250$ MeV (r and R denote the radii of the nucleon and the nucleus, respectively) for photon-gluon processes. This has to be studied in more detail.

The overall situation might change if the production of Higgs bosons required from the minimal supersymmetric extension of the standard model (MSSM) is considered. The electromagnetic production of intermediate mass MSSM Higgs boson may be enhanced over the SM Higgs boson by a factor of about 10 for certain choices of the free model parameters [69]. Therefore the number of $b\bar{b}$ resulting from produced MSSM Higgs Boson decays is enhanced for these specific parameter choices with respect to the SM Higgs signal. On the other hand, the background of directly produced $b\bar{b}$ remains unaffected.

Chapter 4

Single-photon induced processes in relativistic heavy-ion collisions

So far we have discussed two-photon induced particle production processes in relativistic heavy-ion collisions. As the two equivalent photon swarms collide one photon steming from the first swarm fuses with another photon emerging of the second swarm to produce purely electromagnetically the exotic particles. But these are not the only electromagnetic processes occuring in peripheral heavy-ion collisions. Depending on its energy an equivalent photon associated with one nucleus might interact with the other nucleus as a whole, or might penetrate into the latter to interact with one of its nucleons or even with one of its partons. In this Section we will discuss two processes falling into this category: Coulomb dissociation and photon-gluon fusion.
The strong Lorentz-contracted electromagnetic field of one of the nuclei leads to the dissociation of some nucleons or to the disintegration of the other nucleus. This process is of great importance for the design of the relativistic heavy-ion colliders RHIC and LHC as it implies limits to the beam luminosities of the heavy-ion mode with Au and Pb nuclei, respectively.
The fusion of a photon and a gluon leads to the production of a pair of heavy quarks. Its invariant mass spectrum provides direct information about the gluon distribution of a nucleon within a nuclear medium.

4.1 Coulomb dissociation

To describe the interaction of the strong transverse electromagnetic field being associated with nucleus B with the other nucleus A, which leads to its dissociation (or disintegration), we again employ the equivalent photon approach. The cross section for the Coulomb dissociation process can be estimated according to

$$\sigma_{\rm dis} = \int\limits_{b\geq 2R} 2\pi b\, {\rm d}b \int {\rm d}\omega\; n_B(\omega, b)\; \sigma_{\gamma A}(\omega) = \int\limits_{b\geq 2R} P(b)\; 2\pi b\, {\rm d}b \quad . \tag{4.1}$$

Here only peripheral collisions ($b \geq 2R$) are considered in order to avoid any direct hadronic interaction. The equivalent photon spectrum $n(\omega, b)$ indicates the number of real photons with energy ω at the distance b, which represents the impact parameter. The photon spectrum is given by Eq. (2.28) and is displayed in Figure 4.1. Due to its asymptotic behavior (2.29) $n(\omega, b)$ is multiplied with ω and b^2; this explains that the depicted quantity $\omega b^2\, n(\omega, b)/Z^2$ is constant in the low ω-regime and does not depend on the collider energy. Here the effective Lorentz factor $\gamma_{\rm eff}$ taken in the rest frame of the collision partner A enters. It is related to γ in the c.m. system of the two colliding heavy ions by a Lorentz

transformation:

$$\gamma_{\text{eff}} = 2\gamma^2 - 1 \quad . \tag{4.2}$$

This Lorentz boost leads to a tremendous increase of the maximum photon frequency $\omega_{\text{max}} = \gamma_{\text{eff}}/R$ contained in the electromagnetic field of the first nucleus; for Au–Au collisions at RHIC ($\gamma = 108$) we find $\omega_{\text{max}} \approx 500$ GeV and for Pb–Pb collisions at LHC ($\gamma = 2750$) we get $\omega_{\text{max}} \approx 400$ TeV.

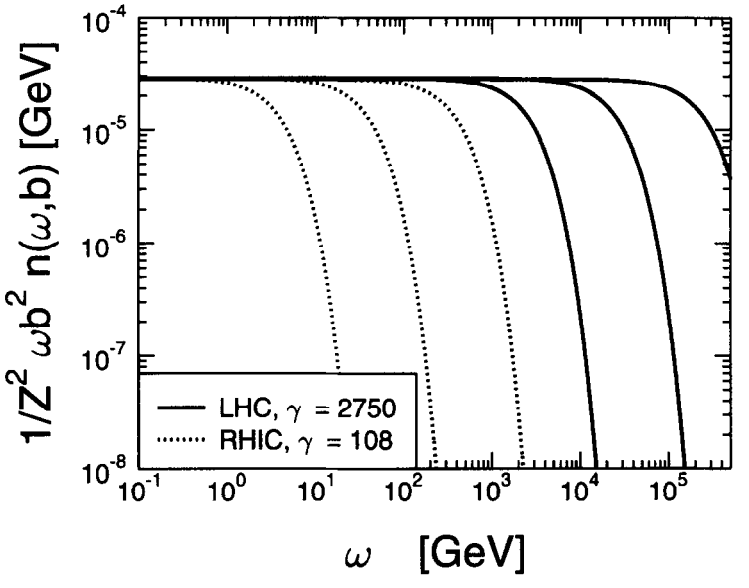

Figure 4.1: Equivalent photon–distributions in the rest frame of nucleus A are displayed for RHIC ($Z = 79, \gamma = 108$; dotted lines) and LHC ($Z = 82, \gamma = 2750$; solid lines). The upper lines refer to $b = 10$ fm, the middle ones to $b = 100$ fm and the lower ones to $b = 1000$ fm.

A modified equivalent photon spectrum was suggested [19, 72], which takes the impact parameter of the single constituent of the nuclei into account because of the strong dependence of the equivalent photon distribution on the impact parameter for close collisions; consult the next Subsection. But as estimated, impact parameters up to 1000 Å are contributing to the dissociation cross section for LHC energies. Therefore the simple form of the equivalent photon distribution can be used.

As far as they are available we will use experimental data for the elementary photo–absorption cross section [11]. At least two sets of data are existing, one is for Pb up to a photon energy of 80 GeV, the other one is for Au up to an energy of 9.5 GeV. So we will use the Pb data scaled down by the mass ratio $\frac{197}{208}$ for gold. In order to take higher energetic photons with $\omega > 80$ GeV into account the photon-nucleus cross section has to be extrapolated up to $\omega \approx \gamma/R$. At these high energies the photon does not interact purely electromagnetically with the nucleus but also by its hadronic structure [117] resulting from vacuum fluctuation of the photon such as $\gamma \to \pi^+\pi^-, \rho, \omega, q\bar{q}, q\bar{q}g$, etc. [133]. To extrapolate $\sigma_{\gamma A}$ we adopt the proton absorption cross section measured extensively for $\omega \leq 200$ GeV and for $\omega \approx 20$ TeV at HERA [136], which results in the actually applied fit

$$\sigma_{\gamma A} = A_{\text{eff}} \left(X \cdot s^{\varepsilon} + Y \cdot s^{-\eta} \right) \quad . \tag{4.3}$$

$s \approx 2M_p\omega$ is the c.m. energy in the γp system, where M_p denotes the proton mass and the used parameters are $\epsilon = 0.0808$, $\eta = 0.4525$, $X = 0.06$ mb/GeV^2 and $Y = 0.16$ mb/GeV^2. $A_{\rm eff} = A^{0.9}$ takes nuclear shadowing into account [59].

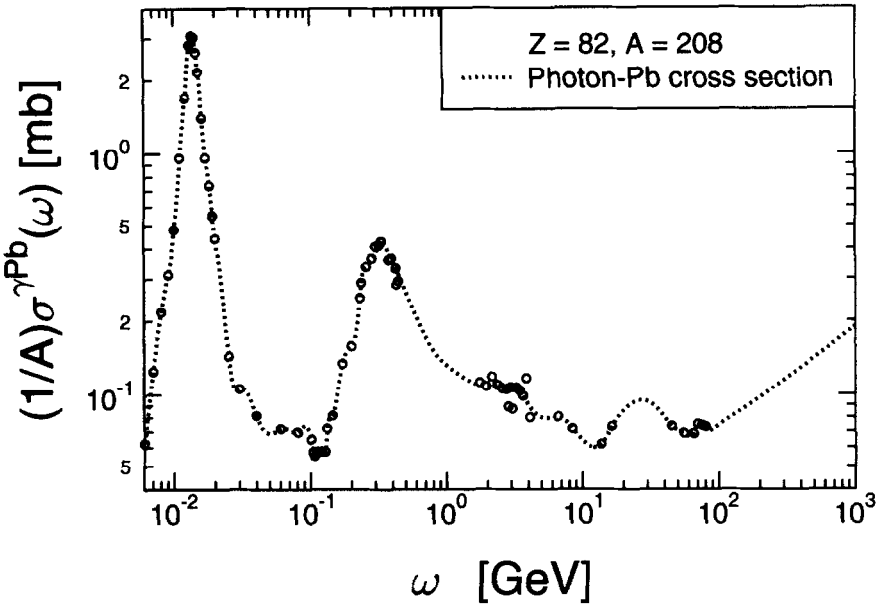

Figure 4.2: The photo–absorption cross section used (dashed line) in comparison with experimental data (little circles). For photon–energies larger than 80 GeV we used (4.3)

The photo–absorption cross section *per nucleon* is displayed in Fig. 4.2. It consists of a superposition of different multipolarities. The main contribution to the dissociation results from the excitation of the giant resonance in the energy region from 6 to 40 MeV, which predominantly leads to the emission of single nucleons. These processes will occur even if the two nuclei pass each other at large distances. At energies from 40 MeV to 2 GeV the formation of quasi–deuterons and Δ–resonances becomes important. At even higher energies the hadronic structure of photons determines the photoabsorption cross section. Some care has to be taken with the straightforward insertion of the interpolated photo absorption cross section $\sigma_{\gamma A}(\omega)$ into the expression (4.1) for the dissociation cross section $\sigma_{\rm dis}$. For small impact parameters the Coulomb dissociation probability $P(b)$ exceeds its maximum value one [127] and therefore violates unitarity, which would be restored by taking into account higher-order corrections like multiphoton exchange. Whenever $P(b)$ becomes larger than one, we artificially reduce it down to one; this procedure has only a minor impact on the dissociation cross section $\sigma_{\rm dis}$.

In Table 4.1 we list the calculated total Coulomb dissociation cross sections for the various heavy-ion collider modes. In order to estimate the contributions from very high-energetic photons ($\omega \geq 80$ GeV) we distinguish between a cross section $\sigma^{\rm uni}_{\rm diss,+}$, which integrates over the total photon frequency spectrum, and $\sigma^{\rm uni}_{\rm diss}$, which integrates only over photon energies up to $\omega = 80$ GeV. Both cross sections have been unitarized, i.e. $P(b) \leq 1$. For the Au-Au mode at RHIC the high energetic equivalent photons practically have no influence on the dissociation cross section; our calculated value is in accordance with

the result of Ref. [109]. On the other hand for the Pb-Pb mode at LHC the photons with $\omega \geq 80$ GeV increase $\sigma_{\rm dis}$ by about 10% from 192 b to 214 b. Results presented in Refs. [19, 23] are systematically lower as they have neglected contributions from the quasi-deuteron region.

Collider	Ions	Energy	$\sigma^{\rm uni}_{\rm dis,+}$ (b)	$\sigma^{\rm uni}_{\rm dis}$ (b)
RHIC	Au–Au	108 GeV/Nucl.	88.15	87.62
LHC	Pb–Pb	2.75 TeV/Nucl.	214.04	191.84
LHC	Ca–Ca	3.75 TeV/Nucl.	2.77	2.40

Table 4.1: Dissociation cross sections for different nuclei colliding at different accelerators. The left column refers to cross sections including the high–energy tail of the photo–absorption cross section of Fig. 4.2, the right column is without this, excluding photon–energies of more than 80 GeV.

These calculations of the dissociation cross sections imply some serious consequences for the heavy-ion collider luminosities. A new calculation of the expected luminosities was presented in Ref. [35]. Taking into account the three contributions which reduce the heavy-ion luminosity, i.e. Coulomb dissociation, electron-positron pair production with caputure and nuclear interactions, the luminosity is expected to be $L = 1.6 \cdot 10^{27}$ cm^{-2} s^{-1} for the Pb-Pb mode and $L = 4.0 \cdot 10^{30}$ cm^{-2} s^{-1} for the Ca-Ca mode at LHC. These results imply that in comparison with the Pb-Pb mode the Ca-Ca mode is more attractive for two-photon fusion and photon-gluon processes in relativistic heavy-ion collisions. Because of the lower charge of Ca compared to Pb, the cross sections for two-photon fusion processes are smaller by a factor of $(20/82)^4 \approx 0.0035$, but on the other hand the more than three orders of magnitude difference in the expected luminosity will lead to about one order of magnitude larger production rates. Furthermore, due to the better Z/A ratio the energy per nucleon is larger for Ca in comparison to Pb. This finding let also to a reconsideration of the electromagnetic Higgs boson production in Ca-Ca collisions [101, 132].

4.2 Deduction of the in–medium gluon distribution via photon-gluon fusion

The production of $c\bar{c}$ and $b\bar{b}$ quark pairs by single photon-gluon fusion processes in peripheral ultrarelativistic heavy-ion collisions offers the possibility to extract informations about the gluon distribution in a nuclear medium [19, 72, 79]. This process has also been suggested for the direct measurement of the gluon distribution of a nucleon in ep collision at HERA [60]. Measuring the gluon distribution of a bound nucleon utilizing the photon-gluon fusion process $\gamma g \to q\bar{q}$ in ultrarelativistic heavy-ion collisions might represent an important supplement for a better understanding of the original EMC effect [103]. Thiw gluon distribution could be quite different form what it is in free nucleons.
The formalism to describe photon-gluon fusion is in close analogy to the impact-parameter dependent equivalent photon method. Two heavy ions moving on classical straight trajectories collide with an impact parameter b. The strong Lorentz-contracted transverse electromagnetic field of one of the two nuclei can be substituted by a swarm of equivalent photons. One of these photons penetrates into the other nucleus and interacts with one of its gluons, which are described by a gluon distribution function. The photon-gluon fusion cross section can be calculated by [19, 72]

$$\sigma = \int_{2R}^{\infty} {\rm d}^2 b \int {\rm d}\omega_1 \int {\rm d}\omega_2 \; \tilde{n}(\omega_1, b) \; g(\omega_2) \, \sigma_{\gamma g \to q\bar{q}}(s) \, , \tag{4.4}$$

where

$$\tilde{n}(\omega_1, b) = \int {\rm d}\vec{x}_\perp \; N(\vec{x}_\perp) \; n(\omega_1, \vec{x}_\perp - \vec{b}) \, . \tag{4.5}$$

$N(\vec{x}_\perp)$ denotes the nucleon number distribution projected onto the transverse plane.

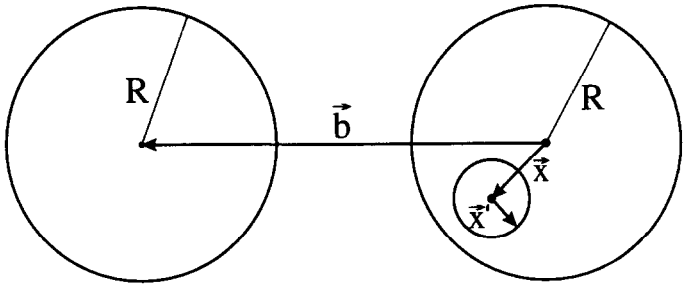

Figure 4.3: Impact parameter, nucleon and gluon coordinates in the transverse reaction plane for photon-gluon-processes in ultrarelativistic heavy-ion collisions.

The expression (4.4) can be deduced from a more complicated approach presented in [72], where the mutual polarisation of the photon and gluon are taken into account in analogy with the impact-parameter dependent equivalent photon cross section in Eq. (2.55): The polarisation dependent two-photon distribution functions are replaced by a polarisation dependent photon-gluon distribution function:

$$\tilde{n}_{\parallel}(\omega_1,\omega_2;\vec{b}) = \int \mathrm{d}\vec{x}_\perp \int \mathrm{d}\vec{x}'_\perp \, n(\omega_1, \vec{x}_\perp + \vec{x}'_\perp - \vec{b})\, N(\vec{x}_\perp)\; g(\omega_2, \vec{x}'_\perp) \left(\frac{(\vec{x}_\perp + \vec{x}'_\perp - \vec{b})\cdot \vec{x}'_\perp}{|\vec{x}_\perp + \vec{x}'_\perp - \vec{b}||\vec{x}'_\perp|} \right)^2 . \tag{4.6}$$

Here $\vec{x}'_\perp$ represents the transverse distance of the gluon to the center of the nucleon, which has the distance $\vec{x}_\perp$ to the center of the nucleus in the transverse plane; see Fig. 4.3. $g(\omega_2, \vec{x}'_\perp)$ is the gluon distribution function for a nucleon, which can be parametized by

$$g(\omega_2, \vec{x}'_\perp) = g(\omega_2)\; h(|\vec{x}'_\perp|)\,, \tag{4.7}$$

with $\int \mathrm{d}\vec{x}'_\perp h(|\vec{x}'_\perp|) = 1$. As a parametrisation for $h(|\vec{x}'_\perp|)$ one can use a gaussian distribution

$$h(|\vec{x}'_\perp|) = \frac{1}{\pi r^2} \exp\left(-\frac{\vec{x}'^2_\perp}{r^2} \right) \quad , \tag{4.8}$$

where r represents the radius of a nucleon. If only peripheral collisions are considered,

$$|\vec{x}'_\perp| \ll |\vec{x}_\perp - \vec{b}| \tag{4.9}$$

holds, and the photon-gluon distribution loses its polarisation dependence. As a result Eq. (4.4) is deduced.

The elementary photon-gluon cross section $\sigma_{\gamma g \to q\bar{q}}$ entering in (4.4) has the same structure as the two-photon cross sections (3.5) and (3.6); we only have to replace

$$3\, \frac{2\pi\alpha^2 e_q^4}{s} \to \frac{2\pi\alpha\alpha_s e_q^2}{2\, s}\,. \tag{4.10}$$

The factor three reflects the color degree of freedom of the quarks in the final state produced by a colour singlet, the two photons. e_q denotes the electric charge of the quarks. The running coupling constant α_s is evaluated at the invariant mass scale $Q^2 = M^2$ with

$$\alpha_s = \frac{12\,\pi}{(33 - 2n_f)\, \ln(\frac{M^2}{\Lambda^2})}\,, \tag{4.11}$$

where n_f represents the number of active flavors ($n_f = 4$) and $\Lambda = 0.2$ GeV.
We discuss three different variations for the nucleon number density $N(\vec{x}_\perp)$. A very crude ansatz is that of a point nucleus with

$$N_{\rm pn}(\vec{x}_\perp) = A_{\rm eff}\,\delta(\vec{x}_\perp)\,, \tag{4.12}$$

where $A_{\rm eff}$ simulates nuclear shadowing [59]. A more realistic distribution, which was adopted in Refs. [19, 72], is represented by the projection of a uniform sphere onto the transverse plane:

$$N_{\rm hs}(\vec{x}_\perp) = 2\sqrt{R^2 - \vec{x}_\perp^{\,2}}\;\frac{A_{\rm eff}}{\frac{4\pi}{3}R^3}\quad . \tag{4.13}$$

In order to introduce a quantity such as an absorption length the following parametrisation of the nuclear number distribution has been proposed [72]:

$$N_{\rm cs}(\vec{x}_\perp) = \frac{A}{\frac{4\pi}{3}R^3}\begin{cases} 2\sqrt{R^2 - \vec{x}_\perp^{\,2}} & \text{for}\quad R \geq |\vec{x}_\perp| \geq \sqrt{R^2 - r_{12}/4} \\ r_{12} & \text{for}\quad 0 \leq |\vec{x}_\perp| \leq \sqrt{R^2 - r_{12}/4} \end{cases}\quad . \tag{4.14}$$

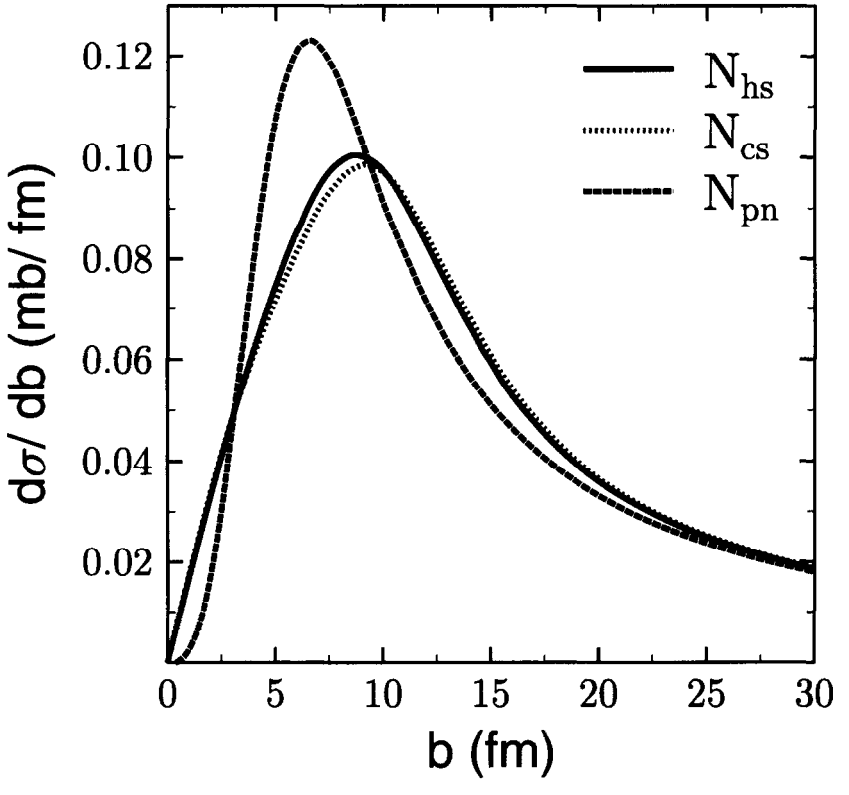

Figure 4.4: The influence of the three different nuclear mass distributions onto the differential cross section $d\sigma/db$ for photon-gluon fusion into $b\bar{b}$ pairs; Pb-Pb collisions at LHC energies ($\gamma = 3000$) have been considered The subscripts *hs*, *cs* and *pn* denote the hard sphere, the cut sphere and the point nucleus forms, respectively.

Here a sphere with radius R is cut from another sphere with the same radius at a center distance r_{12} and the leftover is projected onto the transverse plane. The distance $r_{12} = 0.829 \cdot R$, which simulates the absorption length, is determined such that $\int N_{\rm cs}(\vec{x}_\perp)\,d\vec{x}_\perp = A_{\rm eff}$. This expression for the nuclear

number density is still very simple, e.g., it does not account for a frequency dependence of the absorption lenght.

The dependence of the differential cross section (4.4) with respect to impact parameter on the three different parametrisations of the nuclear number distributions is shown in Figure 4.4. Here, the production of a $b\bar{b}$ pair with $m_b = 4.5$ GeV is considered. For the gluon distribution $g(\omega)$ we use the one of Ref. [98] and for the photon distribution $n(\omega, b)$ we take a Gaussian nuclear charge formfactor. Compared to the pointlike nuclear number distribution (4.12) the impact-parameter dependent cross sections with the distributions (4.13) or (4.14) lead to somewhat larger values for 10 fm $< b <$ 30 fm. This is due to the fact that nucleons closer to the electromagnetic source interact more with equivalent photons of larger energies than more distant nucleons, which encounter equivalent photons of lower energies. Since the equivalent photon spectrum is strongly nonlinear for this impact–parameter region, the contribution of adjacent nucleons to $d\sigma/db$ dominates over those of the more distant nucleons by up to about 20%. As expected, for larger impact parameters the cross sections converge for the three parametrisations of the nucleon number density. Since only peripheral collisions will be considered further the deviations for $b \geq 2R$ are irrelevant. For the remaining calculations we will rely upon the "cut sphere" ansatz (4.14). It is more convenient to employ the rapidity $y = \frac{1}{2}\ln(\omega_1/\omega_2)$ and the invariant mass $M = \sqrt{4\ \omega_1\omega_2}$ of the photon-gluon system instead of the photon and gluon energies ω_1 and ω_2. Then the cross section (4.4) becomes

$$\sigma = \int_{2R}^{\infty} \mathrm{d}^2b \int_{2m_q}^{\infty} \frac{M}{2}\mathrm{d}M \int_{\ln\frac{M}{2p}}^{\infty} \mathrm{d}y\ g\left(\frac{M}{2}e^{-y}\right)\ \tilde{n}\left(\frac{M}{2}e^{y}, b\right)\ \sigma_{\gamma g\to q\bar{q}}(s)\,. \tag{4.15}$$

p is the momentum of the nucleon, which is much larger than the invariant mass. This expression demonstrates explicitly that the double differential cross section $\frac{\mathrm{d}^2\sigma}{\mathrm{d}M\mathrm{d}y}$ with respect to the invariant mass and to the center–of–momentum rapidity of the produced quark pair is directly proportional to the gluon distribution function $g(\omega_2)$ of a nucleon inside a nucleus. It could be directly deduced if the double differential cross section is determined experimentally.

In Fig. 4.5 the double differential cross section $\frac{\mathrm{d}^2\sigma}{\mathrm{d}M\mathrm{d}y}$ is depicted for photon-gluon fusion into a $b\bar{b}$-quark pair in a peripheral Pb-Pb collision at LHC energies ($\gamma = 3000$). It is assumed that the gluon is emerging from the nucleus moving to the "left", i.e. with negative rapidity. Hence, $\frac{\mathrm{d}^2\sigma}{\mathrm{d}M\mathrm{d}y}$ is not symmetric around central rapidity $y = 0$. The main contribution results from small negative rapidities, because on average the gluons carry more momentum than the equivalent photons. With an assumed LHC (Pb-Pb mode) luminosity of $L = 2 \cdot 10^{27}\ \mathrm{cm}^{-2}\,\mathrm{sec}^{-1}$, a running time of $T = 10^6$ sec/year, a rapidity window of $\Delta y = 0.1$ and an invariant mass resolution of $\Delta M = 1$ GeV the contour line of 10 μb/GeV in Fig. 4.5 for the double differential cross section translates into a production rate of $2 \cdot 10^3$ $b\bar{b}$-pairs per year. Usually the gluon distribution is parametrized in terms of the dimensionless variable $x = \omega_2/p = \frac{M}{2p}e^{-y}$, so that $g(\omega_2) = g(x = \frac{\omega_2}{p})/p$. For Pb+Pb collisions at LHC energies the nucleon momentum is equal to $p = 3000$ GeV; hence $x = \frac{M}{6000\ \mathrm{GeV}}e^{-y}$. Then the two points ($y = -3.5, M = 15$ GeV) and ($y = 1.5, M = 15$ GeV) on the contour line 10 μbarn/GeV correspond to x-values of $x = 0.083$ and $x = 0.00056$. The points ($y = -4, M = 20$ GeV), ($y = -2, M = 35$ GeV), ($y = 0, M = 35$ GeV) and ($y = 2, M = 20$ GeV), all belonging to the contour line 1 μbarn/GeV, correspond to x-values of $x = 0.182$, 0.043, 0.0058 and 0.00045, respectively. This demonstrates that the photon-gluon fusion process into a $b\bar{b}$ quark pair occuring in peripheral ultrarelativistic heavy-ion collisions at LHC represents a promising tool to determine the low x and very low x regime, i.e. $0.0005 \leq x \leq 0.15$, of the gluon distribution in a nuclear medium.

The expression (4.15) assumes that we know from which nucleus the gluon originates. In practice this will be hard to distinguish. The initial gluon and hence the produced quarks in the final state represent a color octet. Color conservation will be guaranteed by the exchange of at least one soft gluon with the participating nucleus, which therefore will break into fragments. This would be a clear trigger for the nucleus, from where the gluon emerges. On the other hand, the electromagnetic dissociation cross section of Pb is about 220 barn for LHC energies [127] and thus this process is undistinguishable from

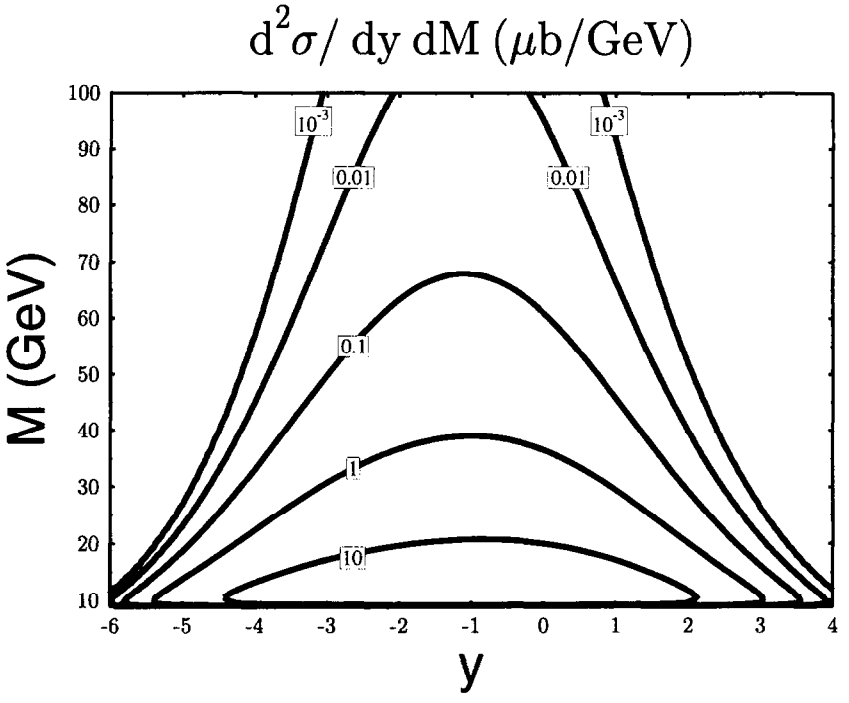

Figure 4.5: Double differential cross section $\frac{\mathrm{d}^2\sigma}{\mathrm{d}M\,\mathrm{d}y}$ for γg-fusion into $b\bar{b}$ pairs production in a Pb-Pb collision at LHC energies ($\gamma = 3000$); here the gluon originates from the nucleus moving with a negative rapidity.

the fragmentation process resulting from color conservation. For Ca+Ca collisions it might be possible to detect from which nucleus the gluon comes, since the electromagnetic dissociation cross section is about two orders of magnitude lower than in Pb-Pb collisions.
In case it is not possible to identify the nucleus from which the gluon originates, the cross section (4.15) has to be symmetrized:

$$\frac{\mathrm{d}^2\tilde{\sigma}}{\mathrm{d}M\mathrm{d}y} = g(\omega_2)\,\xi(\omega_1,\omega_2) + g(\omega_1)\,\xi(\omega_2,\omega_1) \tag{4.16}$$

with

$$\xi(\omega_1,\omega_2) = \int_{2R}^{\infty} \mathrm{d}^2b\;\tilde{n}(\omega_1,b)\;\sigma_{\gamma g\to q\bar{q}}(s=4\omega_1\omega_2) \quad . \tag{4.17}$$

As one can verify from (4.16) the double differential cross section $\mathrm{d}^2\tilde{\sigma}/(\mathrm{d}M\mathrm{d}y)$ is no longer proportional to the in-medium gluon distribution, since in general $\omega_1 \neq \omega_2$. Only if $\omega_1 = \omega_2$ is considered, the gluon distribution again can be directly extracted from the measured double differential cross sections. This particular case corresponds to zero-rapidity: $y = 1/2\ln(\omega_1/\omega_2) = 0$.
In Figure 4.6 the symmetric double differential cross section $\left.\frac{\mathrm{d}^2\tilde{\sigma}}{\mathrm{d}M\mathrm{d}y}\right|_{y=0}$ is displayed in dependence on the invariant mass M of the produced $b\bar{b}$ quark pair in a Pb-Pb collision at LHC energies. Various gluon distributions have been used: two old parametrisations of Duke and Owens [51] and a new parametrisation of Owens [98]; the resolution momentum has been set equal to $Q^2 = M^2$. Also the last parametrisation has been used again, but with a rescaled $Q^2 = 2M^2$; this has been suggested in Ref. [89] for the in-medium gluon distribution. For small invariant masses M the different parametrisations for the gluon distribution result in variations for $\left.\frac{\mathrm{d}^2\tilde{\sigma}}{\mathrm{d}M\mathrm{d}y}\right|_{y=0}$ by a factor of 1.5; for larger invariant masses the deviations are smaller. - For invariant masses in the range 10 GeV $\leq M \leq$ 50 GeV, which corresponds to the range $0.0017 \leq x \leq 0.0083$ for the dimensionless variable x used for the gluon momentum, the values of the double differential cross section $\left.\frac{\mathrm{d}^2\tilde{\sigma}}{\mathrm{d}M\mathrm{d}y}\right|_{y=0}$ lie in the range of 100 μbarn/GeV down

to 0.5 μbarn/GeV. With the assumed LHC luminosity $L = 2 \cdot 10^{27}$ cm^{-2} sec^{-1} and a running time $T = 10^6$ sec/year for the Pb+Pb mode, a rapidity width of $\Delta y = 0.1$ and an invariant mass resolution of $\Delta M = 1$ GeV, these cross sections translate into $2 \cdot 10^4 - 10^2$ produced $b\bar{b}$ quark pairs per year, which should be sufficient to get reasonable statistics. The statistics might even be increased if cross checks for $(\Delta y, \Delta M)$ windows away from zero rapidity are applied [72].

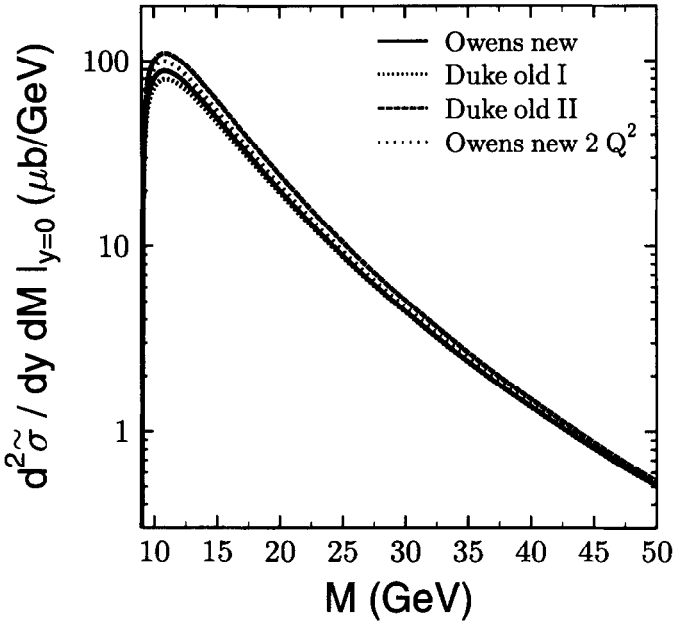

Figure 4.6: Double differential cross section $\frac{d^2\tilde{\sigma}}{dMdy}\Big|_{y=0}$ for γg-fusion into $b\bar{b}$ pairs production in Pb-Pb collisions at LHC energies ($\gamma = 3000$) for various parametrisations of the gluon distribution; the origin of the ingoing gluon is not known.

If one considers the differential cross section $\mathrm{d}\tilde{\sigma}/\mathrm{d}M$ [79, 19] instead of the double differential cross section $\frac{d^2\tilde{\sigma}}{dMdy}\Big|_{y=0}$ the gluon distribution can not directly be deduced. The gluon distribution enters into the calculations as an input parametrisation and one has to compare the experimental results with the calculated output. In Fig. 4.7 the various gluon distributions are taken into account. They lead to about the same variations as in Figure 4.6. On the other hand, due to the full rapidity coverage the production rates are enhanced by a factor of about 50 with respect to the analysis at $y = 0$. The differential cross section $\mathrm{d}\tilde{\sigma}/\mathrm{d}M$ can be used to perform another cross check for the measured in-medium gluon distribution, which can be deduced from the double differential cross sections $\frac{d^2\tilde{\sigma}}{dMdy}\Big|_{y=0}$.
Two important consequences should be noted at the end: First, the produced quark–antiquark pair is in the colour-octet state of the gluon. Before leaving the nucleus or the reaction region, there should be an emission of at least one soft gluon. This is the mechanism to provide colour blanching. Even a soft gluon radiated by this colour source changes of course the reaction kinematics and changes the rapidity and invariant mass assignment. In the same way the hadronisation of the two quarks – a soft reaction as well – changes the results. So far those problems have not been taken into account properly and are still open for further investigations. – Second, in our model we simulated nuclear effects on the gluon-distribution only by the introduction of an effective nucleon number. This represents a rather simple modeling of such effects as for example nuclear shadowing.

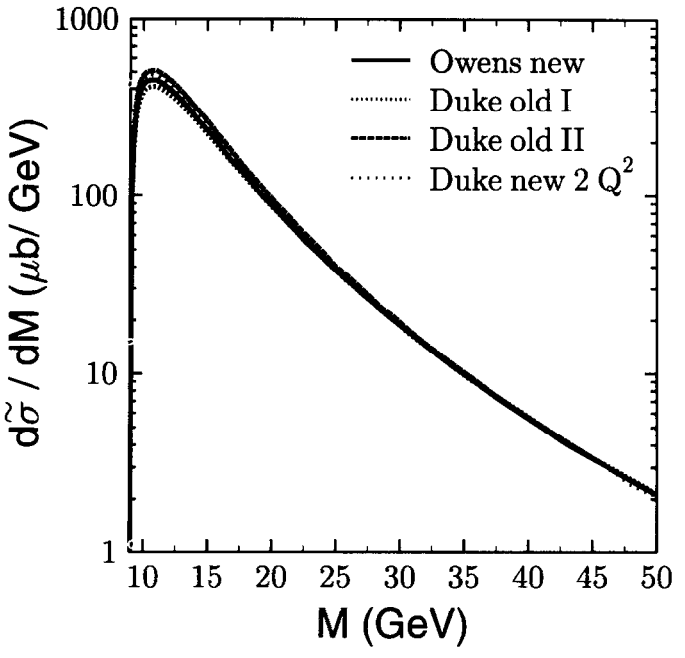

Figure 4.7: Same as Fig. 4.6, but for $\mathrm{d}\tilde{\sigma}/\mathrm{d}M$.

The presented calculations are only premature to deduce the gluon distribution from experiment. More elaborated studies should be performed, which take high order corrections of the quark-pair production into account [60]. The production of $c\bar{c}$ instead of $b\bar{b}$ allows for further extensions for the accessible x-range of the nuclear gluon distribution. The study should also be performed for lighter nuclei, e.g. Ca-Ca collisions, which would lead to a loss of a factor $(Z^2 A_{\mathrm{eff}})_{\mathrm{Ca}}/(Z^2 A_{\mathrm{eff}})_{\mathrm{Pb}} \approx 1/60$ in the cross section, but on the other hand according to luminosity considerations at LHC [35] we would gain more than three orders of magnitude in luminosity. Furthermore, one should answer the question, whether it is possible to distinguish production by single photon-gluon fusion processes from contributions caused by diffractive processes and single gluon-gluon fusion, which result from the overlapping tails of the nucleus distribution at close impact parameters. In addition, the produced quark jets can partially or totally be absorbed by the remaining nucleus. Here parton cascade models might be rather helpful [62]. We conclude that photon-gluon fusion processes in peripheral ultrarelativistic heavy-ion collisions offer the possibility to study the EMC effect and the formation of heavy quarks in a nuclear medium.

Chapter 5

Particle production in central collisions

The production of new and more exotic particles, e.g. the heavy vector mesons, the top quark, the Higgs boson or supersymmetric particles, represents one of the major motivations in high–energy physics. Specific properties of the generated particles are determined experimentally and are compared with predictions from underlying theoretical models within the standard model or within its supersymmetric extensions. An optimal tool for creating particles is provided by an electron-positron collider, e.g. LEP at CERN, since the event environment in electron-positron collisions is relatively clean which allows for precision measurements and for a rigorous analysis of experimental data. But LEP only provides c.m. energies up to about 110 GeV [103]. New high–energy e^+e^- linear colliders called Next Linear Collider (NLC) with c.m. energies larger than 300 GeV are widely discussed [88].
In addition to NLC, a high–energy pp collider (large hadron collider LHC) will be available within a few years. But also heavy-ion collisions being realised at LHC or RHIC could be a suitable tool for the formation of heavy particles. Traditionally, the nuclear colliders at LHC and RHIC are dedicated to the search for a phase transition from hadronic matter into a quark-gluon plasma [112]. But in addition the high–energy photons available due to the strong Lorentz contracted electromagnetic fields of both nuclei may also lead to the formation of new particles in photon-photon fusion processes, confer chapter 2, which is also a relatively clean process. Furthermore, the production of heavy quark pairs by photon-gluon fusion is rather sensitive on the gluon distribution of a bound nucleon inside a nucleus, see chapter 3. In the present chapter we concentrate on particle production in central heavy-ion collisions, which are treated as an ensemble of individual nucleon-nucleon collisions.
The production of new particles in central heavy-ion collisions will not play such a dominant role in the experimental analysis as in single pp collisions. In the framework of the parton model the particle production results from single interactions between the constituents of the nuclei, where collective effects are widely neglected. A simple geometric estimate for the number of nucleon-nucleon collision leads to $A^{4/3}$, which for a Pb-Pb collision yields a factor of about 1230. In this respect heavy–ion collisions are favoured by about three orders of magnitude compared to pp collisions. Contrary to this, the expected c.m. energy in pp collisions is by a factor of about 2.5 and more important the expected luminosity is by about 7 orders of magnitude larger than in Pb-Pb collisions. Consequently, particle production in central heavy-ion collisions is expected to be by typically four orders of magnitude smaller compared with pp collisions. However, considering Ca–Ca collisions, which lead to about three orders of magnitude larger luminosities in contrast to Pb-Pb collisions due to the lower Coulomb-dissociation cross section, confer chapter 3, in total only about two orders of magntitude difference in the particle production yield appears compared to pp collisions. On the other hand, particle production in heavy-ion collisions offers the possibility to deduce relevant informations about the parton content of nuclear matter and of medium effects as well as cooperative phenomena.

5.1 The parton model for ultrarelativistic heavy-ion collisions

Obviously, in central ultrarelativistic heavy-ion collisions we are confronted with produced particles in abundance. More than 200 nucleons are colliding again with more than 200 different nucleons at c.m.

energies up to 2.8 TeV per nucleon in a Pb-Pb collision, i.e. at a total c.m. energy of more than 1000 TeV. Regarding the quarks as individual constituents of nuclei, more than 600 quarks are interacting with more than 600 additional quarks, still without taking the important contributions of gluons and seaquarks into account. Consequently, central ultrarelativistic heavy-ion collisions represent a rather complex scenario.

In order to describe particle production in these extreme heavy-ion collisions we have to employ various assumptions. Considering typical LHC energies of 3 TeV per nucleon one expects a more transparent behavior of the nuclei in contrast to the stopping of impinging nuclei at the current CERN heavy-ion accelerator energy. The constituents of the fast heavy ions are supposed to retain a high fraction of their initial four-momenta. The applied 'incoherence model' includes the underlying assumptions [120]: (1) dominant transparancy of ultrarelativistic heavy-ions in a collision, (2) neglection of single nucleon-nucleon interactions inside a single nucleus, and (3) nuclear cross sections are obtained by an incoherent sum over binary nucleon-nucleon collisions. Clearly, with these assumptions we are reducing the complex problem of an ultrarelativistic heavy-ion collision to the consideration of binary nucleon-nucleon collisions. It should be regarded as a very first step, since the results from experiments at CERN and BNL indicate that nucleus-nucleus collisions cannot be completely described as a straightforward superposition of independent nucleon-nucleon reactions [112].

Following the concept of the parton model, particle production results from numerous independent nucleon-nucleon collisions occuring during the the nucleus-nucleus collision. This immediately leads to the following expression for the total particle production cross section:

$$\sigma_{\mathrm{A_1A_2}}(s_{\mathrm{A}}) = \sum_{i,j} \sigma_{\mathrm{N_iN_j}}(s_{\mathrm{N}}) = \overline{N}_{\mathrm{coll}}\, \sigma_{\mathrm{NN}}(s_{\mathrm{N}})\,. \tag{5.1}$$

Here the assumption of incoherence enters since the total production cross section $\sigma_{\mathrm{A_1A_2}}$ is assumed to consist of an incoherent sum over the individual nucleon-nucleon production cross sections $\sigma_{\mathrm{N_iN_j}}$. The connection between the nucleus-nucleus c.m. energy $\sqrt{s_{\mathrm{A}}}$ for $A = A_1 = A_2$ and the nucleon-nucleon c.m. energy $\sqrt{s_{\mathrm{N}}}$ is simply given by

$$\sqrt{s_{\mathrm{A}}} = A\,\sqrt{s_{\mathrm{N}}}\,. \tag{5.2}$$

Based on the assumption of transparancy the number n_{coll} of nucleon–nucleon collisions prevailing in the nucleus-nucleus collision can be estimated by the following geometrical analysis: A circle is centered around a nucleon of the first nucleus; the area of the circle is equivalent to the total hadronic cross section, for which the parametrization [40]

$$\sigma^{\mathrm{tot}}_{\mathrm{NN}}(s_{\mathrm{N}}) \approx \sigma^{\mathrm{tot}}_{\mathrm{pp}}(s_{\mathrm{N}}) = \left[38.3 + 0.43\,\ln^2\left(\frac{s_{\mathrm{N}}}{100\,\mathrm{GeV}^2}\right)\right]\ \mathrm{mb} \tag{5.3}$$

is utilized. The number of nucleons of the impinging nucleus, which propagate on straight lines, through these circles during the collision will be taken as the number of binary collisions $n_{\mathrm{coll}}(b)$ at a fixed impact parameter b; the circles are of course perpendicular to the straight lines. The impact-parameter averaged number of nucleon-nucleon collisions is finally introduced by

$$\overline{N}_{\mathrm{coll}} = \frac{1}{\sigma^{\mathrm{tot}}_{\mathrm{NN}}} \int \mathrm{d}^2b\; n_{\mathrm{coll}}(b)\,, \tag{5.4}$$

which is normalized to the total nucleon-nucleon cross section $\sigma^{\mathrm{tot}}_{\mathrm{NN}}$. To initialize the proper nucleon distribution and to compute $n_{\mathrm{coll}}(b)$ the relativistic quantum molecular dynamic model (RQMD) was employed [123]. In Figure 5.1 the number of binary collisions n_{coll} depending on the impact parameter b is depicted for a Pb–Pb collision at LHC energies. The mean collision number $\overline{N}_{\mathrm{coll}}$ for LHC energies is $\overline{N}_{\mathrm{coll}} = 1651$ as it has been determined via eq. (5.4), which is somewhat larger than the geometrical estimate $A^{4/3} = 1232$.

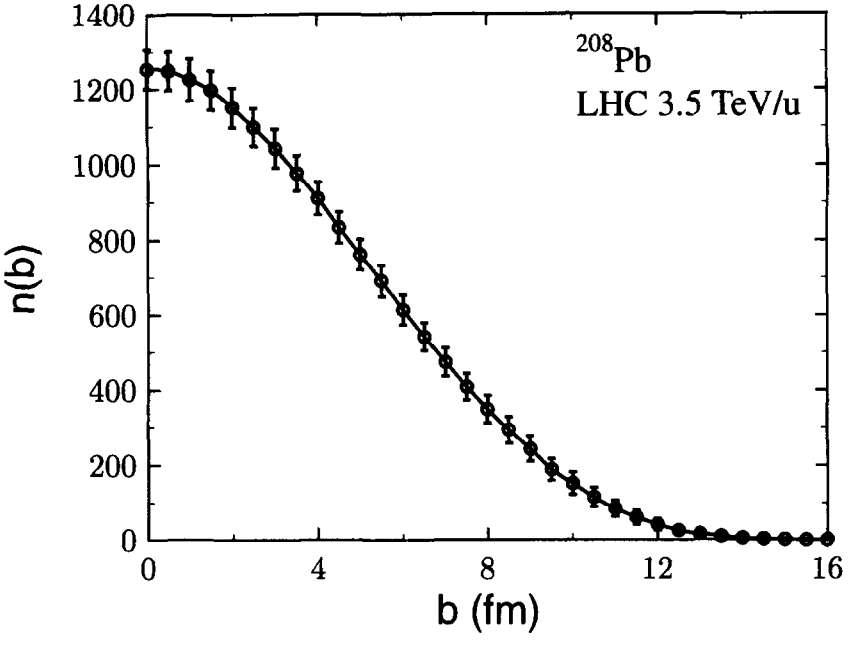

Figure 5.1: Collision number $n_{\mathrm{coll}}(b)$ depending on the impact parameter b for a Pb-Pb collision at a maximum LHC energy of 3.5 TeV/u [116].

The computation of hadronic collisions at relativistic energies is usually performed in the framework of the parton model, i.e. the nucleon is described as a swarm of non-interacting partons (valence quarks, gluons, and sea quarks). Hence the nucleon-nucleon cross section σ_{NN} is reduced to an integral over the parton distributions $f_i(x, Q^2)$ of the impinging nucleons and the associated elementary cross section $\sigma_{ij\to X}(s_{12})$:

$$\sigma_{\mathrm{NN}}(s_{\mathrm{N}}) = K \sum_{i,j} \int_0^1 \int_0^1 \mathrm{d}x_1 \, \mathrm{d}x_2 \, f_i(x_1, Q^2) \, f_j(x_2, Q^2) \, \sigma_{ij\to X}(s_{12}) \, . \tag{5.5}$$

Here s_{N} denotes the squared c.m. energy of the colliding nucleons, Q^2 is the squared four-momentum transfer, and i and j distinguish between the different kinds of partons. The enhancement factor K, which is introduced to simulate higher-oder effects, is set equal to $K = 1$ for simplicity. Furthermore, x_1 and x_2 are the four-momentum fractions of the mother nucleons, carried by the partons, and s_{12} is the squared invariant energy of the parton subprocess, depending on x_1 and x_2:

$$s_{12} = (x_1 - x_2)^2 m_{\mathrm{N}}^2 + x_1 x_2 s_{\mathrm{N}} \, , \tag{5.6}$$

where m_{N} denotes the nucleon mass. The parton distribution functions published by Owens [98] are employed.
In addition, particle production in peripheral collisions should be considered as well by using the equivalent photon method in conjunction with the parton model:

$$\sigma^{\mathrm{periph}}_{\mathrm{A_1A_2}} = A_{\mathrm{eff}} \sum_i \int_0^1 \mathrm{d}x_1 \, f_i(x_1, Q^2) \int_0^\infty \mathrm{d}\omega_2 \, n(\omega_2) \, \sigma_{i\gamma\to X}(s_{12}) \, . \tag{5.7}$$

$A_{\mathrm{eff}} = A^{0.9}$ simulates approximately the nuclear shadowing effect [59]. This prescription of peripheral collisions corresponds to the one presented in chapter 3, the photon-gluon fusion process, but here the central collision region is incorporated.

5.2 The production of Z^0 bosons

In this section various processes which result in the production of Z^0 bosons are studied. It includes processes such as quark-antiquark annihilation and gluon-gluon fusion for central heavy-ion collisions as well as quark-photon fusion for peripheral collisions. The production of neutral intermediate Z^0 bosons during a high-energy heavy-ion collisions can contribute as a background process, e.g. for the production of Higgs bosons in central heavy-ion collisions, and, in general, can serve for further investigations of electroweak phenomena in heavy-ion collisions.

According to the standard model of electroweak interaction several processes on the partonic level $a + b \to Z^0 + X$ have to be considered, where at least one Z^0 is produced in the final state. For a and b being quarks and antiquarks, respectively, the following processes contribute in first-order perturbation theory: $q + \bar{q} \to Z^0 \to l^+l^-$, $q + \bar{q} \to Z^0 + Z^0$, $q + \bar{q} \to Z^0 + \gamma$, $q + \bar{q} \to Z^0 + g$. In the first resonant process l stands for any kind of leptons, i.e. e, μ, τ. Since collinear singularities appear in the last two processes when integrating the differential cross sections cuts for the rapidity ($|y| < 3$) and for the transverse momentum of the produced bosons have to be introduced. Whereas the cut for the transverse momentum is fixed for the next to the last process to $p_t > 10$ GeV, Arnold and Kauffman [16] calculated that perturbation theory for the last process breaks down at transverse momenta below 40 GeV. Consequently, the cut $p_t > 40$ GeV is used for $q + \bar{q} \to Z^0 + g$.

For only one incoming quark or antiquark and additionally one photon or gluon processes such as $(\bar{q})q + \gamma \to q + Z^0$ and $(\bar{q})q + g \to q + Z^0$ have to be taken into account. Furthermore, the gluon fusion processes $g + g \to Z^0 + Z^0$, $g + g \to Z^0 + \gamma$, $g + g \to Z^0 + g$ can only contribute in higher order of perturbation theory, since gluons do not couple directly to Z^0 bosons. Therefore gluon fusion processes occur only via quark loops or triangle diagrams with the Higgs boson. The last kind of process can be neglected because the Z^0ggg coupling contributes at most 3% to the total cross section for Z^0 bosons with large transverse momenta [64]. Although gluon fusion is suppressed by α_s^2, gluon fusion producing a Z^0Z^0 pair [47] or a $Z^0\gamma$ pair [15] via quark loops can make significant contribution at ultrarelativistic heavy-ion collisions. For the computation of these subprocesses as a first assumption a top quark mass of 140 GeV and a Higgs mass of 500 GeV has been used.

On the other hand photon fusion processes occur through quark and additionally through lepton loops and W-boson loops, $\gamma + \gamma \to Z^0 + Z^0$, $\gamma + \gamma \to Z^0 + \gamma$. But it was found that both photon fusion processes can be neglected [83].

The detection of produced Z^0 bosons is assumed to proceed via their decay into dileptons, which will lead to a detectable clear signal. Results of the LEP measurements [115] were used to fix the partial decay rate of the Z^0 boson to

$$\frac{\Gamma_{Z^0 \to l^+l^-}}{\Gamma_{\text{tot}}} = 3.35\,\% \,. \tag{5.8}$$

All results are summarized in Table 5.1. The respective columns indicate the nucleon-nucleon cross sections σ_{NN} and the total heavy-ion cross section σ_{PbPb}.

The results in Table 5.1 demonstrate that the resonant process $q + \bar{q} \to Z^0 \to l^+l^-$ contributes dominantly to Z^0 boson production in ultrarelativistic heavy-ion collisions. Non-resonant contributions are smaller by orders of magnitude, depending on the masses of additionally produced particles. It should be emphasized that the photoproduction process $q + \gamma \to q + Z^0$, which occurs also in peripheral collisions, achieves the highest yield of all non-resonant processes. This high contribution can be traced back to the equivalent photon spectrum which is proportional to the square of the charge number of the colliding nuclei, which is a characteristic feature of ultrarelativistic heavy-ion collisions.

It can be stated that there will be sufficient production rate of Z^0 boson in ultrarelativistic heavy-ion collisions which yields an important background for the search of top quarks and Higgs bosons, but it allows for further investigation of electroweak interactions during ultrarelativistic heavy-ion collisons.

Process	σ_{NN} [pb]	σ_{PbPb} [pb]
$q+\bar{q} \to Z^0 \to l^+l^-$	$1.3 \times 10^{+3}$	$2.2 \times 10^{+6}$
$q+\bar{q} \to Z^0 + Z^0$	$3.5 \times 10^{+0}$	$5.8 \times 10^{+3}$
$q+\bar{q} \to Z^0 + \gamma$	$3.3 \times 10^{+1}$	$5.4 \times 10^{+4}$
$q+\bar{q} \to Z^0 + g$	$2.8 \times 10^{+2}$	$4.7 \times 10^{+5}$
$q+\gamma \to q + Z^0$	-	$8.8 \times 10^{+5}$
$g+g \to Z^0 + Z^0$ with Higgs graph	5.1×10^{-1}	$8.4 \times 10^{+2}$
$g+g \to Z^0 + Z^0$ without Higgs graph	3.9×10^{-1}	$6.4 \times 10^{+2}$
$g+g \to Z^0 + \gamma$	4.3×10^{-1}	$7.0 \times 10^{+2}$

Table 5.1: The production of Z^0 bosons is considered for LHC energies ($\sqrt{s}/2$ = 3.5 TeV/u). For the processes $q+\bar{q} \to Z^0+\gamma$ and $g+g \to Z^0+\gamma$ the cuts $|y| < 3$ and $p_t > 10$ GeV are employed, whereas for $q+\bar{q} \to Z^0+g$ the cuts $|y| < 3$ and $p_t > 40$ GeV are used.

5.3 The production of top quarks

The detection of the top quark at the Fermilab Tevatron is one of the most important recent discoveries. The CDF collaboration has obtained mass values for the top quark of $176 \pm 8 \pm 10$ GeV [2], whereas the D0 collaboration has measured $199^{+19}_{-21} \pm 22$ GeV [1]. Currently the Tevatron is the only machine which generates top quarks on its mass shell, but in future high-energy electron-positron collider and proton-proton collider LHC will also play an important role for the determination of the properties of the top quark, such as its mass, production cross section and branching ratios. The large top quark mass indicates that the top quark experiences the strongest coupling to the symmetry breaking sector of any of the other observed particles. Thus, it provides the possibility to extract some more information about the dynamics of the symmetry breaking, with a scale v which is about the same order of magnitude as the top quark mass m_t ($\approx v/\sqrt{2} = 174$ GeV).

In the following top quark production in central and peripheral ultrarelativistic heavy-ion collisions is discussed. Whereas in central collisions the gluon fusion and the various quark-antiquark annihilation subprocesses are contributing most to the hadronic cross section, in peripheral collisions the photon-gluon and photon-photon fusion subprocess take this place due to the vanishing hard parton-parton subprocesses. Furthermore, the production of toponia, i.e. bound states of top-antitop pairs is considered.

The elementary cross sections are calculated up to second-order perturbation theory. The most dominant elementary cross section for central collisions up to Tevatron energies is the quark-antiquark annihilation subprocess into a free heavy-quark pair because the quark luminosities are larger than the gluon luminosities for large x, i.e. for heavy top-quark production:

$$\sigma_{q\bar{q}} = \frac{2}{9} \frac{4\,\pi\,\alpha_s^2(m_Q^2)}{3\,s} \left(\frac{s-4m_Q^2}{s-4m_q^2}\right)^{1/2} \left(1+\frac{2m_Q^2}{s}\right) \left(1+\frac{2m_q^2}{s}\right), \tag{5.9}$$

where m_q and m_Q are the masses of the ingoing and outgoing quarks, respectively. $\alpha_s(m_Q^2)$ denotes the running coupling constant of the strong interaction, evaluated at the squared mass of the formed quark. Neglecting the light-quark mass m_q, Eq. (5.9) leads to the actually applied formula

$$\sigma_{q\bar{q}} = \frac{2}{9} \frac{4\,\pi\,\alpha_s^2(m_Q^2)}{3\,s^2} (s+2m_Q^2)\,\Delta_T \tag{5.10}$$

with the threshold function

$$\Delta_T = (1-4m_Q^2/s)^{1/2}. \tag{5.11}$$

The calculation of the gluon-gluon fusion subprocess, which becomes most important for LHC energies, yields

$$\sigma_{gg} = \frac{\pi\,\alpha_s^2(m_Q^2)}{3\,s} \left[\frac{1}{4}\left(-7-\frac{31m_Q^2}{s}\right)\Delta_T + \left(1+\frac{4m_Q^2}{s}+\frac{m_Q^4}{s^2}\right) \ln\left(\frac{1+\Delta_T}{1-\Delta_T}\right)\right]. \tag{5.12}$$

The creation of 1^1S_0 quarkonia leads to the gluon fusion cross section

$$\sigma_{gg} = \frac{\pi^2 \alpha_s^2}{3 M_\eta^3} \, |R_S(0)|^2 \, \delta(s - M_\eta^2) \, , \tag{5.13}$$

with M_η the mass of the 1^1S_0 quarkonium and $R_S(0)$ the radial wave function at the origin [115].
Assuming the measured top-quark mass of 176 GeV the total cross section for top quark pair production at LHC energies in central collisions is about 2 μbarn, which corresponds to roughly 3200 top-quark pairs assuming a luminosity of 1.6×10^{27} cm^{-2} s^{-1} and a beam time of 10^6 s ($\approx 1/30$ year).
The production cross sections of toponia is also of definite interest. Assuming $m_\eta = 2\, m_t = 360$ GeV the cross section yields about 50 nbarn, which corresponds to about 80 toponia produced in one year of beam time. The toponium creation cross section is lower by about a factor 40 in contrast to the free top-quark production.
The top-quark pair production cross section in peripheral collisions is roughly two orders of magnitude lower compared within central collisions, cf. chapter 3. But with higher collider energy the peripheral collision becomes more and more important, since the photon luminosities resulting from the strong electromagnetic fields increase considerably.

5.4 Production of Higgs bosons

In this section the production of Higgs bosons in central ultrarelativistic heavy-ion collisions is discussed in contrast to the production in peripheral collisions via two-photon fusion processes, cf. chapter 2. Electron-positron colliders such as LEP represent an optimal tool to produce and to detect Higgs bosons for masses below about 100 GeV. On the other hand Higgs bosons with masses larger than about 160 GeV could be generated utilizing a p-p collider such as the proposed LHC. Alternatively, Higgs boson production also occurs in central heavy-ion collisions, which provide an additional hunting method.
Assuming the mentioned dominant transparency the main elementary production channel of the Higgs boson proceeds from the gluon-gluon fusion mechanism and quark-antiquark annihilation process. Thus the parton cross section reads

$$\sigma_{gg \to H} = \frac{\pi^2}{8\, m_H} \, \Gamma_{H \to gg} \, \delta(s_{12} - m_H^2) \tag{5.14}$$

for the gluon-gluon fusion into a Higgs boson and

$$\sigma_{q\bar{q} \to H} = 2 \, \frac{4}{9} \, \frac{\pi^2}{m_H} \left(1 - \frac{4\, m_q^2}{m_H^2}\right)^{-1} \Gamma_{H \to q\bar{q}} \, \delta(s_{12} - m_H^2) \tag{5.15}$$

for the quark-antiquark annihilation into a Higgs boson. The additional factor 2 in Eq. (5.15) appears because in symmetric collisions the quark might come from the first nucleus and the antiquark from the second nucleus and vice versa. The corresponding decay widths $\Gamma_{H \to gg}$ and $\Gamma_{H \to q\bar{q}}$ are presented both for Higgs bosons required from the standard model (SM) and from the minimal supersymmetric extension of the standard model (MSSM) in Ref. [74, 71].
In Figure 5.2 the production of SM-Higgs boson in central Pb-Pb collisions at LHC energies is displayed in dependence on the mass m_H of the SM-Higgs boson. The dominant contribution to the total cross section for the SM-Higgs boson production results from the gluon-gluon fusion process; the quark-antiquark annihilation subprocess contributes less by about two orders of magnitude. The computed cross sections are in the range 4 - 40 nb, decreasing with increasing Higgs-boson mass. With an expected beam luminosity of $L = 10^{27}$ cm^{-2} s^{-1} and a running time of 10^6 s about 4 - 40 Higgs bosons are produced per one year of beam time. The calculated cross sections are typically one to two orders of magnitude larger than the ones by two-photon fusion processes, cf. chapter 2., and about five to six orders of magnitude larger than the hypothetical collective production [56].

The main decay channel for the intermediate mass Higgs boson is given by the decay into a $b\bar{b}$ pair with a branching ratio of about 90 %. But this channel seems to be overwhelmed completely by background processes, e.g. gluon fusion and quark-antiquark processes. Rare processes such as the two-photon decay $H_{SM} \to \gamma\gamma$ or the decay into a Z^0 boson and a pair of charged leptons $H_{SM} \to Z^0 l^+ l^-$ were proposed for the detection. Taking the two-photon decay branching ratio of about 10^{-3} [45] into account, the detection rates of produced SM-Higgs bosons into two photons is lowered to about 0.04 - 0.4 events per year. One obtains about the same result if the decay $H_{SM} \to Z^0 l^+ l^-$ is considered.

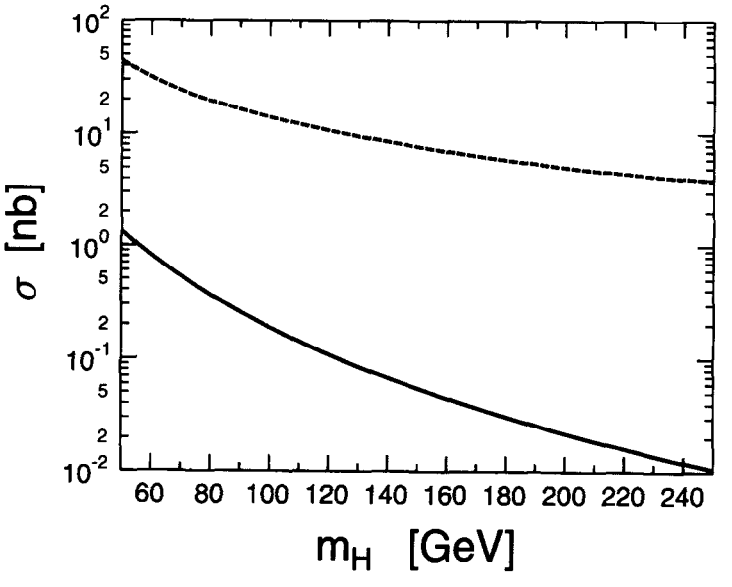

Figure 5.2: Total cross section for SM-Higgs boson production in central Pb-Pb collisions at LHC energies (3.5 TeV/u) in dependence on the SM-Higgs boson mass m_H. Dashed line: gluon-gluon fusion; full line: quark-antiquark annihilation.

Chapter 6

Conclusions

"Non quark gluon plasma" aspects of relativistic heavy-ion collisions have been discussed: Production of exotic particles in peripheral collisions, photon-gluon physics and particle production in central collisions. For the description of these processes the Equivalent Photon Approximation has been employed, which is well justified in relativistic heavy-ion collisions except for e^+e^--production: A rigorous derivation from quantum electrodynamics also allowed for various generalisations as for example the impact-parameter dependence of the cross sections.

For Au-Au collisions at RHIC only light mesons with masses up to 5 GeV can be produced in two-photon fusion processes. This is simply caused by the maximum equivalent photon frequencies contained in the transverse electromagnetic field of the heavy ion, which amount only to about 3 GeV. For LHC the situation is different: In the Pb-mode as well as in the Ca-mode exotic mesons like hybrid mesons, multiquark states and glueballs can be produced in relatively large numbers. This also represents an excellent opportunity to search for unexpected heavy mesons in the mass range of 10 GeV and above. For very heavy exotic particles as Higgs bosons and supersymmetric particles only the Ca-Ca collisions at LHC appear to be promising. This conclusion results predominantly from luminosity arguments. Not all exotic two-photon fusion processes have been calculated so far. It would be interesting to reconsider light mesons as for example pion pair production with capture or even pionium production.

Exotic mesons like D- and B-mesons can also be produced in photon-gluon fusion processes, where the equivalent photon penetrates directly into the other nucleus to fuse with a gluon and to produce a pair of heavy quarks, which then fragment into the mesons. From a different perspective the γg-fusion into a $q\bar{q}$-pair is also very enlightening, as it allows to deduce directly the gluon distribution in a nuclear medium. Here some additional studies are still necessary; for example the deflection and absorption of the produced jets in the nuclear medium, the calculation of the in-medium K-factor and the nuclear reactions after the γg-fusion. In conclusion, the photon-gluon processes contribute to a better understanding of the behaviour of heavy quarks in nuclear medium.

As a further fascinating topic we have to consider the hadronic component of the photon, which interacts with the other photons' hadronic component or with the other nucleus. QCD-parametrisations turn out to be necessary to understand these processes. Also photon-pomeron or additional diffractive processes play an interesting role in the framework of relativistic heavy-ion collisions and could be studied.-

All these findings, presented here in this review, and all the perspectives outlined emphasize that "Non quark gluon plasma" physics will fruitfully contribute to the relativistic heavy-ion collision programm at RHIC and LHC.

Acknowledgement: We are grateful to Mario Vidovic for many enlightning discussions which contributed to the organisation of this review. Over the years this work has been supported by GSI, DFG, BMBF, DAAD and AvH.

Bibliography

[1] S. Abachi et al. (D0 Collaboration); Phys. Rev. Lett. 74, 2632 (1995).

[2] F. Abe et al. (CDF Collaboration); Phys. Rev. Lett. 74, 2626 (1995).

[3] F. Abe et al. (CDF Collaboration); Phys. Rev. Lett. 68, 447 (1992).

[4] F. Abe et al. (CDF Collaboration); Phys. Rev. Lett. 62, 1825 (1989).

[5] K.J. Abraham, R. Laterveer, J.A.M. Vermaseren, D.. Zeppenfeld; Phys. Lett. B 251, 186 (1990).

[6] K. J. Abraham, M. Drees, R. Laterveer, E. Papageorgiu, A. Schäfer, G. Soff, J. Vermaseren, D. Zeppenfeld; *Large Hadron Collider Workshop*; eds.: G. Jarlskog and D. Rein, Proceedings Vol. II, 1224, (Aachen 1990), CERN 90-10, ECFA 90-133.

[7] N. N. Achasov, G. N. Shestakov; Phys. Lett. B 156, 434 (1985).

[8] B. Adeva et al. (L3 Collaboration); Phys. Lett. B 251, 311 (1990).

[9] C.K. Agger and A.H. Sorensen; Phys. Rev. A 55, 402 (1997).

[10] F. del Aguila, F. Cornet, J. I. Illana; Phys. Lett. B 271, 256 (1991).

[11] J. Ahrens; Nucl. Phys. A446, 229c (1985).

[12] ALICE collaboration; *Technical Proposal*; CERN/LHCC/95-71 (1995).

[13] J.D. Almeida, A.A. Natale, S.F. Novaes; Phys. Rev. D 44, 118 (1991).

[14] G. Altarelli, M. Traseira; Phys. Lett. B 245, 658 (1990).

[15] L. Ametller, E. Gava, N. Paver, D. Treleani; Phys. Rev. D 32, 1699 (1985).
E.W.N. Glover, J.J. van der Bij; Phys. Lett. B 206, 701 (1988).

[16] P. B. Arnold, R. P. Kauffman; Nucl. Phys. B 349, 381 (1991).

[17] A. Aste, K. Hencken, D. Trautmann; Phys. Rev. A 50, 3980 (1994).

[18] A.J. Baltz; preprint physics/9701008.

[19] N. Baron, G. Baur; Phys. Rev. C 48, 1999 (1993).

[20] N. Baron, G. Baur; Phys. Rev. C 49, 1127 (1994).

[21] S. E. Baru et al.; Z. Phys. C 48, 581 (1990).

[22] R. Bates, J. N. Ng; Phys. Rev. D 33, 657 (1986).

[23] G. Baur, C. A. Bertulani; Nucl. Phys. A 505, 835 (1989).

[24] G. Baur, L. Ferreira Filho; Nucl. Phys. A 518, 786 (1990).

[25] G. Baur; Phys. Rev. A 42, 5736 (1990).

[26] G. Baur, N. Baron; Nucl. Phys. A 561, 628 (1993).

[27] C. Berger, W. Wagner; Phys. Rep. 146, 1 (1987)

[28] C. A. Bertulani, G. Baur; Phys. Rep.163, 299 (1988).

[29] C. Best, W. Greiner, G. Soff; Phys. Rev. A 46, 261 (1992).

[30] C. Best, J. M. Eisenberg, G. Soff, W. Greiner; *QCD Vacuum structure*; eds.: H. M. Fried and B. Müller, Proceedings, 270, (World Scientific, Singapore, 1993)

[31] C. Bottcher, M. R. Strayer; Phys. Rev. D 39, 1330 (1989).

[32] C. Bottcher, M. R. Strayer; J. Phys. G 16, 975 (1990).

[33] C. Bottcher, A. K. Kerman, M. R. Strayer, J. S. Wu; Particle World, Vol. 1, No. 6, 174 (1990).

[34] C. Bottcher, M. R. Strayer; Nucl. Phys. A 544, 255c (1992).

[35] D. Brandt, K. Eggert, A. Morsch; LHC Note 264, CERN AT/94-05 (DI).

[36] V. M. Budnev, I. F. Ginzburg, G. V. Meledin and V. G. Serbo; Phys. Rep. 15C, 183 (1975).

[37] R. N. Cahn, J. D. Jackson; Phys. Rev. D 42, 3690 (1990).

[38] F. Caruso, E. Predazzi, A. C. B. Antunes, J. Tiomno; Z. Phys. C 30, 493 (1986).

[39] F. Close; Rep. Prog. Phys. 51, 833 (1988).

[40] P. D. B. Collins and A. D. Martin; *Hadron Interactions* (Hilger, Bristol, 1984).

[41] S. Cooper; Ann. Rev. Nucl. Part. Sci. 38, 705 (1988).

[42] B. L. Berman, S.C. Fultz; Rev. Mod. Phys. 47, 713 (1975).
A. Lepretre, H. Beil, R. Bergere, P. Carlos, J. Fagot, A. De Miniac, A. Veyssiere; Nucl. Phys. A367, 237 (1981).
P. Carlos, H. Beil, R. Bergere, J. Fagot, A. Lepretre, A. De Miniac, A. Veyssiere; Nucl. Phys. A431, 573 (1984).
J. Arends, J. Eyink, A. Hegerath, K. G. Hilger, B. Mecking, G. Nöldeke, H. Rost; Phys. Lett. 98B, 423 (1981).
G. R. Brookes et al.; Phys. Rev. D 8, 2826 (1973).
D. O. Caldwell, V. B. Elings, W. P. Hesse, R. J. Morrison, F. V. Murphy, D. E. Yount; Phys. Rev. D 7, 1362 (1973).
D. O. Caldwell et al.; Phys. Rev. Lett. 42, 553 (1979).

[43] A. Veyssiere, H. Beil, R. Bergere, P. Carlos, L. Lepretre; Nucl. Phys. A159, 561 (1970).
A. Lepretre, H. Beil, R. Bergere, P. Carlos, J. Fagot, A. De Miniac, A. Veyssiere; Nucl. Phys. A367, 237 (1981).

[44] Michalowski S. Michalowski, D. Andrews, J. Eickmeyer, T. Gentile, N. Mistry, R. Talman, K. Ueno; Phys. Rev. Lett. 39, 737 (1977).

[45] S. Dawson; Comments Nucl. Part. Phys. 20, 161 (1991).

[46] W. Deans; Nucl. Phys. B 197, 307 (1982).

[47] D.A. Dicus, C. Kao, W.W. Repko; Phys. Rev. D 36, 1570 (1987).
D.A. Dicus; Phys. Rev. D 38, 394 (1988).
E.W.N. Glover, J.J. van der Bij; Phys. Lett. B 219, 488 (1989); Nucl. Phys. B 321, 564 (1989).

[48] H. G. Dosch, Yu. A. Simonov; Z. Phys. C 45, 147 (1989).

[49] M. Drees, J. Ellis, D. Zeppenfeld; Phys. Lett. B223, 454 (1989).

[50] M. Drees, M. Krämer, J. Zunft, P. M. Zerwas; Phys. Lett. B306, 371 (1993).

[51] D. W. Duke, J. F. Owens; Phys. Rev. D 30, 49 (1984).

[52] J. Eichler; Phys. Rep. 193, 165 (1990).

[53] J. Eichler and W.E. Meyerhof; *Relativistic Atomic Collisions* (Academic Press, San Diego, 1995).

[54] E. Eichten, I. Hinchliffe, K. Lane, C. Quigg; Rev. Mod. Phys. 56, 579 (1984).

[55] J. Ellis; Beyond the Standard Model IV Conference, Granlibakken, California, December 1994; CERN-TH.95-28.

[56] T. Elze, J. Rafelski; Phys. Lett. B 276, 501 (1992).

[57] E. Fermi; Z. Physik 29, 315 (1924).

[58] M. Frank, P. J. O'Donnel; Phys. Rev. D 32, 1739 (1985).

[59] L. Frankfurt, M. Strikman; Phys. Rep. 160, 235 (1988).

[60] S. Frixione, M. L. Mangano, P. Nason, G. Ridolfi; Phys. Lett. B 308, 137 (1993).

[61] K. Geiger, B. Müller, W. Greiner; Z. Phys. C 48, 257 (1990).

[62] K. Geiger, B. Müller; Nucl. Phys. B 369, 600 (1992).

[63] I. F. Ginzburg; Nucl. Phys. B (Proc. Suppl.) 37, 303 (1994).

[64] E. W. N. Glover, J. J. van der Bij; Nucl. Phys. B 313, 237 (1989).

[65] E. Gotsman, D. Lissauer; Phys. Lett. B 240, 16 (1990).

[66] M. Grabiak, B. Müller, W. Greiner, G. Soff, P. Koch; Preprint GSI 87-78.

[67] M. Grabiak, B. Müller, W. Greiner, G. Soff, P. Koch; J. Phys. G15, L25 (1989).

[68] M. Greiner, M. Vidović, J. Rau, G. Soff; J. Phys. G 17, L45 (1991).

[69] M. Greiner, M. Vidović, G. Soff; Phys. Rev. C 47, 2288 (1993).

[70] M. Greiner, M. Vidović, G. Soff, C. Best; Rev. Mex. Fis. 39, Supl. 2, 114 (1993).

[71] M. Greiner, D. Hilberg, C. Hofmann, G. Soff; J. Phys. G: Nucl. Part. Phys. 19, 261 (1993).

[72] M. Greiner, M. Vidović, Ch. Hofmann, A. Schäfer, G. Soff; Phys. Rev. C 51, 911 (1995).

[73] M. C. Guclu, J. C. Wells, A. S. Umar, M. R. Strayer, D. J. Ernst; Phys. Rev. A 51, 1836 (1995).

[74] J. F. Gunion, H. Haber, G. Kane, S. Dawson; *The Higgs Hunter's Guide*; (Addison-Wesley, Reading, 1991).

[75] H. E. Haber, J. P. Perrier; Phys. Rev. D 32, 2961 (1985).

[76] K. Hencken, D. Trautmann, G. Baur; Phys. Rev. A 49, 1584 (1994).

[77] K. Hencken, D. Trautmann, G. Baur; Phys. Rev. A 51, 1874 (1995).

[78] K. Hencken, D. Trautmann, G. Baur; Z. Phys. C 68, 473 (1995).

[79] C. Hofmann, G. Soff, A. Schäfer, W. Greiner; Phys. Lett. B 262, 210 (1991).

[80] C. Hofmann, S. Schneider, M. Vidovic, C. Best, D. Hilberg, A. Schäfer, W. Greiner, M. Greiner and G. Soff; *Production of exotic particles in central and peripheral heavy-ion collisions*; eds.: I. Iori; Ricerca Scientifica ed. Educazione Permanente, Supplemento n.91, 406 (1992)

[81] C. Itzykson, J.B. Zuber; *Quantum Field Theory*; (Mc Graw-Hill, New York, 1985).

[82] J. D. Jackson; *Klassische Elektrodynamik*, (deGruyter, Berlin, 1983).

[83] G. Jikia; preprint IHEP 93-37.

[84] K. Karch et al.; Z. Phys. C 54, 33 (1992).

[85] W. Keung, W.J. Marciano; Phys. Rev. D 30, 248 (1984).

[86] S. Klein; LBL-37295, Presented at "Photon '95", April 8-13, 1995, Sheffield University, Sheffield, UK.

[87] L. Köpke, N. Wermes; Phys. Rep. 174, 67 (1989).

[88] J. Kuhn; *Physics and Experiments with Linear e^+e^- Colliders*; eds.: F. Harris, S. Olsen, S. Pakvasa, and X. Tuta; (World Scientific, Singapore, 1993).

[89] S. Kumano; Phys. Lett. B 298, 171 (1993).

[90] B. Müller; *The Physics of the Quark-Gluon Plasma*, Lecture Notes in Physics, vol. 225; (Springer, Berlin, 1985).

[91] H. J. W. Müller-Kirsten, A. Wiedemann; *Supersymmetry*; (World Scientific, Singapore, 1987).

[92] B. Müller, A. J. Schramm; Phys. Rev. D 42, 3699 (1990).

[93] B. Müller, A. J. Schramm; Nucl. Phys. A 523, 677 (1991).

[94] A.A. Natale; Mod. Phys. Lett. A 9, 2075 (1994).

[95] A.A. Natale; hep-ph/9509280 (1995).

[96] J. W. Norbury; Phys. Rev. D 42, 3696 (1990).

[97] J. W. Norbury; Phys. Rev. C 43, R368 (1991).

[98] J. F. Owens; Phys. Lett. B 266, 126 (1991).

[99] E. Papageorgiu; Phys. Rev. D 40, 92 (1989).

[100] E. Papageorgiu; Phys. Lett. B 250, 155 (1990).

[101] E. Papageorgiu; Phys. Lett. B 352, 394 (1995).

[102] Particle Data Group; Phys. Rev. D 45, Part 2 (1992).

[103] Particle Data Group; Phys. Rev. D 50, 1173 (1994).

[104] Particle Data Group; Phys. Rev. D 50, 1173 (1996).

[105] Proceedings to the 10th. International Workshop on Photon-Photon Collisions (Photon '95), Sheffield University, England, April 8-13 1995.

[106] M. Poppe: Int. Jour. of Mod. Phys. A, Vol. 1, No. 3, 545 (1986).

[107] Proceedings of the IXth. Workshop on Photon-Photon Collisions, UC, San Diego, La Jolla, California, 1992, edited by D.O. Caldwell and H.P. Paar (World Scientific, Singapore, 1992).

[108] J. Rau, B. Müller, W. Greiner, G. Soff; J. Phys. G 16, 211 (1990).

[109] M. J. Rhoades-Brown, J. Weneser; AD/RHIC-110, Informal Report No. BNL-47806 (1992).

[110] S. Sadovsky; Internal Note ALICE 93-07 (1993).

[111] A. Schäfer, O. Nachtmann, R. Schöpf; Phys. Lett. B 249, 331 (1990).

[112] H. R. Schmidt, J. Schukraft; J. Phys. G 19 (1993) 1705.

[113] J. Schukraft for the ALICE collaboration; Nucl. Phys. A 566, 311c (1995).

[114] J. Smith, W. van Neerven; Nucl. Phys. B 374, 36 (1992).

[115] S. Schneider, H. Sorge, G. Soff, W. Greiner; J. Phys. G 17, L149 (1991).

[116] S. Schneider, W. Greiner, G. Soff; Phys. Rev. D 46, 2930 (1992).

[117] S. M. Schneider, W. Greiner, G. Soff; J. Phys. G 19, L39 (1993).

[118] H. Schopper; Phys. Bl. 47, 907 (1991).

[119] G. Soff, J. Rau, M. Grabiak, B. Müller, W. Greiner; *The Nuclear Equation of State*, eds.: W. Greiner, H. Stöcker; Part B, p. 579, Plenum Press, New York (1989).

[120] G. Soff, W. Mittelbach, M. Greiner, M. Vidović, C. Best, S. Schneider, D. Hilberg, and C. Hofmann; *Heavy Ion Physics Today and Tomorrow*; eds. : R. Caplar and W. Greiner; Proceedings, 353, (World Scientific, Singapore, 1991).

[121] G. Soff, D. Hilberg, Ch. Hofmann, Ch. Best, S. Schneider, M. Vidović, M. Greiner; Rev. Mex. Fis. 38, Supl. 2, 196 (1992).

[122] M. F. Sohnius; Phys. Rep. 128, 39 (1985).

[123] H. Sorge, H. Stöcker, and W. Greiner; Ann. Phys. 192, 266 (1989).

[124] E. Teller; Nucl.Instruments and Methods in Phys. Research B 24/25, 1 (1987).

[125] M. Vidović, diploma thesis, GSI-91-32.

[126] M. Vidović, M. Greiner, C. Best, G. Soff; Phys. Rev. C 47, 2308 (1993).

[127] M. Vidović, M. Greiner, G. Soff; Phys. Rev. C 48, 2011 (1993).

[128] M. Vidović, M. Greiner, G. Soff; *15. Arbeitsbericht der Arbeitsgruppe Energiereiche Atomare Stöße*; ed.: C. Düsterhöft et al.; S. 165, ISSN 0724-4975, Riezlern (1994).

[129] M. Vidović; Thesis 1994 unpublished.

[130] M. Vidović, G. Soff, M. Greiner; *Coulomb dissociation of* ^{208}Pb *and* ^{197}Au *collisions*; ed.: I. Iori; Ricerca Scientifica ed Educazione Permanente, Supplemento n. 97, 371 (1994).

[131] M. Vidović, M. Greiner, G. Soff; J. Phys. G 21, 545 (1995).

[132] M. Vidović, M. Greiner, G. Soff; Mod. Phys. Lett. A 10, 2471 (1995).

[133] W. Weise; Phys. Rep. 13, 53 (1974).

[134] C. F. v. Weizsäcker; Z. Physik 88, 612 (1934).

[135] E. J. Williams; Proc. Roy. Soc. A139, 163 (1933).

[136] G. Wolf; Phys. Lett. B 293, 465 (1993).

[137] J. S. Wu, C. Bottcher, M. R. Strayer; Phys. Lett. B 252, 37 (1990).

[138] J. S. Wu, C. Bottcher, M. R. Strayer, A. K. Kerman; Ann. Phys. 210, 402 (1991).

[139] J. S. Wu, J. J. Rhoades-Brown, C. Bottcher, M. R. Strayer; Nucl. Instrum. Methods A 311, 249 (1992).

[140] C. N. Yang; Phys. Rev. 77, 242 (1950).